

**Landslide risk analysis for Clifton Beach,  
Cape Kidnappers, Hawke's Bay**

Cl Massey  
S de Vilder

B Lukovic  
GC Archibald

**GNS Science Consultancy Report 2020/28  
May 2020**



### **DISCLAIMER**

This report has been prepared by the Institute of Geological and Nuclear Sciences Limited (GNS Science) exclusively for and under contract to Hastings District Council and the Department of Conservation. Unless otherwise agreed in writing by GNS Science, GNS Science accepts no responsibility for any use of or reliance on any contents of this report by any person other than Hastings District Council and the Department of Conservation and shall not be liable to any person other than Hastings District Council and the Department of Conservation, on any ground, for any loss, damage or expense arising from such use or reliance.

#### **Use of Data:**

Date that GNS Science can use associated data: April 2020

### **BIBLIOGRAPHIC REFERENCE**

Massey CI, Lukovic B, de Vilder S, Archibald GC. 2020. Landslide risk analysis for Clifton Beach, Cape Kidnappers, Hawke's Bay. Lower Hutt (NZ): GNS Science. 101 p. Consultancy Report 2020/28.

The risk data and calculations used in this report were independently reviewed by T Taig, TTAC Ltd.

## CONTENTS

<b>EXECUTIVE SUMMARY.....</b>	<b>IV</b>
<b>1.0 INTRODUCTION .....</b>	<b>1</b>
1.1 Project Objectives.....	5
1.2 Report Structure .....	6
1.3 Personnel .....	6
<b>2.0 SITE DESCRIPTION.....</b>	<b>7</b>
2.1 Setting .....	7
2.2 Topographic Mapping .....	8
2.3 Geology and Geomorphology .....	8
2.4 Hazard Areas.....	8
2.5 Previous Landslides in the Area .....	9
2.5.1 Rockfall.....	9
2.5.2 Debris Slides and Avalanches.....	9
2.5.3 Exclusions .....	10
2.5.4 Landslide Data for the Study Area .....	11
2.6 Visitor and DOC, HDC and GBA Staff Exposure.....	11
2.7 Data Used in this Study .....	12
<b>3.0 RISK METRICS AND METHODOLOGY.....</b>	<b>13</b>
3.1 Risk Metrics.....	13
3.2 Assessment Methodology.....	14
3.2.1 Probability of the Initiating Event.....	16
3.2.2 Landslide Source Locations .....	22
3.2.3 Probability of Being in the Path of Landslide Debris, if Present.....	25
3.2.4 Vulnerability: Probability that a Person is Killed, if Present and in the Path of Landslide Debris .....	44
3.2.5 Local Personal Risk.....	47
3.2.6 Probability that a Person is Present .....	48
<b>4.0 RISK ANALYSIS RESULTS.....</b>	<b>50</b>
4.1 The Local Personal Risk.....	50
4.1.1 General Results for the Study Area.....	75
4.2 The Annual Individual Fatality Risk and Risk per Trip .....	75
4.3 Societal Risk.....	77
4.4 Consistency with Actual Experience .....	79
4.5 Sensitivity to Key Uncertainties.....	80
<b>5.0 RISK IN CONTEXT.....</b>	<b>83</b>
5.1 Visitor Individual Risk in Context.....	83
5.2 Staff Risk in Context .....	86
5.3 Societal Risk in Context.....	87

<b>6.0</b>	<b>RISK MANAGEMENT .....</b>	<b>88</b>
6.1	Warning Staff and Visitors that the Hazard is Present.....	88
6.2	Informing Staff and Visitors of the Measures in Place to Make it Safer .....	88
6.3	Closing the Operations during Periods when the Hazard Might be Increased	89
<b>7.0</b>	<b>CONCLUSIONS .....</b>	<b>90</b>
<b>8.0</b>	<b>RECOMMENDATIONS.....</b>	<b>92</b>
<b>9.0</b>	<b>ACKNOWLEDGEMENTS.....</b>	<b>93</b>
<b>10.0</b>	<b>REFERENCES .....</b>	<b>93</b>

## FIGURES

Figure 1.1	Photographs of the Cape Kidnappers debris avalanche, captured via drone on the 25/01/2019.	1
Figure 1.2	Location map showing the study area. ....	3
Figure 2.1	Photographs of the study area, taken 5–6 March 2020. ....	7
Figure 2.2	Cartoons of the three main type of landslides found in the study area. ....	9
Figure 3.1	Landslide source volume and surface area for 240 landslides derived from differencing the March to April 2019 DSM from the July and September 2019 DSM.....	20
Figure 3.2	The number of landslides within each volume and LSR class for the slopes on which the different volume classes of landslide triggered by the Kaikōura Earthquake occurred.....	24
Figure 3.3	Schematic representation of the source area and debris inundation area (source, transport and deposit zones) of a landslide .....	26
Figure 3.4	Schematic representation of runout exceedance probability based on empirical relationships ..	27
Figure 3.5	Empirical relationship between $\Delta H/L$ ratio and volume in dry (i.e. earthquake-induced) debris avalanches ( $<100,000 \text{ m}^3$ ) and rock avalanches ( $>100,000 \text{ m}^3$ ). ....	28
Figure 3.6	Conceptual representation of the landslide runout model stopping rules as implemented in GIS. ....	29
Figure 3.7	Landslide hazard footprints. ....	31
Figure 3.8	Rockfall simulations showing the simulated rockfall trajectories and runout distances for the mean boulder size of $1 \text{ m}^3$ . ....	40
Figure 3.9	Schematic diagram showing how the probability of a person being in the path of one landslide is calculated in the risk analysis. ....	43
Figure 4.1a	Map showing the LPR from earthquake-induced landslides for the study area. ....	51
Figure 4.1b	Map showing the LPR from non-earthquake-induced landslides for the study area.....	59
Figure 4.1c	Map showing the LPR from combining earthquake- and non-earthquake-induced landslides for the study area.....	67
Figure 4.2	The risk per trip and AIFR: earthquake-induced landslides only. ....	77
Figure 4.3	The risk per trip and AIFR: non-earthquake- and earthquake-induced landslides combined. ....	77
Figure 4.4	Lower overall visitor societal risk, in terms of charts of frequency ( $f$ ) of events causing a number ( $N$ ) or more deaths for the representative routes in the study area .....	78
Figure 4.5	Upper overall visitor societal risk, in terms of charts of frequency ( $f$ ) of events causing a number ( $N$ ) or more deaths for the representative routes in the study area .....	79
Figure 5.1	Fatality risk per single round trip for some popular adventure tourism activities compared with the fatality risk per trip to visit the gannets.....	84
Figure 5.2	Fatality risk per day for visiting the gannets compared to the fatality risk per day from some popular New Zealand sport and leisure activities for the period January 2001 to June 2014. ....	85

Figure 5.3	The total fatalities per employee per year for DOC and GBA staff at Cape Kidnappers compared with those from other New Zealand industries.....	86
Figure 5.4	The annual frequency ( $f$ ) of events with a given number ( $N$ ) of more deaths for the study area, compared to those from New Zealand earthquakes and storms and/or floods.....	87

## TABLES

Table 2.1	Summary of data types, sources and uses within this study. ....	12
Table 3.1	Details of the multiple linear regression model adopting the ‘least squares’ method to fit a line through the observations made from debris avalanches that occurred on cliffs in the Port Hills of Christchurch cliffs during the CES.....	18
Table 3.2	Total volumes of debris generated using the RoARS model for Hazard Areas 1–4. ....	19
Table 3.3	Landslide source volume classes, their representative source areas and the contribution of each landslide volume class as a proportion of the total landslide volume generated per year .....	21
Table 3.4	Annual frequency of a given PGA occurring in the study area obtained from the NSHM, and the representative event PGA for each earthquake band.....	21
Table 3.5	Annual frequency of non-earthquake-induced landslides per volume class and per hazard area. ....	22
Table 3.6	Summary of the estimated potential landslide source volume as a function of the LSR calculated in the 30 m radius from the Kaikōura earthquake landslides.....	24
Table 3.7	Summary of Fahrböschung values for each volume class of dry debris avalanche and rock avalanche used in this project .....	28
Table 3.8	RAMMS Rockfall model parameters used for forecasting rockfalls. ....	41
Table 3.9	Physical vulnerability values used in the study.....	45
Table 3.10	Physical vulnerability values for a walker on their own.....	46
Table 3.11	Physical vulnerability values for a group member on a GBA tour.....	46
Table 3.12	Exposure data. ....	49
Table 4.1	AIFR and risk per trip results for the Neap and Spring low tide routes, for earthquake- (EQ) and non-earthquake- (Non-EQ) induced landslides, and both combined.....	76
Table 4.2	Uncertainties and their implications for risk. ....	81

## APPENDICES

<b>APPENDIX 1</b>	<b>EARTHQUAKE-INDUCED LANDSLIDE FREQUENCY MAGNITUDE</b>	<b>99</b>
-------------------	---	-----------

### APPENDIX TABLES

Table A1.1	Hazard Area 1, adopting the study area landslide distribution.....	99
Table A1.2	Hazard Area 2, adopting the study area landslide distribution.....	99
Table A1.3	Hazard Area 3, adopting the study area landslide distribution.....	100
Table A1.4	Hazard Area 4, adopting the study area landslide distribution.....	100
Table A1.5	Hazard Area 1, adopting the Kaikōura earthquake landslide distribution .....	100
Table A1.6	Hazard Area 2, adopting the Kaikōura earthquake landslide distribution .....	101
Table A1.7	Hazard Area 3, adopting the Kaikōura earthquake landslide distribution .....	101
Table A1.8	Hazard Area 4, adopting the Kaikōura earthquake landslide distribution .....	101

## EXECUTIVE SUMMARY

This report has been prepared by the Institute of Geological & Nuclear Sciences Limited (GNS Science) in response to a request from Hastings District Council (HDC) and the Department of Conservation (DOC) for a quantified landslide risk analysis for the Clifton Beach to Cape Kidnappers study area in Hawke's Bay.

The quantitative landslide risk assessment is based on risk-estimation methods that follow appropriate parts of the Australian Geomechanics Society framework for landslide risk management. It provides landslide risk estimates suitable for use under AS/NZS ISO 31000: 2009.

The objectives of this study are: 1) to inform HDC and DOC of the spatial variation of risk and the factors that most contribute to landslide risk in the study area; and 2) to use the information from the landslide risk analysis to provide advice that will help HDC and DOC manage visitor and staff safety so that the landslide risk is as low as reasonably practicable (ALARP).

The risk assessment quantifies the risk – in this case, the loss of life – to visitors and to DOC and Gannet Beach Adventures (GBA) staff from landslide hazards in the study area. The landslide risk metrics adopted for this study are described in Section 2; these are:

1. the local personal risk (LPR),
2. the annual individual fatality risk (AIFR),
3. the individual risk for visitors (risk per trip and per multiple trips), and
4. the risk of major multi-fatality accidents ('societal risk').

The risks presented in this report for the Cape Kidnappers study area do not include any consideration of the potential reduction in risk caused by the control measures that are currently in place. This is because it is difficult to quantify the relative reduction in risk that they may provide.

The method used for this risk analysis follows the new DOC guideline for natural hazard risk analysis on Public and Conservation Lands and Waters, adopting the advanced level of analysis at the local scale (nominally 1:5000) set out in the report: Part 3: Analysing landslide risk to point and linear features (de Vilder and Massey, in press).

The main conclusions of the report are:

1. Landslides have and will continue to occur from the slopes in the study area. The main landslide hazard types affecting the representative routes along the beach to visit the gannet colonies are rockfalls and debris avalanches.
2. The risk from other natural hazards present along the beach, such as tsunami and drowning, has not been quantified. The risk from these hazards would be in addition to the risk from landslides.
3. The LPR varies along the length of each route as a function of the proximity of the route to the steep slopes (cliffs). The LPR along the Spring low tide route is marginally less than the LPR along the Neap low tide route. This is because the Spring tide route is further away from the steep slopes.

4. The main contributor to the risk is from non-earthquake-induced landslides. There is about an order of magnitude difference in the risks calculated for earthquake- and non-earthquake-induced landslides.
5. The risk levels per trip associated with visiting the gannets are slightly less than those from eruption hazards when walking the Tongariro Alpine Crossing without risk control measures, such as monitoring volcanic unrest. They are higher than those from visiting Fox Glacier and Franz Josef Glacier with or without risk control measures in place, where the control measures mainly comprise closing the valleys during heavy rain, which is when landslides can occur.
6. The risk levels per trip are at the upper end of the range of the risk levels associated with other popular New Zealand tourist activities and are higher than those associated with several other 'adventure' activities, such as visiting the glaciers, rafting and jet boating.
7. The fatality risk per day for visiting the gannets is high compared to the fatality risk per day from some other popular New Zealand sport and leisure activities.
8. The people at greatest risk from landslides in the study area are GBA staff, as they spend the most time in the hazard areas. GBA staff (the main operator) is the person most exposed to landslide hazards and therefore the person at highest risk.
9. The fatality risk per year (AIFR) to GBA staff is high when compared to other mortality data, but, for DOC staff, it is lower than the risk those staff at Fox and Franz Josef are exposed to with the risk management controls put in place by DOC in the glacier valleys.
10. The risk expressed as total fatalities per employee per year for GBA staff is slightly higher than those in the forestry and mining industries, two of New Zealand's high-risk industries. However, not many GBA employees (2–3) are exposed to these levels of risk.
11. The societal risk from visiting the gannets is slightly lower than the risk from people visiting the Fox and Franz Josef glaciers and the risk from past New Zealand earthquake, storm and flood events that have killed multiple people.
12. While the contribution to the AIFR and the risk per trip from earthquake-induced landslides is lower than that from non-earthquake-induced landslides, earthquakes could trigger lots of landslides at the same time. Therefore, societal risk is driven by earthquake-induced landslides, as these could potentially kill many people if an earthquake were to occur when a large group of GBA passengers were on the beach.
13. One of the largest uncertainties in the risk estimates is the frequency (number) and magnitude (volume) of non-earthquake-induced landslides. Other potentially significant uncertainties are: a) the time spent walking or driving along the beach by the different users, b) the route a person walks along the beach between the Neap and Spring tides and c) the vulnerability of a person walking or driving along the beach.
14. These uncertainties combine to give a total factor of difference of between 6 and 8, which is between half to an order of magnitude difference in the uncertainty on the risk estimates, in either direction.
15. Although the risk model performs well for walkers, for GBA passengers, the model over-predicts the number of people likely to be hit and killed at those risk levels calculated adopting the upper estimates. This is thought to be because the upper estimates of non-earthquake-induced landslide frequencies are possibly too high.

16. The risk (not hazard) from landslides could be controlled by:

- understanding, for non-earthquake-induced landslides, when they are most likely to happen and not going on the beach at those times of the year;
- warning staff and visitors that the hazard is present;
- informing staff and visitors of the measures in place to make it safer; and
- recommending that they take advantage of the local knowledge, and reduced exposure time, by going on an organised tour.



## 1.0 INTRODUCTION

This report has been prepared by the Institute of Geological & Nuclear Sciences Limited (GNS Science) in response to a request from Craig Thew, Group Manager: Asset Management for Hastings District Council (HDC), and Reg Kemper, Director Operations Lower North Island, Department of Conservation (DOC), for a quantified landslide risk analysis for the Clifton Beach to Cape Kidnappers study area in Hawke's Bay. Walking, driving or taking a tractor from Clifton to visit the plateau gannet colonies is a popular tourist activity. The DOC reserve containing the gannet colonies is about a 4–5-hour return trip along the beach. The journey from Clifton along the beach to and from the colony is subject to periodic landslides and rockfall and can only be attempted around low tide, as high tides and big seas block the beach access at certain places, making it impossible (or very hazardous) to get around the coastline. On the 23<sup>rd</sup> of January 2019, at approximately 2.30 pm, a large landslide occurred from the coastal cliffs of Cape Kidnappers (Figure 1.1). The landslide avalanche injured two tourists, one critically, who were walking along the beach below the cliff at the time. Due to the perceived landslide risk, the DOC access track from the beach to the gannet reserve has since been closed, and the commercial tourist operation using this access route is currently on hold. The study area is shown in Figure 1.2.

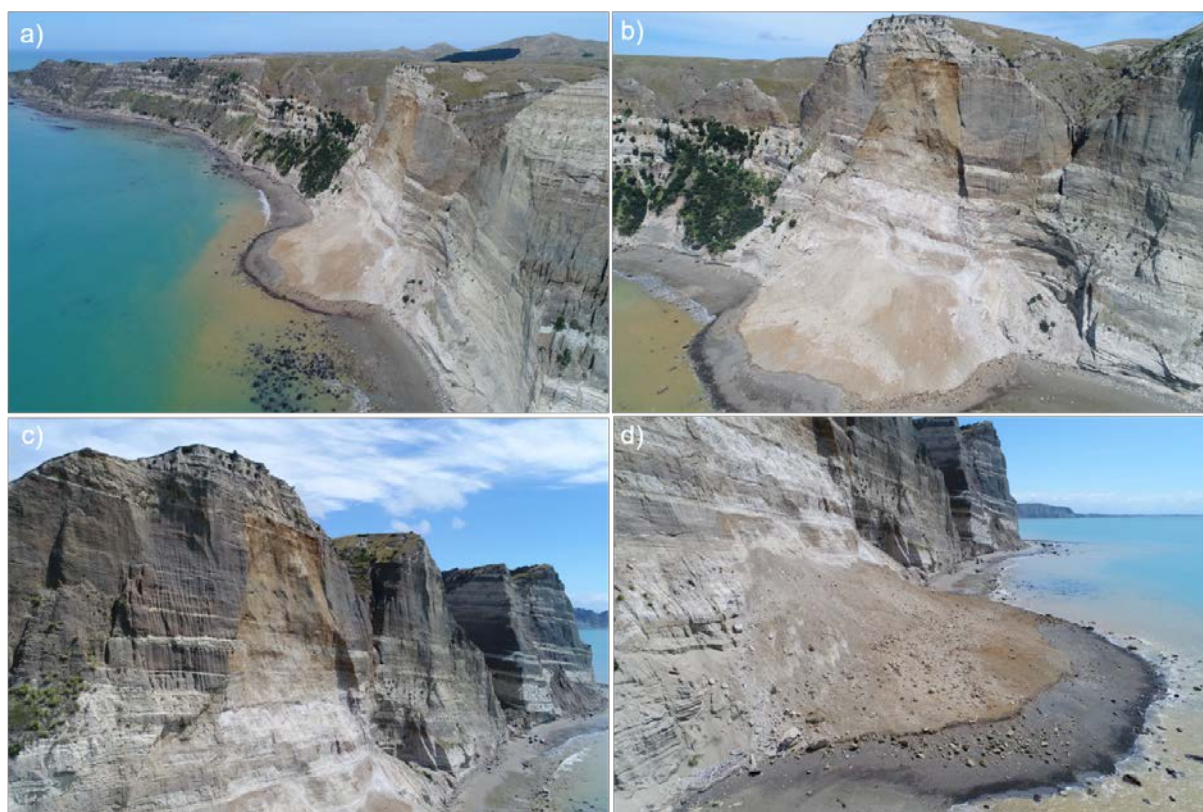
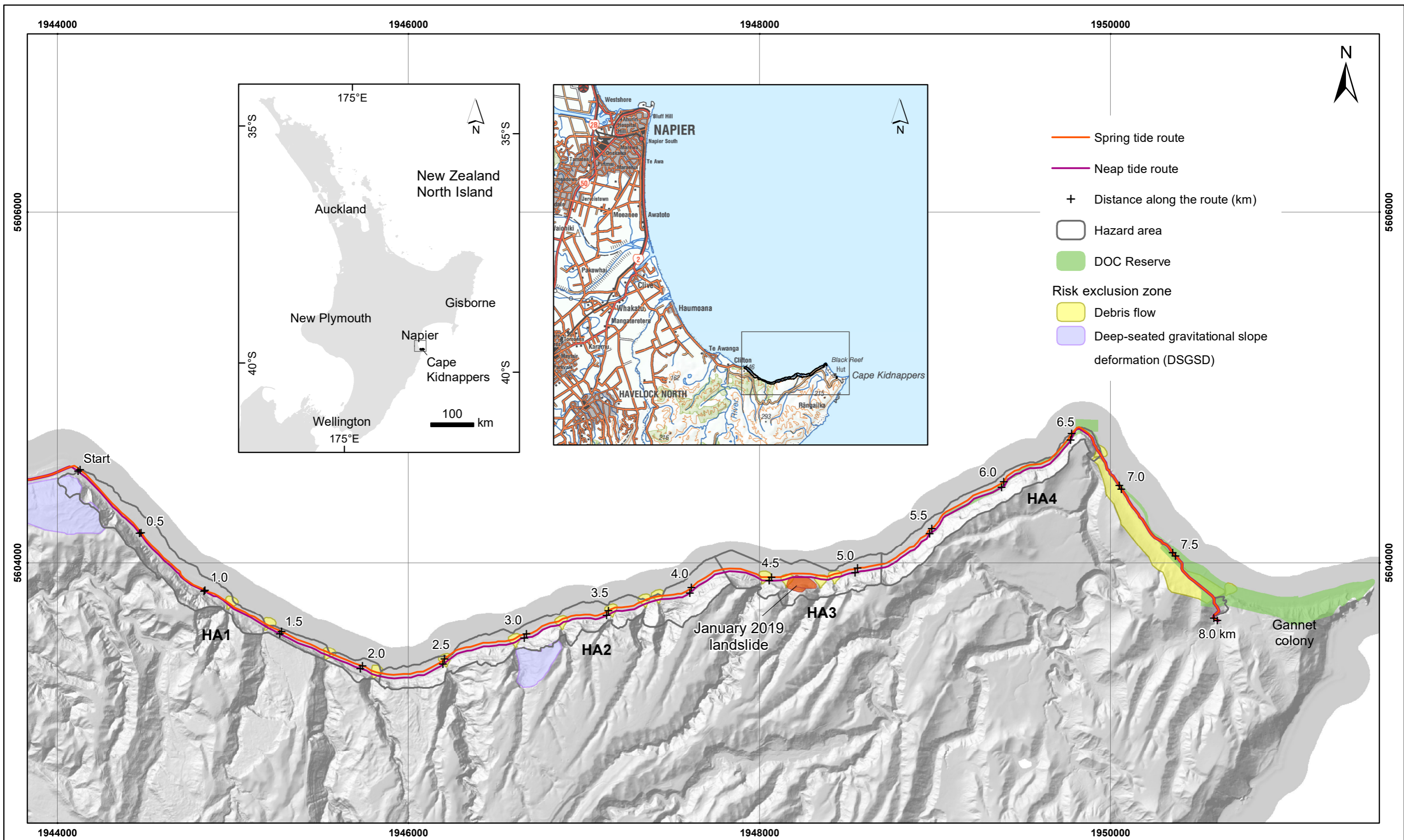


Figure 1.1 Photographs of the Cape Kidnappers debris avalanche, captured via drone on the 25/01/2019. a) and b) Images of the debris avalanche, c) source area of the debris avalanche and d) deposit of the debris avalanche. Images are taken from de Vilder et al. (2019).

This page left intentionally blank.



SCALE BAR:			<b>LOCATION MAP</b>	<b>FIGURE 1.2</b>	
EXPLANATION:  Background shade model derived from a LiDAR based Digital Elevation Model (1m ground resolution) which was resampled to 3 m for the analysis	DRW: BL  CHK: CM, SDV			<b>Cape Kidnappers</b>	<b>FINAL</b>
PROJECTION: New Zealand Transverse Mercator 2000				REPORT: CR2020/28	DATE: May 2020

This page left intentionally blank.

In 2019, Stantec Ltd were commissioned by HDC and DOC to carry out an assessment of the landslide hazards and risk within the study area. GNS Science reviewed this report in December 2019. In January 2020, HDC and DOC approached GNS Science to revise the analysis of the landslide risk part of the work carried out by Stantec. Stantec revised their initial hazard and risk analysis report to contain only an assessment of the landslide hazards (Stantec 2020). This GNS Science report presents the results from the quantified landslide risk analysis carried out by GNS Science for the study area shown in Figure 1.2. This analysis has quantified the landslide hazards identified in Stantec (2020); the life-safety risks to walkers, GBA passengers and DOC, HDC and GBA staff within the study area; and the factors that contribute to risk, which can be used by HDC and DOC to inform their risk management planning. The results of this risk analysis have been independently reviewed by T Taig (TTAC Ltd).

The method used for this risk analysis follows the new DOC guideline for natural hazard risk analysis on Public and Conservation Lands and Waters, adopting the advanced level of analysis at the local scale (nominally 1:5000) set out in Part 3: Analysing landslide risk to point and linear features (de Vilder and Massey, in press).

## 1.1 Project Objectives

The objectives of this study are: 1) to inform HDC and DOC of the spatial variation of risk and the factors that most contribute to landslide risk in the study area; and 2) to use the information from the landslide risk analysis to provide advice that will help HDC and DOC manage visitor and staff safety so that the landslide risk is as low as reasonably practicable (ALARP).

GNS Science has carried out a regional-scale, quantified landslide risk assessment for the representative routes along Clifton Beach, as shown in the study area in Figure 1.2, triggered by earthquake- and non-earthquake-related events. The quantitative landslide risk assessment is based on risk-estimation methods that follow appropriate parts of the Australian Geomechanics Society framework for landslide risk management (Australian Geomechanics Society 2007). It provides risk estimates suitable for use under SA/SNZ ISO1000: 2009.

The risk assessment quantifies the risk – in this case, the loss of life – to visitors and to DOC and Gannet Beach Adventures (GBA) staff from landslide hazards in the study area. The landslide risk metrics adopted for this study are described in Section 2; these are:

1. the local personal risk,
2. the annual individual fatality risk,
3. the individual risk for visitors (risk per trip and per multiple trips), and
4. the risk of major multi-fatality accidents ('societal risk').

The uncertainties relating to the parameters used in the risk assessment, and their impact on the risk estimates, have also been quantified to give some indication of the accuracy of the risk assessment results. This work does not include any assessment of the river-related (fluvial) sedimentation hazards (i.e. debris flows) associated with the streams that exit onto the beach (Figure 1.1) or the risk from other hazards, such as tsunami and drowning.

The project comprises the following tasks, which were carried out for the study area shown in Figure 1.2:

- Review of the hazard assessment contained in Stantec (2020). The risk calculations contained in this report rely on the hazard information contained in Stantec (2020). No re-assessment of the hazard information presented in their report has been carried out by GNS Science.
- Completion of a quantified risk analysis for the study area. This task takes the information from the hazard assessment (Stantec 2020) and uses it to estimate the landslide risk to people at different locations along the beach. The risk analysis also assesses the uncertainties associated with the information used in the risk analysis and the impact such uncertainties may have on the risk estimates.
- Field validation of the hazard assessment and risk analysis results, as listed above.

## 1.2 Report Structure

The report has been structured into six sections:

- Section 1: Introduction and background to this report.
- Section 2: Site descriptions.
  - Geology and geomorphology.
  - Historical and recent landslides.
- Section 3: Risk metrics and methodology.
  - Explanation and calculation of risk metrics.
- Section 4: Risk analysis results.
  - Sensitivity of the risk to key uncertainties.
  - Explanation of key risk drivers.
- Section 5: Risk in context.
  - Visitors risk.
  - DOC and GBA staff risk.
  - Other risks in New Zealand.
  - Societal risk.
- Section 6: Risk management.
  - Warning and information.

## 1.3 Personnel

This report has been prepared by Chris Massey, Saskia de Vilder, Bilijana Lukovic and Garth Archibald (GNS Science). The risk calculations have been independently reviewed by Tony Taig (TTAC Ltd, a UK-based risk consultancy). Members of the team visited the study areas on 5–6 March 2020 to carry out field surveys.

## 2.0 SITE DESCRIPTION

### 2.1 Setting

The study area extends from the end of Clifton Road (labelled 'Start' in Figure 1.2) to about 1 km west of the gannet colony (labelled 'the 8.0 km' in Figure 1.2). Visitors who want to visit the gannet colony either walk along the beach from the end of Clifton Road, or take a guided tour on a tractor operated by GBA. The tractor drives about 7.5 km along the beach, where visitors alight and travel on foot for the last ~1 km to the gannet colony viewing area. The walk takes about 5 hours (return trip) and the tour about 4 hours (return trip). The route can only be walked at low tide, which is therefore an assumption we have made for the representative routes used in the risk model.

The route along the beach is spectacular as it traverses beneath steep cliffs, some being >100 m in height (Figure 2.1). More information about the gannets and GBA can be found on the following websites:

- <https://www.DOC.govt.nz/parks-and-recreation/places-to-go/hawkes-bay/places/cape-kidnappers-gannet-reserve/>
- <https://www.gannets.com/>

Visitors who do not want to take the walk along the beach can take a guided tour that accesses the gannet colony via a private road belonging to the Cape Kidnappers station. Details can be found here:

- <https://gannetsafaris.co.nz/>

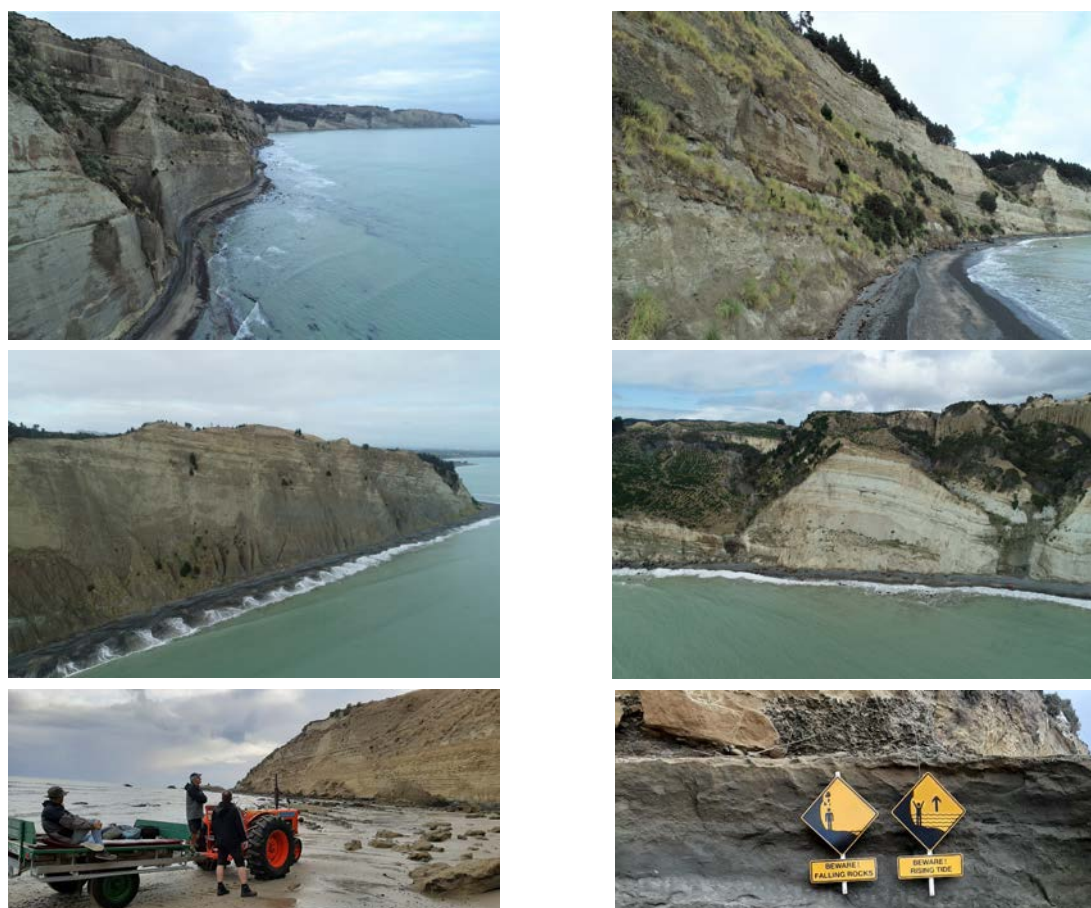


Figure 2.1 Photographs of the study area, taken 5–6 March 2020.

## 2.2 Topographic Mapping

For this analysis, the topographic data used was derived from a LiDAR survey carried out by New Zealand Aerial Surveys. The data was captured between 25 November 2011 and 25 April 2012 using New Zealand Aerial Mapping's Optech ALTM 3100EA LiDAR system and Trimble AIC medium format digital camera. This data was used to generate a digital elevation model (DEM) of the ground surface at 1 m by 1 m resolution. For this risk analysis, the DEM was resampled to a ground resolution of 3 m by 3 m. This 3 m by 3 m DEM of the study area has been used as the basis for the numerical simulations of landslide runout and for the landslide risk analysis modelling.

## 2.3 Geology and Geomorphology

The geology and geomorphology of the study area is described in Stantec (2020). In summary, the main cliffs are formed of four dominant materials, youngest to oldest:

- Modern beach and landslide deposits at the base of the cliffs.
- Quaternary deposits: comprising beach deposits of sand, silt, mud, gravel; commonly containing loess, palaeosols and tephra, with some landslide colluvium. These deposits are mapped on top of the cliffs and represent old marine benches.
- Kidnappers Group: comprising Lower-Pleistocene-age fossiliferous sandstone overlain by conglomerate, sandstone, carbonaceous mudstone, tephra and ignimbrite. These form most of the cliffs in the study area.
- Pakaututu Formation: comprising Pliocene-age massive calcareous and fossiliferous mudstone with minor interbedded sandstone at Cape Kidnappers.

The bedding within the cliffs is shown on the published geological map to dip towards the northwest at 8° to 15°. Due to the east-west strike of the cliff, this equates to obliquely out of slope (Stantec 2020). The New Zealand Active Faults Database shows that two active faults are present in the study area; these, and other faults, can be seen exposed in the cliffs, where they offset bedding.

The geomorphology of the study area is dominated by the steep (50° to 90°) and high (20 to >100 m) coastal cliffs. In parts, the tops of the cliffs are relatively flat, representing relict, and now uplifted, marine benches. In many locations, these have been incised by streams to create several mainly first and second order drainage catchments. Several of the streams within these catchments exit onto the beach where, in some cases, they have deposited small debris fans. The cliffs and drainage line are being actively eroded by the sea.

Additional information can be found at: <https://www.geotrips.org.nz/trip.html?id=182>.

## 2.4 Hazard Areas

The geological and geomorphological characteristics were used by Stantec (2020) to define a series of domains that had similar physiographic characteristics, such as slope height, angle and geology. For this risk analysis, we have grouped the domains into four hazard areas (HA1–4 in Figure 1.2). These are used in the risk analysis to estimate the numbers of earthquake- and non-earthquake-induced landslides that could source from them. The up-slope limit of the hazard areas are defined by the cliff crest. The downslope, seaward extents of the hazard areas are defined by the distance that debris from the largest simulated landslide might travel into the sea. The way this is defined is discussed in Section 3.2.3. Therefore, the seaward



hazard area boundaries do not represent the edge of the land and start of the sea, because the level of the sea, and how much beach is exposed at a given time of day, varies greatly.

## 2.5 Previous Landslides in the Area

Many documented landslides have occurred from the cliffs within the study areas, and the debris from such hazards has made it onto the beach and, in some cases, hit and injured people.

These landslides can be broadly classified into rockfall, debris avalanche and debris flow events (Figure 2.2). The locations of these different landslide hazards within the study area have been mapped and described by Stantec (2020), are shown on Figure 1.2 and are summarised below.

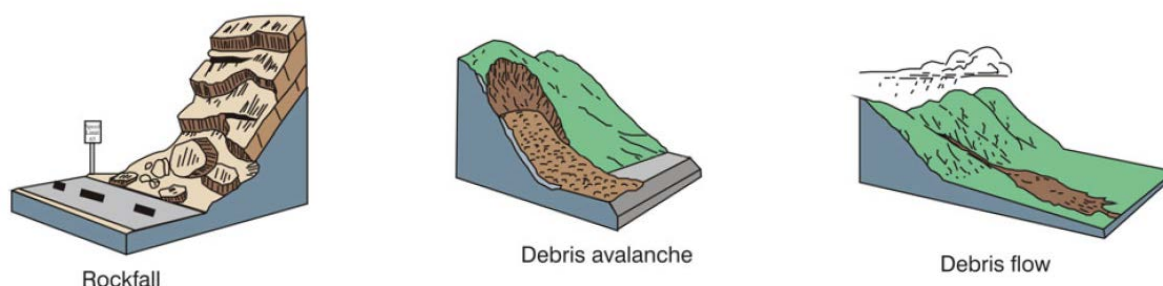


Figure 2.2 Cartoons of the three main type of landslides found in the study area.

### 2.5.1 Rockfall

Rockfall, as described by Hungr et al. (2014), comprises the detachment, falling, rolling and bouncing of rock blocks. They may occur singly or in clusters, but there is little dynamic interaction between the moving blocks, which interact mainly with the substrate (path). Fragmentation of the moving block can occur during movement and/or on impact with objects along the path. The detachment of rock blocks from cliffs occurs by a range of mechanisms, such as sliding and toppling, but they are often limited in scale (size) by the spacing and orientation of the discontinuities (fractures, joints, etc.) that define the blocks in the source area.

Rockfalls have occurred from many of the slopes in the study area and are documented by Stantec (2020) as being one of the dominant landslide hazards along the route.

### 2.5.2 Debris Slides and Avalanches

Debris avalanches are a type of landslide comprising many blocks falling simultaneously from a slope. The avalanching mass starts by sliding, toppling or falling before descending the slope rapidly ( $>5$  m/sec) (following Hungr et al. 2014) by any combination of falling, bouncing, rolling and sliding. Debris avalanches can comprise a few individual blocks of rock and other debris or a mass of many tens of thousands or millions of blocks and debris, depending on the volume of the landslide source area. In a debris avalanche the blocks interact with one another, which can lead to the debris travelling considerable distance down a slope and out to sea. A debris avalanche usually initiates as a debris slide, which is defined by Hungr et al. (2014) as a:

*“sliding of a mass of granular material on a shallow, planar surface parallel with the ground. Usually, the sliding mass is a veneer of colluvium, weathered soil, or pyroclastic deposits sliding over a stronger substrate. Many debris slides become flow-like after moving a short distance and transform into extremely rapid debris avalanches.”*

Debris slides are not analysed separately in this project, and this definition is only provided to describe the initial stage of a debris avalanche.

Debris slides and avalanches have occurred from many of the slopes in the study area and, along with rockfalls, are documented by Stantec (2020) as being the dominant landslide hazards along the route.

### 2.5.3 Exclusions

The results from this project exclude debris inundation from debris flows sourcing from the streams and gullies and where they flow out onto the beach.

Debris flows are defined by Hungr et al. (2014) as a

*“very rapid to extremely rapid surging flow of saturated debris in a steep channel. Strong entrainment of material and water from the flow path can occur along the runout path. Debris flows often occur simultaneously with floods. The debris flow may be initiated by a debris slide, debris avalanche or rockfall from a steep bank, or by spontaneous instability of the steep stream bed.”*

Following Hungr et al. (2014), a debris flow refers exclusively to a channelised landslide, whereas a landslide consisting of flowing debris on an open slope is referred to as a debris avalanche. It is possible that debris flows become debris avalanches if the channel they flow down becomes less confined and, conversely, debris avalanches may become debris flows if the debris enters a channel. Where the erosion rate outpaces the depositional environment (e.g. river or coastal erosion rate greater than deposition rate), the landslide deposits from multiple debris flows form debris fans. Within the study area, debris flows are confined to where the gullies/streams flow onto the beach. In some of these gullies above the high tide zone, debris fans can be observed. Fans are generated when confined watercourses (e.g. gullies, creeks, rivers) become wider and the water course becomes less confined, e.g. when watercourses enter valleys, plains or lakes – in this case, the beach. The resulting decrease in flow velocity promotes sediment deposition. Along the beach, such deposits are relatively shallow and limited in extent, being confined by the steep slopes forming the flanks of the gullies.

It also excludes ground movement by slow-moving landslides such as rotational sliding (slumps), earthflows and deep-seated gravitational slope deformation (DSGSD). While DSGSD landslide types represent a lower life safety risk, as they tend to move slowly, they can still result in significant infrastructure damage (e.g. Massey et al. 2013). Slow-moving landslides can, under certain conditions, evolve into or be associated with rapid landslides (e.g. Reid et al. 2003; Loew et al. 2017), in which case, if they meet the topographic criteria defined in Section 3.2.2, they will be covered by the analyses conducted in this project. What is not covered by this project is the slow displacement component of such landslides and other erosional processes, e.g. the high rates of coastal erosion driven by the sea. These risk exclusion zones are shown on Figure 1.2.

The risk analysis results from this project exclude those from hazards associated with inundation from water, including tsunami and sediment and/or debris resulting from fluvial flooding.

## 2.5.4 Landslide Data for the Study Area

The main sources of landslide data for the study have been compiled by Stantec (2020); these are:

1. Historical records and anecdotal information from locals and the GBA operator. The main ones are listed below:
  - a. January 2019 – large debris avalanche; two walkers (tourists) hit, one of which severely injured.
  - b. September 2018 – large landslide, inundated part of the lower gannet colony.
  - c. March 1988 – large debris avalanche, two walkers (tourists) hit. Both suffered severe lower body injuries.
  - d. February 1973 – large debris avalanche, three GBA workers were present at the time clearing debris from a previous landslide. One was partially buried by debris and injured, the other two ran into the sea. The GBA tractor and trailer were damaged.
  - e. GBA records of landslides.
  - f. Media reports of landslides.
2. Historical aerial photographs and Google Earth imagery, 1948–2018.
3. Survey information from:
  - a. Comparing the differences between DEMs generated from airborne LiDAR surveys carried out in 2003 and 2011–2012.
  - b. Comparing the differences between the 2011–2012 LiDAR DEM and the digital surface model (DSM) generated from the March to April 2019 UAV survey.
  - c. Comparing the differences between the March to April 2019 DSM and the DSM generated from a second UAV survey carried out between July and September 2019 (four- to five-month period over winter).

The media accounts of those landslides that have hit and injured people indicate that, in all three instances, the people appear to have heard something and took evasive action by running into the sea, away from the cliffs and the landslide debris. In all cases, the people hit by debris appear to have sustained injuries to their lower body only.

## 2.6 Visitor and DOC, HDC and GBA Staff Exposure

Details of the visitor and DOC, HDC and GBA staff exposure data relating to route within the study area was compiled by Stantec (2020). On average, there are currently about >8000 and up to 13,000 trips per year made along the coastal route to see the gannet colonies, based on GBA and DOC records for the period 2015–2019 but excluding the 2019–2020 season as the beach route was closed. Approximately 1200 to 2000 trips per year are made by independent walkers and 7000 to 11,000 by tourists taking the GBA tour. There is a DOC track counter located on the route in the DOC reserve, but records for this counter are unreliable and incomplete. The number of visitors per season appears to have increased in the last two seasons since DOC started to market the walk as a “great walk”. These numbers may reduce in the future.

## 2.7 Data Used in this Study

The main data used in this landslide risk assessment are listed in Table 2.1.

Table 2.1 Summary of data types, sources and uses within this study.

Data	Description	Source	Date	Where Used in Analysis
Light Detecting and Ranging (LiDAR), DEMs	DEM derived from LiDAR survey sampled to 1 m ground resolution and subsequently resampled to a 3 m ground resolution.	New Zealand Aerial Surveys	2011–2012	Used as base topography for the rockfall (RAMMS) and landslide runout modelling and the risk modelling.
Stantec (2020). Hazard assessment report	Recent and historical accounts of landslides and their estimated date of occurrence and size.	Media reports, aerial photographs, local knowledge and UAV survey data	2020	Used to estimate the volume and frequency of landslides from the cliffs in the study area.
	Visitor numbers for both walkers and people paying to take the GBA tours.	Interviews with the GBA operator, DOC and HDC staff	2020	Used to assess visitor exposure and total number of visitors to the study area per year.
	Numbers of people hit by debris and what they did at the time, and the type of injuries sustained.	Media reports and interviews with the GBA operator	2020	Used in the vulnerability part of the risk analysis.
Olsen et al. (2019). Port Hills, Christchurch landslide hazard assessments	The size and frequency of landslides that fell from the coastal cliffs in the Port Hills during the 2010/11 Canterbury Earthquake Sequence.	Terrestrial laser scan surveys carried out by GNS Science	2011–2016	Used to estimate the number and volume of landslides that could be generated at different levels of earthquake ground shaking – peak ground acceleration.
Brideau et al. (In press). Empirical landslide runout modelling	Empirical relationships between landslide volume and runout for different types of landslide.	GNS Science	2020	Used to forecast the distance that different volumes of landslide will travel from the cliff's downslope onto the beach.
Stirling et al. (2012). The New Zealand National Seismic Hazard Model	The annual exceedance probability of different levels of peak ground acceleration.	GNS Science	2016	Used to estimate the annual frequency of different levels of earthquake shaking (peak ground acceleration).

### 3.0 RISK METRICS AND METHODOLOGY

This report estimates the life safety risk from landslide hazards to visitors and DOC and GBA staff on the beach in the study area. A hazard is a dangerous (or adverse) future event with the potential to cause harm. Within the study area, the dangerous future events of concern are landslides falling from the steep coastal cliffs onto visitors and DOC and GBA staff. While there are other hazards within the study area, these are not discussed in this report.

This report estimates the life risk from rockfalls and debris avalanches (two types of landslide) to visitors and DOC and GBA staff on the routes shown in the study area (Figure 1.2). Two 'risk scenarios' were adopted using different estimates of the variables used in the risk analysis; these were:

1. Lower scenario – adopting the lower estimates for the landslide production rates and exposure data.
2. Upper scenario – adopting the upper estimates for the landslide production rates and upper estimates for the exposure data.

The sensitivity of the risk model to changes in the other variables used, such as the distance landslide debris may travel down a slope and the vulnerability of a person, was also carried out; these are discussed in Section 4.5.

#### 3.1 Risk Metrics

To assist in comparing the landslide risk within the study areas with that of other activities, we have calculated risk parameters as follows:

1. The local personal risk (LPR), which is a widely used risk metric in the Netherlands and represents the annual probability of death for a theoretical imaginary person present at a particular location for 100% of the time (24 hours a day and 365 days of the year). It is a useful metric to visualise the spatial distribution of risk in the study area and can be used to help plan and/or re-align tracks and roads.
2. The annual individual fatality risk (AIFR): This is expressed in terms of the fatality risk experienced by an individual (probability of death) over one full year of working in the study area. The risk is calculated for the DOC and GBA member of staff most at risk, which is the person that spends the most time in the study area per year. This risk can then be compared with the risk experienced in a year at work in other New Zealand workplaces.
3. Individual risk for visitors: This is expressed in terms of the fatality risk experienced by an individual (probability of death) resulting from one return trip along routes within the study area. In most cases, a person might only visit the site once in their lifetime. The risk is calculated separately for a visitor walking or taking a tour along the routes within the study area. This risk can then be compared with the risk of participating in other leisure, travel or tourism activities in New Zealand.

4. Risk of major accidents (societal risk): There are several different metrics available of the aggregate risk impact on a community (typically a country) of a specified event (e.g. landslide of a given magnitude) or a category of events (e.g. landslides triggered by an earthquake). One widely used measure, often termed 'Societal' or 'Group' risk, is defined as the relationship between the frequency of occurrence of a specified hazard and the number of people in a given population being killed if the hazard were to occur (Lee and Jones 2014). A key issue within the study area is that a large landslide, or several smaller landslides triggered by a single event (such as an earthquake), could cause multiple fatalities in a single event. Societal risk, in terms of the frequency of an accident killing  $N$  or more people in a single event (a so-called 'f/N curve'), is used in this study to show the potential for multiple fatality events. Curves are calculated for visitors, whose numbers dominate greatly over those of staff for higher consequence events. This risk can then be compared with the known frequency of other major (multiple death) incidents in New Zealand.

### 3.2 Assessment Methodology

The landslide risk assessment follows appropriate parts of the Australian Geomechanics Society framework for landslide risk management (Australian Geomechanics Society 2007). Using the Australian Geomechanics Society guidelines for landslide risk management, we calculated the annual probability of death (life risk) of an individual,  $R_{(D)}$ , from:

$$R_{(D)} = P_{(H)} \times P_{(S:H)} \times P_{(T:S)} \times V_{(D:T)} \quad \text{Equation 3.1}$$

where:

- $R_{(D)}$  is the annual risk (probability) of loss of life (death) of a person from landslides;
- $P_{(H)}$  is the annual probability of the initiating event;
- $P_{(S:H)}$  is the probability that a person, if present, is in the path of the debris at a given location;
- $P_{(T:S)}$  is the probability that a person is present at that location when the debris reaches or passes through it; and
- $V_{(D:T)}$  is the vulnerability, or probability, that a person is killed if present and in the path of debris.

The risk assessment method, as outlined in the sections below, comprises the following steps:

1. Consider the possible range of triggering events in terms of a set (bands) of earthquake triggers and a set of non-earthquake triggers (e.g. rain, time, etc.).
2. Consider the locations where landslides are most likely to source from in the study area.
3. Define the areas that could be inundated by landslides in the study area and divide these into a series of 3 m by 3 m grid cells.

#### For Earthquake Triggers:

4. Choose a small set of representative events (earthquake bands) spanning the range of event severity, from the lowest to the highest.
5. For each representative event, estimate:
  - a. The number of landslides of a given volume class produced in that event ( $P_{(H)}$ ).
  - b. The probability of debris reaching or passing a given grid cell from each landslide within each volume class, and the probability of a person at that location being in the path of debris from a landslide ( $P_{(S:H)}$ ).

- c. The probability of a person being in the path of debris and killed, if present, for each landslide class within each earthquake band. This is done for each landslide volume class by multiplying  $P_{(S:H)}$  by the probability that a person is killed, if present, and in the path of one or more landslides ( $V_{(D:T)}$ ). These values are calculated for the cliff toe and the estimated area of slope inundated by a landslide of a given volume class – for debris avalanches, this is the maximum estimated distance that debris from a landslide of a given volume will travel out from the cliff toe, referred to as the F-angle line; for rockfalls, this is the maximum simulated distance that a rockfall may travel out from the cliff toe, referred to as the rockfall limit line. Enter these values into a GIS programme and interpolate between them to produce contours of equal probability of death (being in the path of debris and killed) across the area.
- d. The combined probability of a person being in the path of debris and killed, if present, for all landslide classes triggered within each earthquake band, ensuring that a person can only be killed once.
- e. The annual frequency of the representative earthquake event, taken from the National Seismic Hazard Model for New Zealand.
- f. The probability that a person is present (walking, on a tour or working) in a given cell as the debris moves through it ( $P_{(T:S)}$ ).
- g. The LPR, calculated by multiplying 5 (d)–(f), assuming a person is present in each grid cell in the debris inundation areas for 24 hours a day and 365 days of the year, using the GIS programme to create a grid of LPR for each earthquake event.

#### For Non-Earthquake Triggers:

6. Choose a small set of landslide volumes that span the range that could occur and, for each representative landslide volume class, calculate:
  - a. the annual frequency of the landslide occurring ( $P_{(H)}$ );
  - b. the probability of debris reaching or passing a given grid cell, and the probability of a person at that location being in the path of debris ( $P_{(S:H)}$ );
  - c. the probability that a person is present (on a trip) in a given cell as the debris moves through it ( $P_{(T:S)}$ );
  - d. the probability that a person is killed if present and in the path of debris ( $V_{(D:T)}$ );
  - e. multiply 6 (a)–(d) to estimate the LPR contributed by each landslide volume class, assuming a person is present in each grid cell in the debris inundation areas for 24 hours a day and 365 days of the year; and
  - f. enter the LPR values for the cliff toe and estimated runout distance (F-angle) into a GIS programme and interpolate between the risk values to produce contours of equal LPR across the area.

#### For All Triggers:

7. Sum the risks from all events 5 (g) and 6 (f) to estimate the combined LPR due to earthquake and non-earthquake-induced landslides.
8. Multiply the LPR by the fraction of a year visitors and DOC and GBA staff spend in a grid cell while walking, taking a tour and/or working to sum the contribution to the AIFR and risk per trip from each grid-cell location visited along the route.

9. Estimate the number of people that could be killed by landslides triggered by each of the representative events (the societal risk) – for earthquakes, this is done for each earthquake band, and for non-earthquake induced landslides, this is done for each landslide volume class – as a function of the number of people present in the inundation areas at any one time.

The following sections describe the calculation of the annual frequency of a landslide occurring for both earthquake and non-earthquake triggers, the assessment of the source areas for the different landslide volumes in order to understand where along the cliffs and steep slopes behind the beach such landslides could occur, and landslide and rockfall runout simulations are outlined and described in order to understand how far debris from rockfalls and landslides of a given volume travel out towards and/or into the sea from the cliff toe.

The subsequent sections include an assessment of the probability of a person at that location being in the path of a rockfall or landslide and the probability that a person is killed if present and in the path of a rockfall or landslide. The data are then used to calculate the LPR, AIFR, risk per trip and societal risk based on the exposure data for visitors and DOC and GBA staff.

### **3.2.1 Probability of the Initiating Event**

#### **3.2.1.1 Earthquake Triggers**

The frequency (number) and volume of landslides likely to be generated at different magnitudes of ground shaking intensity were determined from the Rockfall Activity Rate System (RoARS) described by Olsen et al. (2019). The RoARS provides an indication/forecast of the volume of rock that could fall from a slope (of a given height, angle and surface area) at different levels of earthquake shaking. These forecasts are derived from an empirical relationship between the volumes of rock that fell from selected Port Hills rock slopes during the 2010/11 Canterbury Earthquake Sequence (CES). In this report, we use a modified version of the RoARS, which uses only the slope height and peak ground acceleration (PGA) to derive landslide volume estimates; this is because the slope angles within the hazard areas are all similar. The RoARS is underpinned by the assumption that, if a slope is strongly shaken by an earthquake, the volume of debris that falls from it is a function of the magnitude of the shaking (e.g. PGA) and the geometry of the slope (e.g. slope height) and angle.

The total volumes of debris estimated from the RoARS for the slopes in each hazard area (Figure 1.2) were then distributed across the different volume classes of landslide that could occur from them. This determined the number of landslides of a given volume that could occur at different levels of earthquake shaking. To do this, we used two approaches:

1. the frequency (number) and volume distribution of landslides derived from the UAV surveys and historical data compiled in the Stantec (2020) report; and
2. the frequency (number) and volume distribution of landslides derived in similar materials to those at Cape Kidnappers that were triggered by the 16 November 2016 Kaikōura earthquake (Massey et al. 2020, In press).

The CES and Kaikōura earthquakes occurred in areas where the topography, bedrock geology and earthquake mechanisms are somewhat different to those in the study area. Therefore, applying relationships based on these data sets to those cliffs in the study area does add a level of uncertainty into the risk analysis, which is difficult to quantify. However, no site-specific data is available for the study area, although there are anecdotal reports of dust clouds (assumed to be from landslides) visible from these cliffs during the 1931 Hawke's Bay



M7.8 earthquake, also known as the Napier earthquake, which occurred in New Zealand at 10:47 am on 3 February, killing 256 people.

The assessment was carried out in four stages:

- Stage 1: Estimate the surface area of all potential debris avalanche and rockfall sources within each hazard area (Figure 1.2).
- Stage 2: Using the RoARS, estimate the total volume of debris that could fall from the cliffs in the study area at different levels of earthquake shaking, adopting four different bands of increasing PGA.
- Stage 3: Estimate the number of landslides of a given volume (adopting eight classes of increasing landslide volume) that could be triggered by each representative event PGA for each earthquake band. Then distribute these volumes (from stage 2) using the landslide frequency and volume distributions derived from: i) the Stantec (2020) landslide distribution for the study area and ii) the Kaikōura earthquake landslide distribution (Massey et al. 2020, In press), using only those landslides in similar materials to those within the study area.
- Stage 4: Combine estimates of the annual frequency of the representative event PGA for each earthquake band from the National Seismic Hazard Model (NSHM) for New Zealand with the relationship between landslide frequency and volume and PGA (from Stages 2 and 3). Then, using this relationship, estimate the probability of a landslide of a given volume class occurring within each study area for each PGA band considered, along with the annual frequency of the representative PGA in the band occurring.

### Potential Landslide Source Areas and Their Volumes

Potential landslide source areas were defined using the 3 m resolution LiDAR-derived DEM. For debris avalanches, any slopes  $\geq 30^\circ$  were assumed to be potential source areas, and for rockfalls, any slopes  $\geq 45^\circ$  were assumed to be potential source areas. This was done in ArcGIS to generate a series of source area polygons that could deliver rockfalls and debris avalanches onto the beach. Note that there is little difference in the source area extents between those defined using  $30^\circ$  and those using  $45^\circ$ . A slope angle of  $45^\circ$  was used for rockfalls, as they tend to only initiate from steeper slopes. The surface areas of these source polygons were then calculated in ArcGIS for each hazard area.

Although Stantec (2020) have visually identified a few potentially more unstable slopes within the study area, it is not currently possible to quantify the susceptibility of each slope to landslides using more sophisticated models, as the data required by such models does not yet exist. Over time, as more data is compiled, it will be possible to use such models to identify which slopes within the different hazard areas (Figure 1.2) are more unstable (susceptible to landslides). The results from such models could then be used to forecast numbers of landslides generated from specific slopes, rather than using the surface area of the slopes within each hazard area, which is what is currently used in this study.

For the risk assessment, we have adopted eight landslide volume bins; these were:

- $\leq 1 \text{ m}^3$
- $>1 \text{ to } 10 \text{ m}^3$
- $>10 \text{ to } 100 \text{ m}^3$
- $>100 \text{ to } 1000 \text{ m}^3$

- >1000 to 10,000 m<sup>3</sup>
- >10,000 to 25,000 m<sup>3</sup>
- >25,000 to 50,000 m<sup>3</sup>
- >50,000 to 100,000 m<sup>3</sup>.

These volume bins were based on those adopted by Stantec (2020), which we modified to also consider smaller ( $\leq 1$  m<sup>3</sup>) rockfalls and larger (>25,000 m<sup>3</sup>) debris avalanches that could potentially occur from the slopes in the study area.

A maximum volume class of 100,000 m<sup>3</sup> was assumed to represent the largest landslide that could feasibly occur within the study area, based on the slope morphology and historical records. It should be noted that each volume class represents landslide source volumes that range from the lower class to the given class. For example, the landslide volume class of 1000 m<sup>3</sup> represents landslides >100 m<sup>3</sup> and up to 1000 m<sup>3</sup>.

### Landslide Volume and Earthquake Shaking

The total volume of debris produced at different levels of PGA were derived from the RoARS (Olsen et al. 2019), which is based on a multiple linear regression analysis adopting the 'least squares' method to fit a line through the observations made from debris avalanches that occurred on cliffs in the Port Hills of Christchurch during the CES. The model relates slope height and PGA to the volume of debris per unit area of slope (vol/area m<sup>3</sup>/m<sup>2</sup>) that could fall off. It is given by the equation:

$$\frac{Vol}{area} = C_{SH} \times SH + C_{PGA} \times PGA \quad \text{Equation 3.2}$$

where *SH* is slope height in metres (adopting the lower values from each hazard area) and *PGA* is the representative peak ground acceleration (m/s/s) for each earthquake band, which was assumed to be the mid value for each band. The coefficients  $C_{SH}$  and  $C_{PGA}$  were derived from model fitting (Olsen et al. 2019) and are shown in Table 3.1. The surface area of those slopes that could generate landslides (landslide source areas), within each hazard area, were used to then estimate the total landslide volume.

The performance of the model and summary statistics are shown in Table 3.1. The estimated total volume of debris produced from the cliffs in each hazard area at different levels of shaking are shown in Table 3.2. Volumes were derived adopting the lower and 85% model fits in order to accommodate the uncertainty in the relationship.

Table 3.1 Details of the multiple linear regression model adopting the 'least squares' method to fit a line through the observations made from debris avalanches that occurred on cliffs in the Port Hills of Christchurch cliffs during the CES. The model is modified from Olsen et al. (2019).

Variables	Coefficients (Lower)	Coefficients (Upper 84%)	Standard Error
Intercept	0	N/A	N/A
Slope Height (m)	0.002	0.004	0.002
PGA Horizontal (m/s/s)	0.06	0.09	0.02

Table 3.2 Total volumes of debris generated using the RoARS model for Hazard Areas 1–4.

Hazard Area	Source Slope Surface Area (Slopes $\geq 30^\circ$ )	Model	Total Landslide Volume per Earthquake Band ( $m^3$ )			
			1 (3 m/s/s)	2 (7 m/s/s)	3 (15 m/s/s)	4 (34 m/s/s)
1	227,430	Lower	67,034	123,999	237,929	522,755
		Upper (84%)	114,575	196,718	361,005	771,722
2	277,670	Lower	82,441	151,989	291,085	638,825
		Upper (84%)	141,190	241,478	442,054	943,494
3	132,811	Lower	40,531	73,797	140,327	306,652
		Upper (84%)	69,928	117,896	213,832	453,672
4	184,329	Lower	52,546	98,715	191,052	421,897
		Upper (84%)	88,974	155,549	288,700	621,577

### Landslide Frequency and Volume

The number of landslides and their volumes that have fallen from the cliffs in the study area were taken from those listed in Stantec (2020). In addition to these landslides, Stantec provided GNS Science with the DSMs derived from their two 2019 surveys. We differenced these two DSMs to make a surface change model, from which we extracted the surface areas and volumes of change. Change volumes  $< 1.0 m^3$  were assumed to be either errors in the surveys or changes from rilling and gullyng (other types of erosion processes) and were not included in the data. Changes  $\geq 1.0 m^3$  were assumed to be landslides, although some may also have been changes caused by rilling and gullyng or errors in the DSMs caused by vegetation effects. We fitted a power law relationship to the landslide source volume and area (Figure 3.1). This was done so that we could derive a representative source surface area for each volume class of landslide.

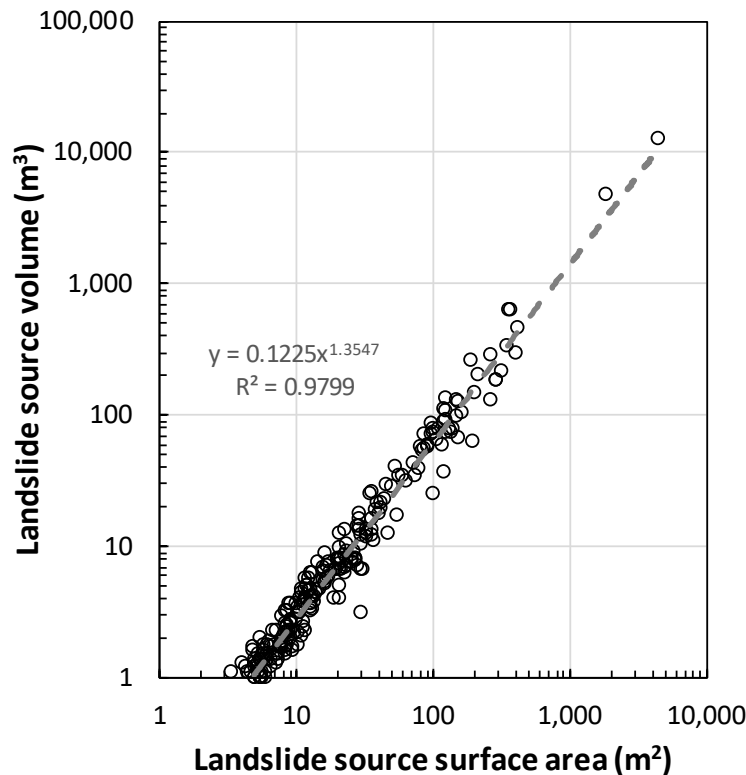


Figure 3.1 Landslide source volume and surface area for 240 landslides derived from differencing the March to April 2019 DSM from the July and September 2019 DSM. Each area of change was modelled using 3DReshaper to estimate the volumes of change. Volumes  $<1.0 \text{ m}^3$  were assumed to be either errors in the surveys or changes from rilling and gullyng (another type of erosion process) and were not included in the data. The relationship fitted to the data is a power law.

Using the volume data in Figure 3.1, we then added in the volumes of some of the larger historical landslides listed in Stantec (2020), including the volume of the January 2019 landslide from de Vilder et al. (2019). For each volume class of landslide, we summed the total volume of all landslides in the given volume class and then estimated the annual volume of landslides in each of the different volume classes (considering the time over which each landslide data set was compiled) as a proportion of the total annual landslide volume. It should be noted that we do not use these annual volumes to represent the number of landslides of a given volume occurring in the study area. This is because the landslides derived from the DSM surveys occurred between a maximum five-month period, which may not have captured: 1) many of the medium volume landslides (in the 1000 to 10,000  $\text{m}^3$  range) that occur less frequently than the survey period or 2) the variation of landslide rates over time. As a result, these rates are possibly not representative of the longer-term rates of landslides across the full volume range considered in this analysis. However, the larger landslides listed in Stantec (2020), going back to 1973, are possibly representative of those that have fallen from the cliffs over the years, as people tend to notice such large landslides.

We therefore only use the data in Table 3.3 as a way to proportion the total volume of debris generated within each earthquake band (Table 3.2) across the different volume classes of landslide. We do this to derive estimates of the number of landslides of a given volume that could be generated by the representative PGA within each band and hazard area (Appendix 1). As a check on the study area data, and to consider that the landslide frequency magnitude distributions could be different for earthquake-induced events compared to those triggered by non-earthquake events, we also use data from landslides triggered by the  $M_w 7.8$  14 November 2016, Kaikōura earthquake (Massey et al. 2020). These proportions per

landslide volume class were derived from only those landslides (N = 1230) that occurred in similar materials and slopes to those located within the study area. It should be noted that the relative proportions of landslides in the lower volume classes (1–100 m<sup>3</sup>) are unlikely to be representative, as such small landslides were not all mapped by Massey et al. (2020). We also used these values (Table 3.3) to proportion the total volume of debris generated within each earthquake band (Table 3.2) across the different volume classes of landslides (Appendix 1).

Table 3.3 Landslide source volume classes, their representative source areas and the contribution of each landslide volume class as a proportion of the total landslide volume generated per year. The representative landslide source areas are derived from the power law relationship in Figure 3.1 and the assumed source area widths are based on the square route of the source area.

Landslide Volume Class (m <sup>3</sup> )	Representative Landslide Source Surface Area (m <sup>2</sup> )	Representative Landslide Source Area Width (m)	Volume per Year (m <sup>3</sup> /yr)	Study Area: Proportion of Total Volume per Year (%/yr)	Kaikōura EQ: Proportion of Total Volume per Year (%/yr)
1	5	2	178	0.4%	0.0%
10	25	5	1704	3.5%	0.01%
100	134	12	7160	14.9%	0.7%
1000	707	27	13,977	29.0%	12.8%
10,000	3736	61	17,230	35.8%	42.1%
25,000	7249	85	2522	5.2%	19.2%
50,000	11,967	109	2922	6.1%	18.9%
100,000	19,758	141	2500	5.2%	6.3%

### Annual Frequency of the Representative Earthquake Event

For the representative earthquake event within each PGA Band, the annual frequency of a given free-field PGA occurring was obtained from the New Zealand National Seismic Hazard Model (NSHM; Stirling et al. 2012) for the study area (Table 3.4). It should be noted that the study area is located close to the Hikurangi subduction zone, and several active faults in the GNS Science Active Faults Database are shown as passing through and nearby the study area.

Table 3.4 Annual frequency of a given PGA occurring in the study area obtained from the NSHM, and the representative event PGA for each earthquake band.

Earthquake Band	Band 1	Band 2	Band 3	Band 4
PGA Range (g)	0.2–0.4	0.4–1.0	1.0–2.0	>>2.0
Representative PGA (m/s/s)	3	7	15	34
Annual Frequency	0.0122	0.0037	0.0005	0.0001

#### 3.2.1.2 Non-Earthquake Triggers

For non-earthquake triggers, we use the annual frequency of landslides of a given volume from Stantec (2020). We then proportion these across the four hazard areas. To do this we:

- calculate the surface area of the potential landslide source-area slopes (source slopes) that could generate debris avalanches within each hazard area, which are all slopes  $\geq 30^\circ$  within the given hazard area – as per those used for earthquake-induced landslides; and

- calculate the percentage of source slopes ( $\geq 30^\circ$ ) within each hazard area as a proportion of the total surface area of all source slopes in the study area.

The estimated numbers of landslides of a given volume for each hazard area are shown in Table 3.5. Stantec (2020) did not separate out volume classes of 1 and 10 m<sup>3</sup>, and we proportioned the number of landslides in their volume class of <10 m<sup>3</sup> equally into the 1 and 10 m<sup>3</sup> classes used in this analysis. Stantec (2020) also only had one large volume class of >10,000 m<sup>3</sup>. However, landslides of up to 100,000 m<sup>3</sup> could potentially occur in the study area, based on slope morphology and the size of some of the possible historical landslide source areas apparent in the area. For example, the volume of the landslide in 1988 is estimated to be about 30,000 m<sup>3</sup>, we estimate that a landslide that occurred in 1990 (pers. com. GBA operator) had a source volume of up to 70,000 m<sup>3</sup> and another in 2015 had an estimated volume of about 40,000 m<sup>3</sup> (estimated from the airborne LiDAR surveys), assuming that all of the debris from these landslides failed as single events. We have therefore subdivided the Stantec (2020) >10,000 m<sup>3</sup> landslide class into three classes and estimated the annual frequency of landslides within the given volume class occurring.

Table 3.5 Annual frequency of non-earthquake-induced landslides per volume class and per hazard area.

Landslide Volume Class (m <sup>3</sup> )	Number of Landslides in Class per Year		Number of Landslides per Year, per Hazard Area (HA) (% of Hazard Area Source Slopes as a Proportion of ALL Source Slopes)							
	Lower ALL Source Slopes	Upper ALL Slopes	HA1 (28%)		HA2 (34%)		HA3 (16%)		HA4 (22%)	
			Lower	Upper	Lower	Upper	Lower	Upper	Lower	Upper
1	100	400	28	111	34	135	16	65	22	90
10	100	400	28	111	34	135	16	65	22	90
100	50	200	14	55	17	68	8	32	11	45
1000	12	50	3	14	4	17	2	8	3	11
10,000	3	12	0.8	3	1.0	4	0.5	2	0.7	3
25,000	1.0	3.0	0.3	0.8	0.3	1.0	0.2	0.5	0.2	0.7
50,000	0.1	1.0	0.03	0.3	0.03	0.3	0.02	0.2	0.02	0.2
100,000	0.01	0.1	0.003	0.03	0.003	0.03	0.002	0.02	0.002	0.02

### 3.2.2 Landslide Source Locations

To estimate which parts of the study area are likely to be inundated by debris from landslides of a given volume, the locations of potential landslide source areas need to be defined to understand how far the debris could travel downslope from a source. These debris inundation areas were calculated from landslide runout simulations (runout is the distance the debris travels downslope from the source) and are discussed in Section 3.2.3.

Determining the locations of future landslide source areas within each hazard area is difficult to quantify, as there is a certain amount of randomness in most landslide distributions. This is because it is not realistic, given the size and geological complexity of the study area, to assess potential source area on a slope and estimate its likely probability of failure.

To help identify a suite of potential landslide source areas for each of the landslide volume classes for the numerical runout simulations, we adopted the following multi-stage approach:

- Step 1: Identify slopes  $\geq 30^\circ$  from the DEMs in the study area. In general, it was assumed that only slopes  $\geq 30^\circ$  could generate debris avalanches and slopes  $\geq 45^\circ$  could generate rockfalls. However, some of the larger landslide volume classes could include failure of lower angle slopes.
- Step 2: Use the local slope relief (LSR) – the difference between the elevation of the grid cell and the lowest point in a 30 m radius circle, projected from each grid cell. The 30 m radius value was selected to capture the representative difference in elevation of the slope of interest while minimising situations where the relief of a neighbouring slope is attributed to the grid cell. In this project, we use the 3 m resolution DEM resampled from the 1 m resolution DEM derived from the 2011–2012 LiDAR survey. We then use the LSR to landslide volume relationship established by Massey et al. (In press), which is based on 16,736 landslides that were triggered by the 2016 Kaikōura Earthquake. We used it to identify which slopes would be large enough in height (LSR) to generate landslides of a given volume (Figure 3.2). Table 3.6 summarises the LSR values assumed for each landslide volume class considered in this project. The LSR was calculated for sections of the hillside based on the elevation difference in the DEM cells within the 30 m radius that had a gradient greater than  $30^\circ$ . For this study, we use the lower minus one standard deviation (1SD) LSR values. We have assumed that any slope  $\geq 45^\circ$  can generate rockfalls.
- Step 3: Use the representative landslide source area for each volume class (Table 3.3) to screen (remove) slopes not large enough to generate a landslide of the given volume class. To do this, we assumed each landslide source area to be square, with a total surface area equal to the representative source surface area. We then projected these surface areas onto a horizontal plane by assuming a lower slope angle for the study area of  $60^\circ$  in order to create representative plan areas (polygons) for each source volume class. We then used ArcGIS to fit the source areas for each volume class to the slopes in the study area.

This three-step process allowed slopes, which could potentially generate landslides up to a given source volume, to be systematically identified within the project area. This is important because larger landslides generally result in longer landslide debris inundation zones.

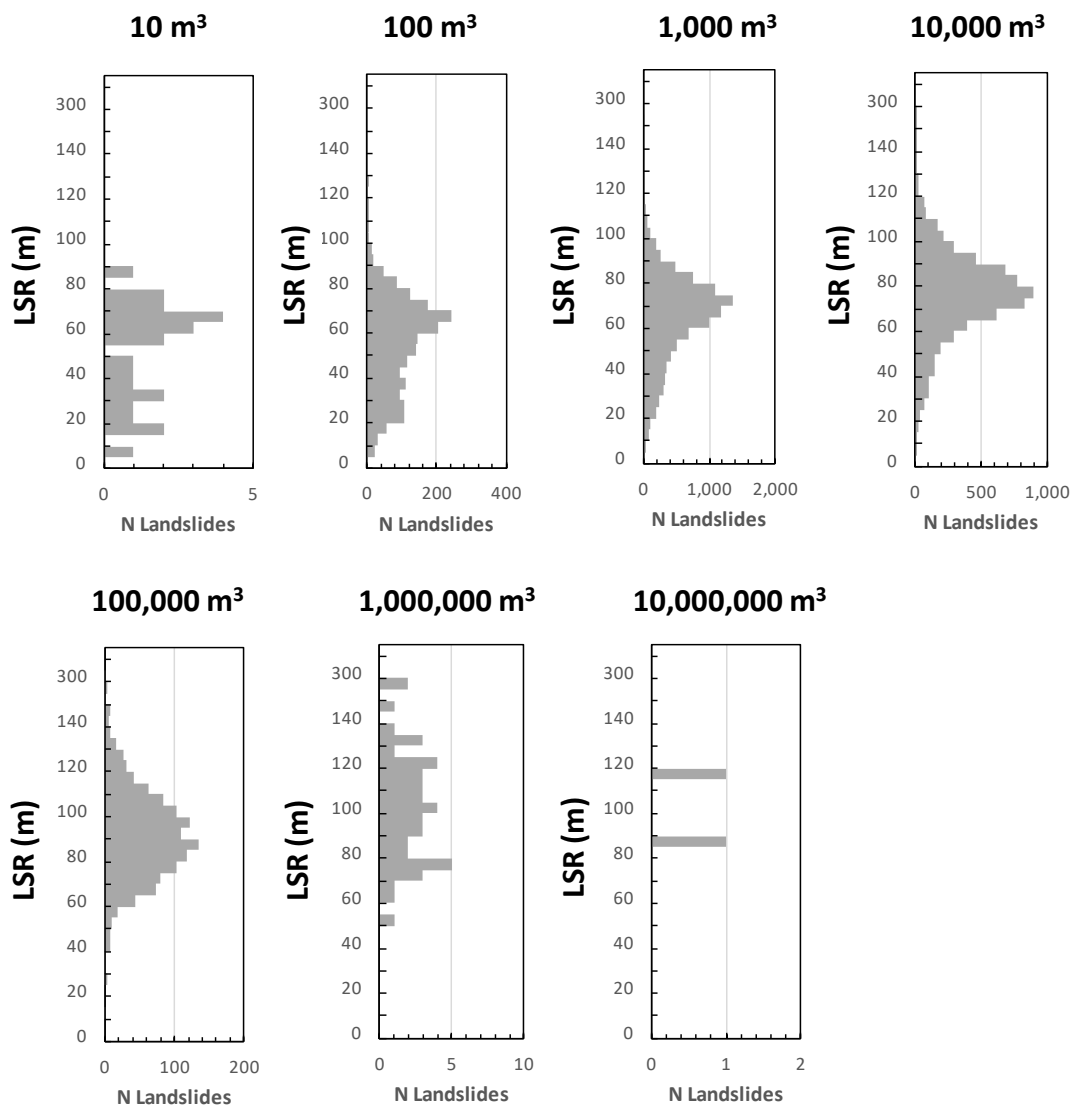


Figure 3.2 The number of landslides within each volume and LSR class for the slopes on which the different volume classes of landslide triggered by the Kaikōura Earthquake occurred (Massey et al. In press). N landslides = 16,736.

Table 3.6 Summary of the estimated potential landslide source volume as a function of the LSR calculated in the 30 m radius from the Kaikōura earthquake landslides (Massey et al. 2020).

Volume Bin Range (m <sup>3</sup> )	Representative Volume (m <sup>3</sup> )	Lower-1SD LSR in the 30 m Radius (m)
1–10	10	15
>10–100	100	15
>100–1000	1000	17
>1000–10,000	10,000	22
>10,000–25,000	25,000	28
>25,000–50,000	50,000	32
>50,000–100,000	100,000	32



### 3.2.3 Probability of Being in the Path of Landslide Debris, if Present

The probability of being in the path of landslide debris was calculated in several steps:

- Step 1: Estimate the downslope distance and area inundated by debris from each volume class of landslide as it travels from the source areas.
- Step 2: For each volume class of landslide, estimate the probability of a person being in the path of one landslide in the given volume class at: 1) the cliff bottom (toe) and 2) at the limit of the assessed area that could be inundated by debris (debris limit, defined using F-angles), if the landslide occurred.
- Step 3: For earthquake-induced landslides, calculate the probability of being in the path of a given number of landslides, of a given volume, triggered by the representative PGA in each earthquake band at the cliff bottom, rockfall limit line and debris limit.

#### 3.2.3.1 Step 1: Landslide Debris Inundation

The probability of being in the path of landslide debris depends on the distance that landslide debris travels down a slope from a potential source area. It is usually referred to as the landslide travel distance or runout distance (e.g. McDougall 2017).

The debris inundation area is defined as the area of ground that falling debris may cover as it travels, which comprises the source zone, transport zone, and the deposition zone (Figure 3.3). Numerous techniques exist to estimate the potential landslide debris runout and inundation area. These typically fall into two categories: 1) empirical- or 2) physics-based methods. Empirically based methods rely on the debris inundation area of past landslides of a given type to estimate the anticipated debris inundation area of future landslides of a similar type. They are relatively simple to apply, which makes them appropriate for regional-scale studies. Because empirically based methods record the actual behaviour of landslides, they are not limited by our current understanding of landslide mechanics, as can be the case in physics-based models. A limitation of the empirically based debris inundation model used in this project is that it cannot incorporate the site-specific conditions in the forward-looking estimates of the debris inundation area. However, given that the slopes in the study area are relatively simple in shape, empirical methods are thought to be adequate.

Physics-based methods include a range of techniques that consider the site-specific topography (usually in 2D or 3D) landslide volume and equivalent rheological parameters of the failed landslide mass (e.g. Hungr and McDougall 2009; Christen et al. 2012). Such techniques need to be calibrated by back-analysing a suite of data from representative landslides of varying types, from which detailed information about the landslide can be obtained and used in the calibration. Iverson (2014) noted that, because there is often not enough information available to fully constrain a physics-based debris flow model, empirical methods (i.e. back analyses of historical events) continue to play a dominant role in estimating the hazard associated with debris flows.

For this study, we use empirical methods to define the runout of debris avalanches for volume classes 10–100,000 m<sup>3</sup>, and a physics-based approach for rockfalls for the volume class of 1 m<sup>3</sup>. Using such physics-based approaches for the regional-scale assessment of debris avalanches is not possible, as they take considerable input data and time to set up, calibrate and run and, as such, we have adopted the empirically based methodology. However, for rockfalls, we use a physics-based approach, using a model that has been calibrated to the site, as the empirical models are not appropriate for rockfalls.

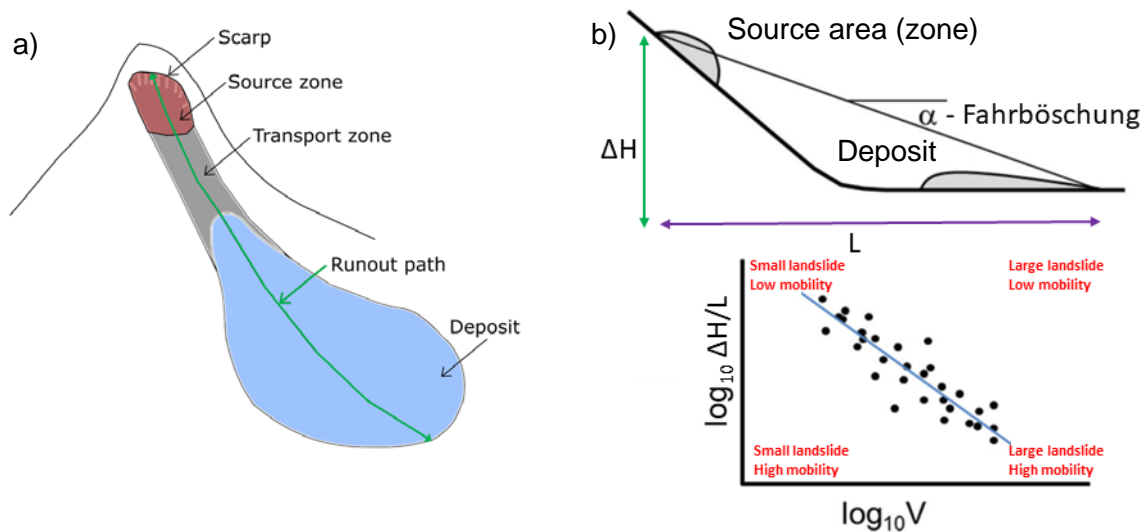


Figure 3.3 a) Schematic representation of the source area and debris inundation area (source, transport and deposit zones) of a landslide. Drawing modified from Brideau et al. (2020). b) Schematic representation of the fall height ( $\Delta H$ ) and runout distance ( $L$ ) parameters for a landslide and the conceptual relationship between  $\Delta H/L$  and the landslide volume ( $V$ ). Modified from McDougall (2017).

### Empirical Relationship: Debris Avalanches

Heim (1932) proposed that the distance a landslide travels is proportional to its fall height. The tangent of the ratio of the fall height ( $\Delta H$ ) to horizontal runout distance ( $L$ ) between the crest of the source area and toe of the deposit, known as the 'Fahrböschung' (referred to as the F-angle in this report) (Figure 3.3), has subsequently been correlated with landslide volume ( $V$ ). Empirical relationships between the F-angle and landslide volume have been derived for different landslide types (e.g. Corominas 1996). Measurement of the slope crest and deposit toe can be compiled for many different landslide types and trigger conditions to generate empirical relationships similar to the one in Figure 3.4. From these compilations, a best-fit linear regression (in log-log space) between  $\Delta H/L$  and  $V$  was derived for the debris avalanches, assuming dry conditions. Dry conditions were assumed because: 1) most of the non-earthquake-induced landslides are noted to occur during periods of dry weather; 2) the cliff-forming material is mainly unsaturated; 3) most landslides appear to occur from the cliff toe and propagate upwards towards the crest, indicating wave action as being a dominant trigger (Stantec 2020); and 4) earthquake-induced landslides tend to be relatively dry.

Empirically based relationships between  $\Delta H/L$  and  $V$  represent the compilation of landslides with different site conditions (e.g. source geology, local topography, grain-size of failed material, water content of source material and erodible material along travel path, vegetation, buildings, the presence [or not] of mitigation measures). This range of site-specific conditions results in the variability of observed landslide debris runout and inundation area. The variability in the landslide debris runout and inundation data also allows for the probability of runout exceedance, or limits of confidence to be defined for the prediction of runout for each landslide volume (e.g. Li-Tianchi 1983). For example, the best-fit (orange) line in Figure 3.4 represents an exceedance probability of 50%, i.e. half of the landslides of the given volume and type will travel further than this line, while the 10% line (yellow) represents a 10% chance that a similar landslide will travel further (Brideau et al. In press).

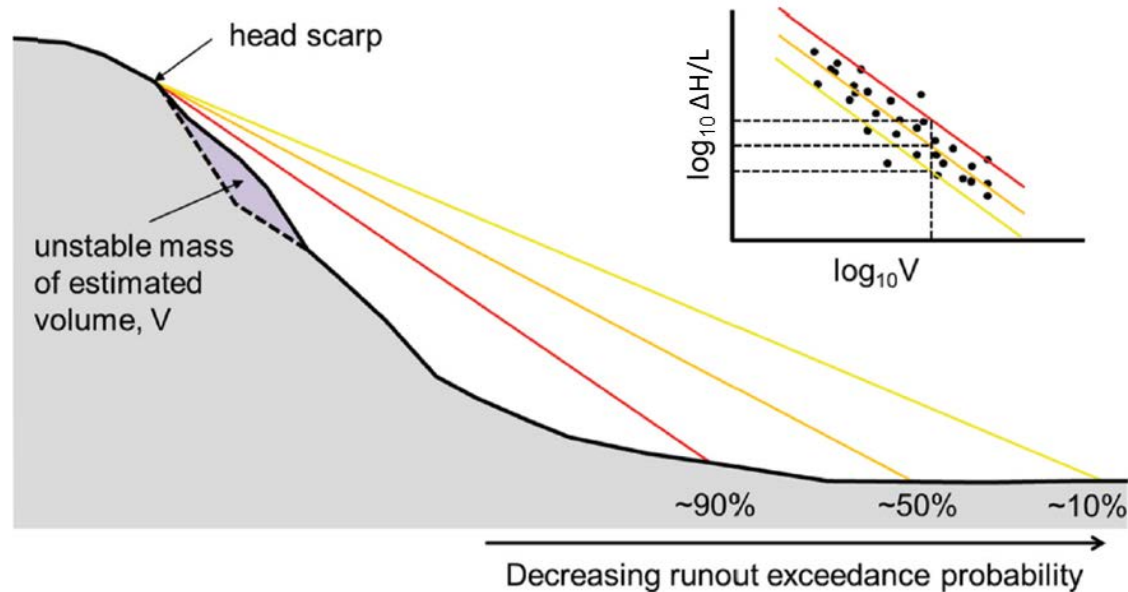


Figure 3.4 Schematic representation of runout exceedance probability based on empirical relationships. Modified from Brideau et al. (In press).

To minimise variability in empirical relationships, tools to estimate landslide runout need to be calibrated to the region-specific characteristics over which they will be applied. To address these contributing factors in the empirical runout-relationships, a plot showing the relationship between the  $\Delta H/L$  and volume was compiled from the relevant Kaikōura earthquake and other New-Zealand-specific landslide runout information available (Brideau et al. 2020), (Figure 3.5). Figure 3.5 represents earthquake-induced dry open-slope debris avalanches, which transition into rock avalanches (at volumes greater than  $100,000 \text{ m}^3$ ) from landslides in similar materials to those in the study area.

Implementation of the empirical runout methodology was carried out in ArcGIS. It was done in two steps:

- Step 1: Identify potential landslide source areas of a given volume class, adopting the slope angle of  $\geq 30^\circ$  to define the source areas in each hazard area.
- Step 2: Carry out dry open-slope debris avalanche/rock avalanche runout modelling using the given F-angles for each landslide volume class from the lower relationship in Figure 3.5.
- Step 3: Screen the source and corresponding runout areas, as per the method in Section 3.2.2, to identify where landslides of a given volume class could feasibly occur.

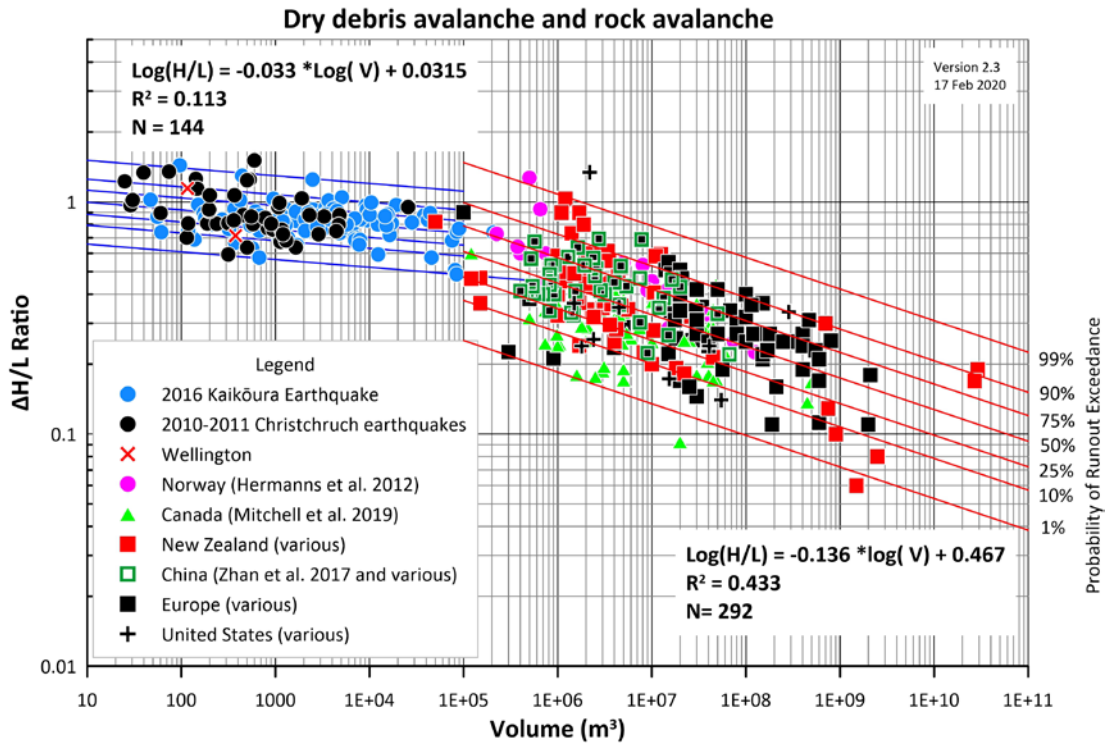


Figure 3.5 Empirical relationship between  $\Delta H/L$  ratio and volume in dry (i.e. earthquake-induced) debris avalanches ( $<100,000 \text{ m}^3$ ) and rock avalanches ( $>100,000 \text{ m}^3$ ).

GNS Science developed a GIS script that combines the Fahrböschung method with methodology used in the ArcGIS Visibility Tool. The visibility tool assesses which areas can be seen from a location. In this project, for each landslide source area of a given volume class, the elevation of each grid cell within the potential source area was projected in eight directions (i.e. to each adjacent grid cell) using the Fahrböschung. This projected elevation was compared with the elevation obtained from the DEM. All the cells with the projected elevation above the DEM were deemed to be ‘visible’ and within the inundated area, but only if they were downhill from the processing cell. The process was continued using these inundated cells as sources until no more cells were inundated (Figure 3.6). The 3 m resolution DEM was used for processing, and the Fahrböschung for each landslide volume class is listed in Table 3.7.

Table 3.7 Summary of Fahrböschung values for each volume class of dry debris avalanche and rock avalanche used in this project. For the landslide volume class of  $100,000 \text{ m}^3$ , the  $50,000 \text{ m}^3$  F-angle was adopted, as this projected far out into the sea.

Representative Landslide Volume ( $\text{m}^3$ )	Fahrböschung ( $^\circ$ ) 50% Runout Exceedance Probability
10	45
100	43
1000	41
10,000	38
25,000	38
50,000	37
100,000	37

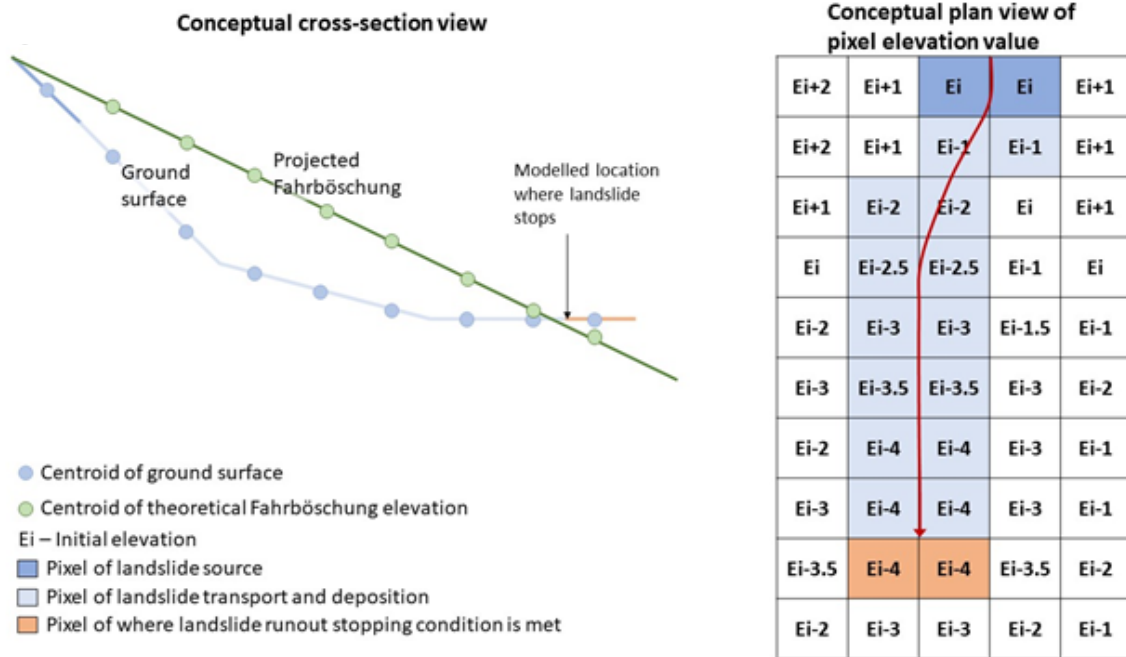
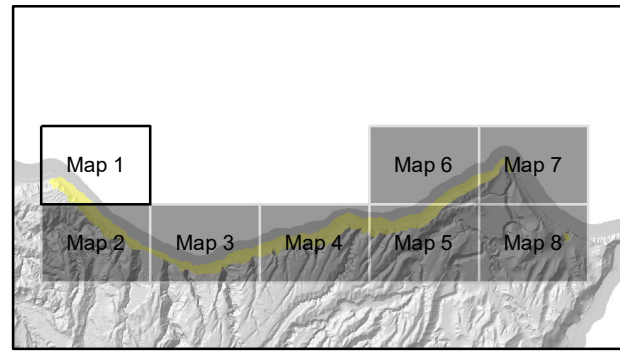


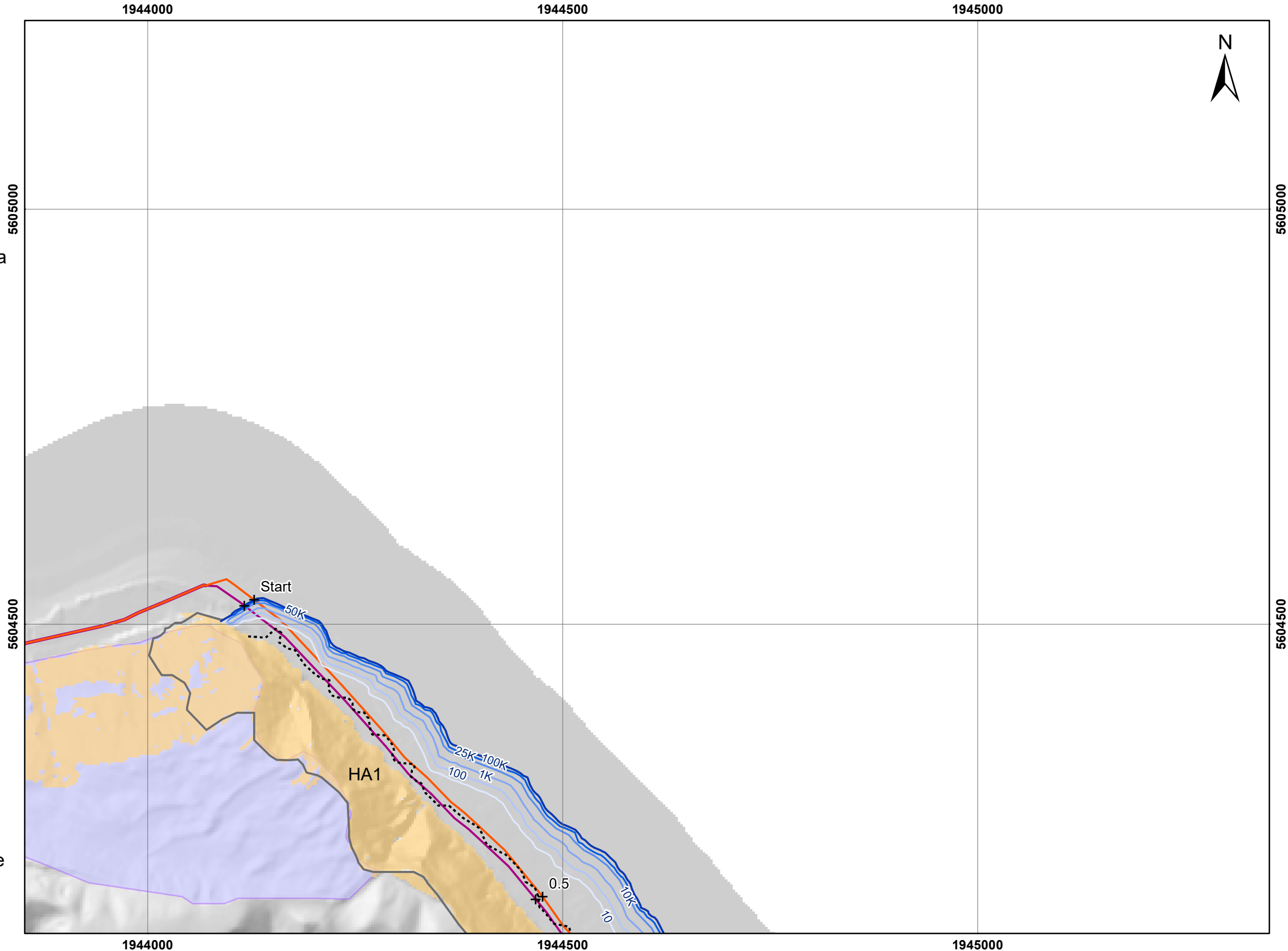
Figure 3.6 Conceptual representation of the landslide runout model stopping rules as implemented in GIS. The modelled travel path (red arrow) intersects the Fahrböschung for the landslide volume class investigated. Modified from Brideau et al. (2020).

The simulated landslide source areas and runout extents based on the F-angle lines are shown in Figure 3.7. The area of slope extending from and including the simulated sources (potential landslide source areas) to the runout extents (F-angle lines) for each landslide volume class are called the ‘hazard footprints’. The F-angle lines are drawn where they project the furthest out from the cliff bottom.

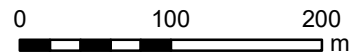
This page left intentionally blank.



- Simulated landslide source area  
(slopes  $\geq 30^\circ$ )
- Landslide runout extent (F-angles)**  
(Landslide volume class  $m^3$ )
- 10
- 100
- 1000
- 10000
- 25000
- 50000 & 100000
- Rockfall limit line
- Spring tide route
- Neap tide route
- + Distance along the route (km)
- Hazard area
- Risk exclusion zone**
- Debris flow
- Deep-seated gravitational slope deformation (DSGSD)
- DOC Reserve



SCALE BAR:



EXPLANATION:

Background shade model derived from a LiDAR based Digital Elevation Model (1m ground resolution) which was resampled to 3 m for the analysis

PROJECTION: New Zealand Transverse Mercator 2000

DRW:  
BL  
CHK:  
CM, SDV



## LANDSLIDE HAZARD FOOTPRINTS

### Cape Kidnappers

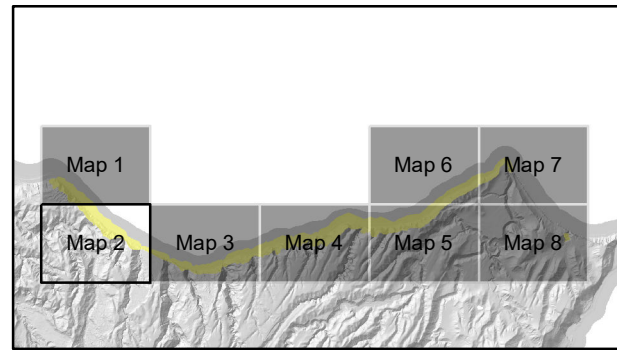
**FIGURE 3.7**

Map 1

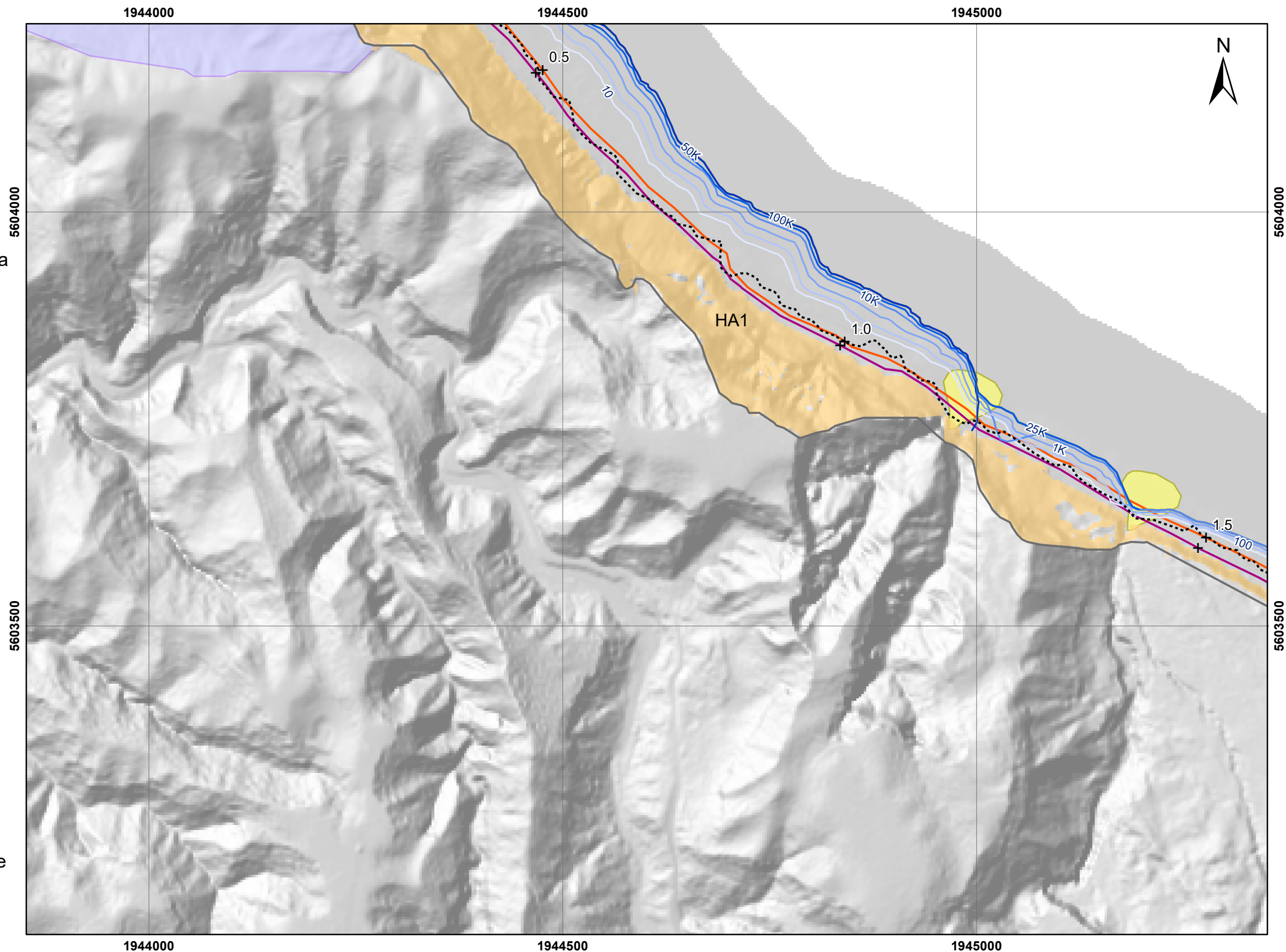
**FINAL**

REPORT:  
CR2020/28

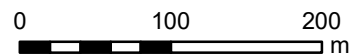
DATE:  
May 2020



- Simulated landslide source area (slopes  $\geq 30^\circ$ )
- Landslide runout extent (F-angles)**  
(Landslide volume class  $m^3$ )
- 10
- 100
- 1000
- 10000
- 25000
- 50000 & 100000
- Rockfall limit line
- Spring tide route
- Neap tide route
- + Distance along the route (km)
- Hazard area
- Risk exclusion zone**
- Debris flow
- Deep-seated gravitational slope deformation (DSGSD)
- DOC Reserve



SCALE BAR:



EXPLANATION:

Background shade model derived from a LiDAR based Digital Elevation Model (1m ground resolution) which was resampled to 3 m for the analysis

PROJECTION: New Zealand Transverse Mercator 2000

DRW:  
BL  
CHK:  
CM, SDV



## LANDSLIDE HAZARD FOOTPRINTS

### Cape Kidnappers

**FIGURE 3.7**

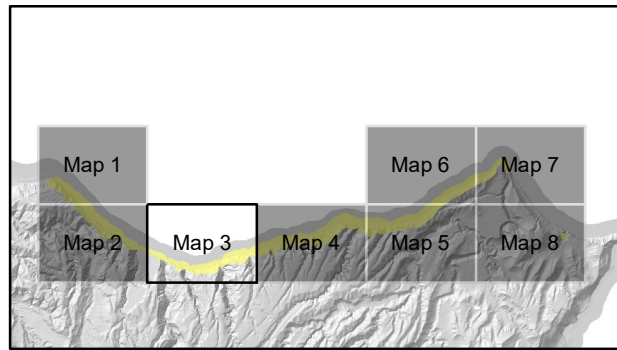
Map 2

**FINAL**

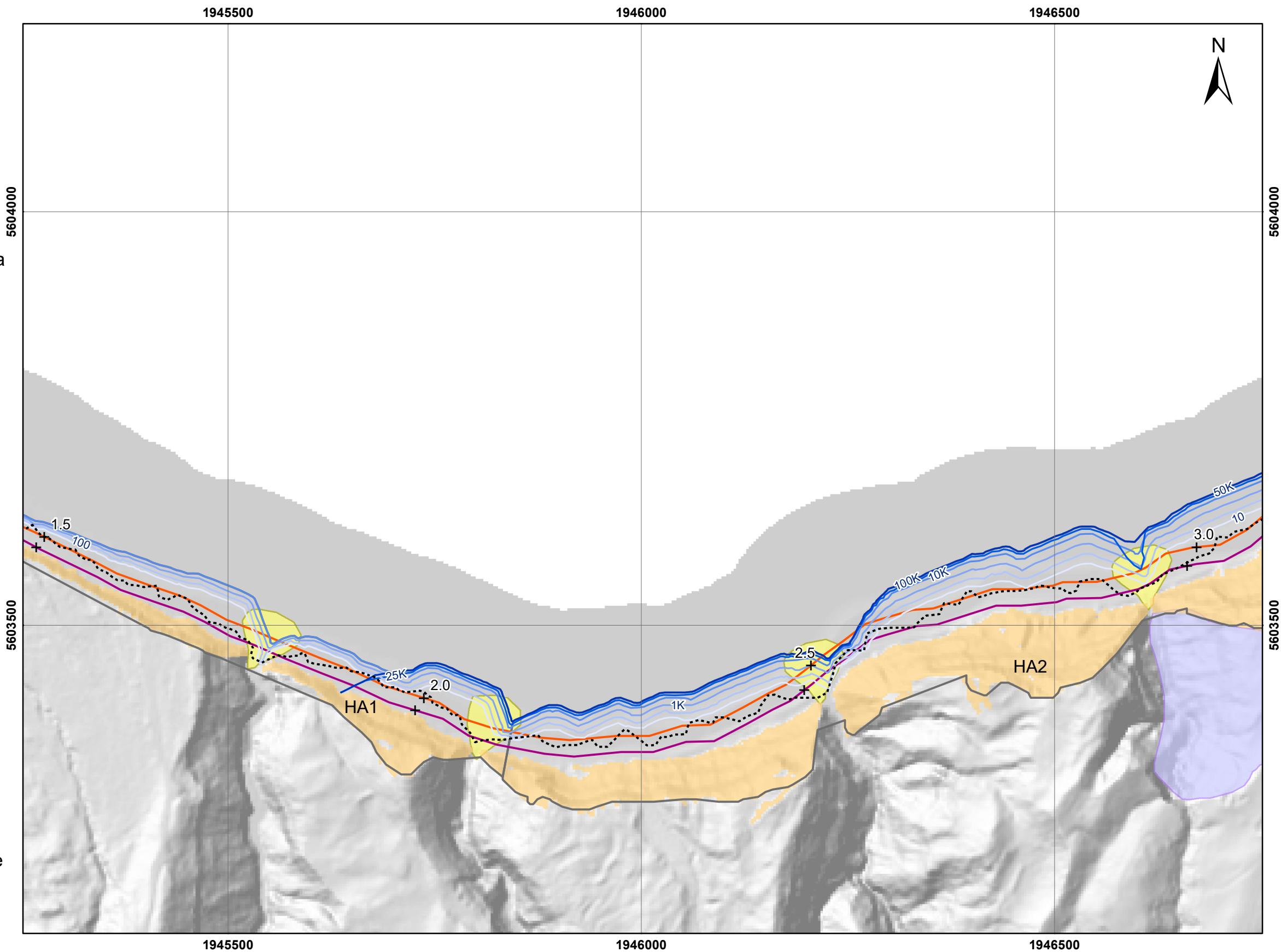
REPORT:  
CR2020/28

DATE:  
May 2020

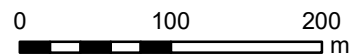




- Simulated landslide source area (slopes  $\geq 30^\circ$ )
- Landslide runout extent (F-angles)**  
(Landslide volume class  $m^3$ )
- 10
- 100
- 1000
- 10000
- 25000
- 50000 & 100000
- Rockfall limit line
- Spring tide route
- Neap tide route
- + Distance along the route (km)
- Hazard area
- Risk exclusion zone**
- Debris flow
- Deep-seated gravitational slope deformation (DSGSD)
- DOC Reserve



SCALE BAR:



EXPLANATION:

Background shade model derived from a LiDAR based Digital Elevation Model (1m ground resolution) which was resampled to 3 m for the analysis

PROJECTION: New Zealand Transverse Mercator 2000

DRW:  
BL  
CHK:  
CM, SDV



## LANDSLIDE HAZARD FOOTPRINTS

### Cape Kidnappers

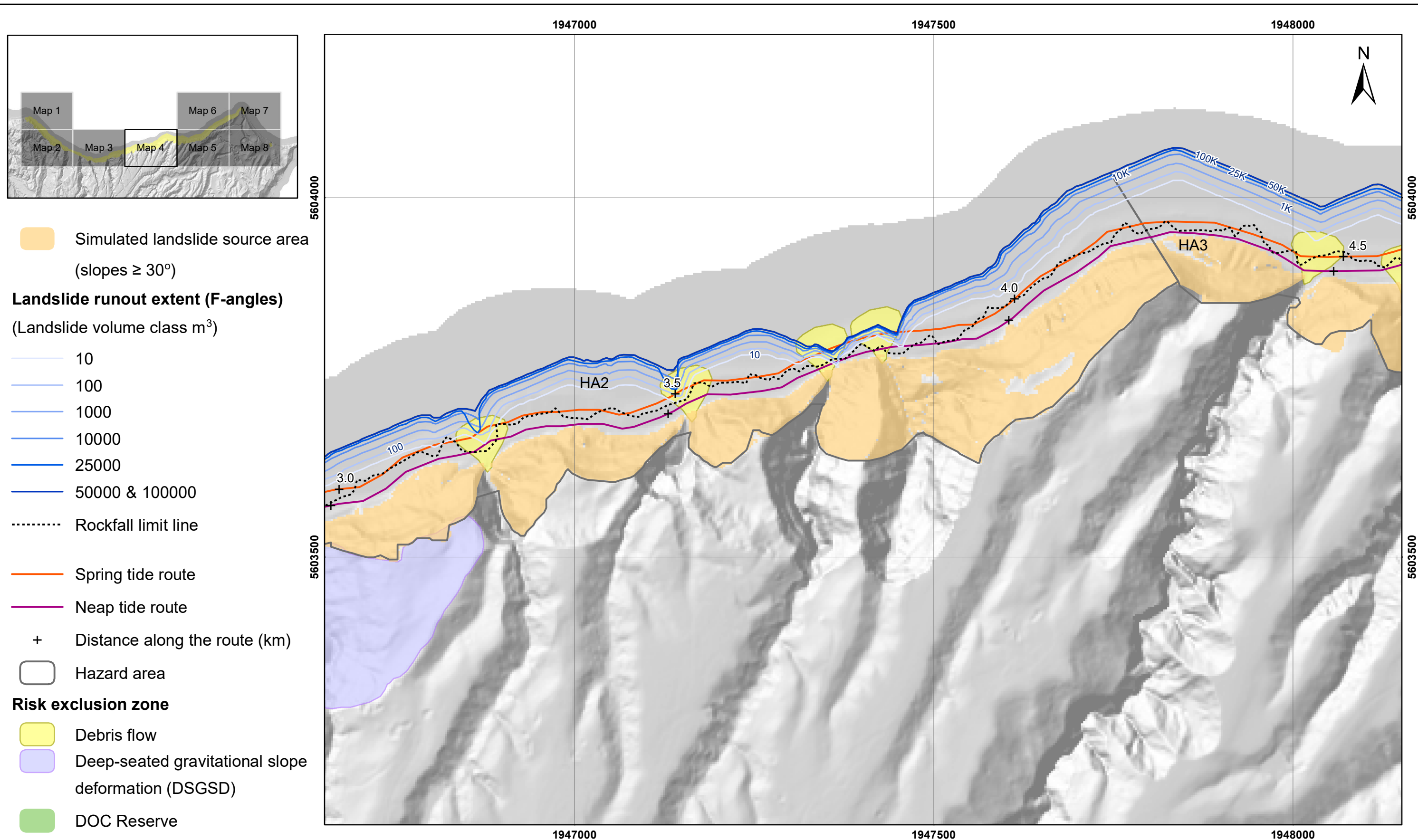
FIGURE 3.7

Map 3

**FINAL**

REPORT:  
CR2020/28

DATE:  
May 2020



SCALE BAR: 0 100 200 m

EXPLANATION:

Background shade model derived from a LiDAR based Digital Elevation Model (1m ground resolution) which was resampled to 3 m for the analysis

PROJECTION: New Zealand Transverse Mercator 2000

DRW:  
BL

CHK:  
CM, SDV



**LANDSLIDE HAZARD FOOTPRINTS**

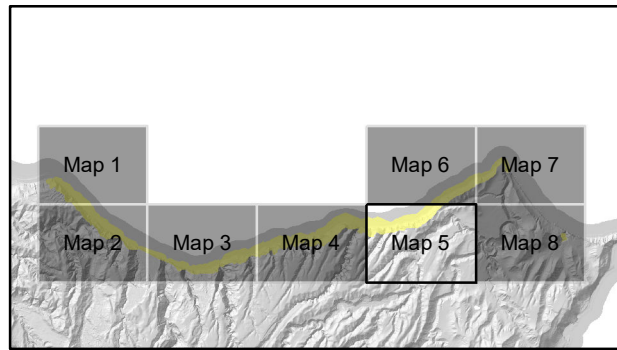
**Cape Kidnappers**

**FIGURE 3.7**

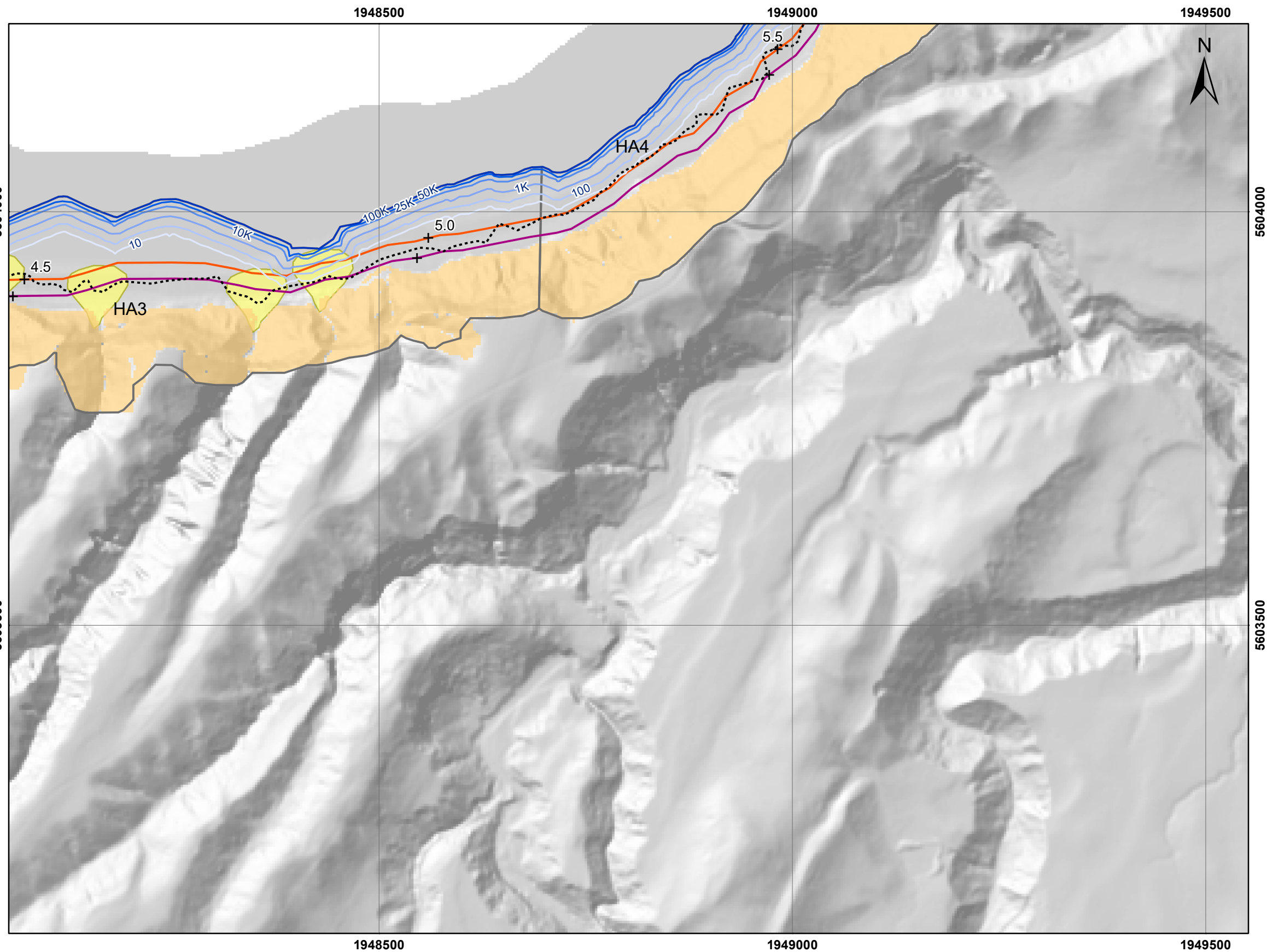
Map 4

**FINAL**

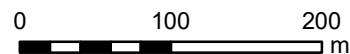
REPORT: CR2020/28      DATE: May 2020



- Simulated landslide source area (slopes  $\geq 30^\circ$ )
- Landslide runout extent (F-angles)**  
(Landslide volume class  $m^3$ )
- 10
- 100
- 1000
- 10000
- 25000
- 50000 & 100000
- Rockfall limit line
- Spring tide route
- Neap tide route
- + Distance along the route (km)
- Hazard area
- Risk exclusion zone**
- Debris flow
- Deep-seated gravitational slope deformation (DSGSD)
- DOC Reserve



SCALE BAR:



EXPLANATION:

Background shade model derived from a LiDAR based Digital Elevation Model (1m ground resolution) which was resampled to 3 m for the analysis

PROJECTION: New Zealand Transverse Mercator 2000

DRW:  
BL

CHK:  
CM, SDV



## LANDSLIDE HAZARD FOOTPRINTS

### Cape Kidnappers

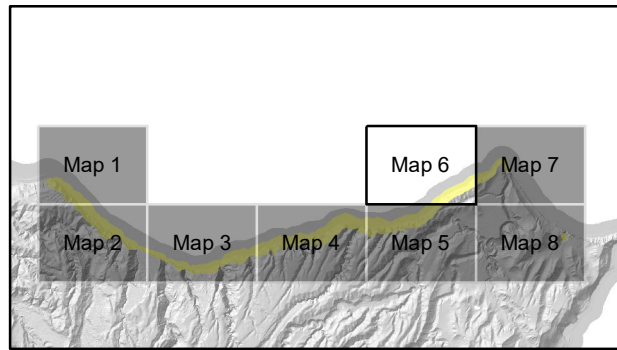
**FIGURE 3.7**

Map 5

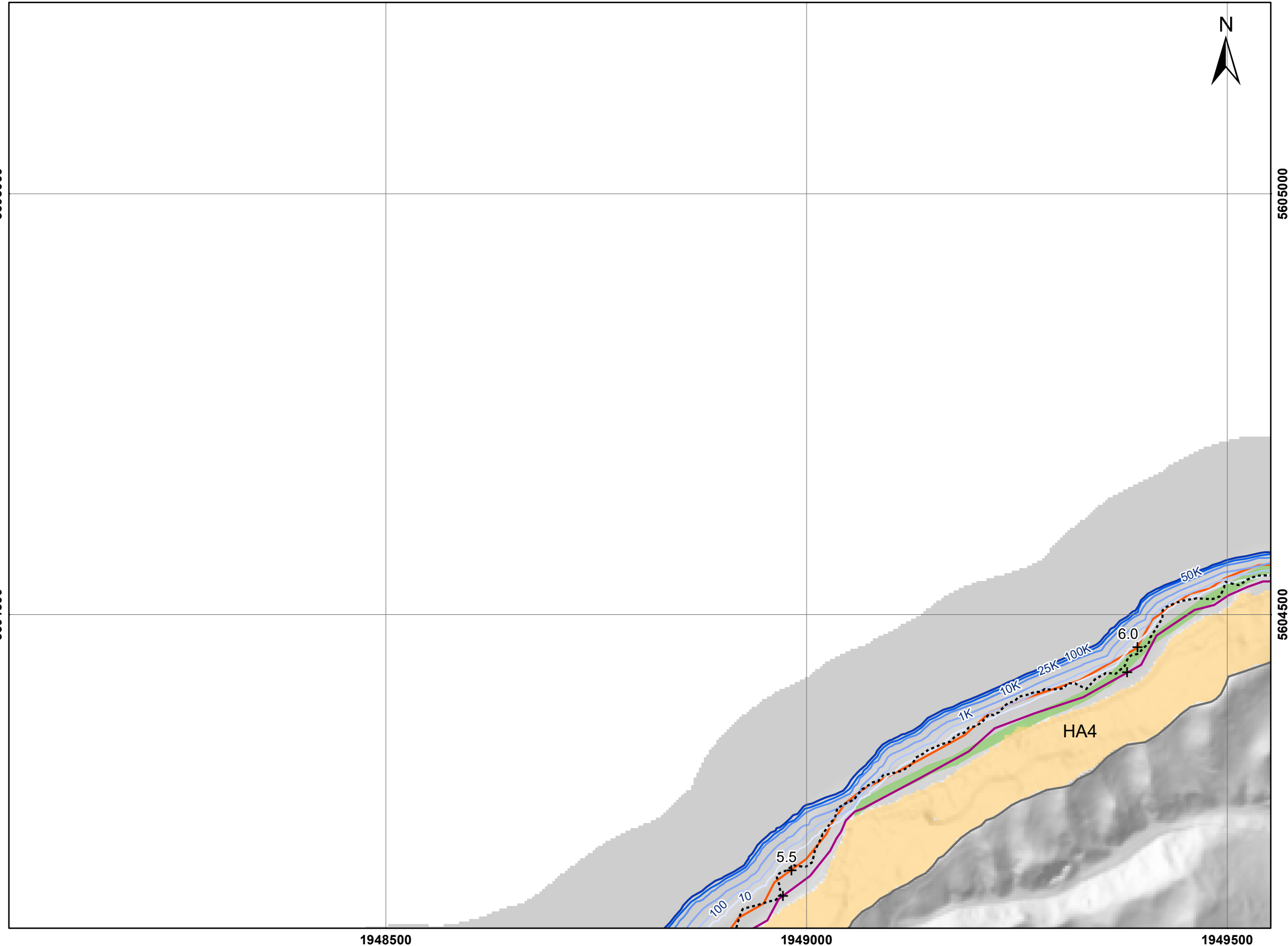
**FINAL**

REPORT:  
CR2020/28

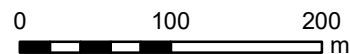
DATE:  
May 2020



- Simulated landslide source area (slopes  $\geq 30^\circ$ )
- Landslide runout extent (F-angles)**  
(Landslide volume class  $m^3$ )
- 10
- 100
- 1000
- 10000
- 25000
- 50000 & 100000
- Rockfall limit line
- Spring tide route
- Neap tide route
- + Distance along the route (km)
- Hazard area
- Risk exclusion zone**
- Debris flow
- Deep-seated gravitational slope deformation (DSGSD)
- DOC Reserve



SCALE BAR:



EXPLANATION:

Background shade model derived from a LiDAR based Digital Elevation Model (1m ground resolution) which was resampled to 3 m for the analysis

PROJECTION: New Zealand Transverse Mercator 2000

DRW:  
BL  
CHK:  
CM, SDV



## LANDSLIDE HAZARD FOOTPRINTS

### Cape Kidnappers

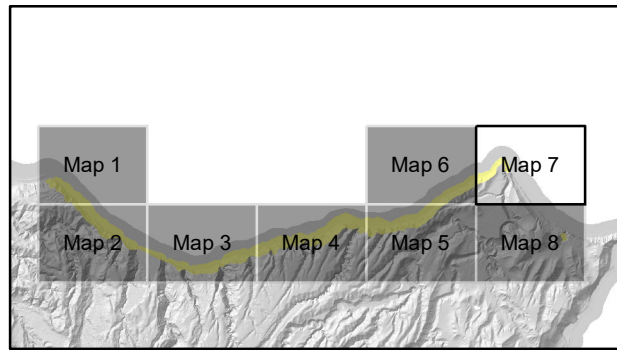
**FIGURE 3.7**

Map 6

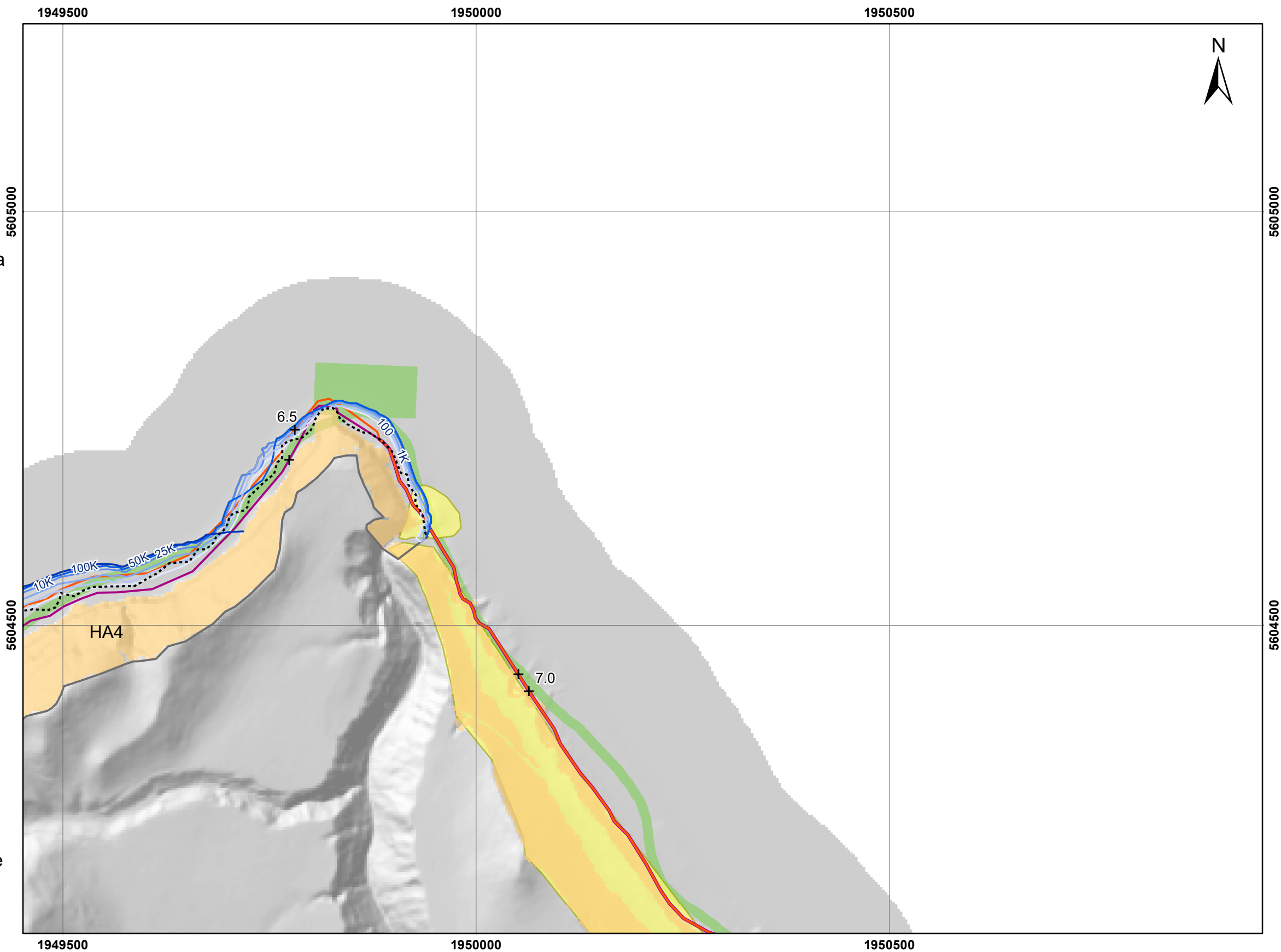
**FINAL**

REPORT:  
CR2020/28

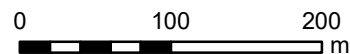
DATE:  
May 2020



- Simulated landslide source area (slopes  $\geq 30^\circ$ )
- Landslide runout extent (F-angles)**  
(Landslide volume class  $m^3$ )
- 10
- 100
- 1000
- 10000
- 25000
- 50000 & 100000
- Rockfall limit line
- Spring tide route
- Neap tide route
- + Distance along the route (km)
- Hazard area
- Risk exclusion zone**
- Debris flow
- Deep-seated gravitational slope deformation (DSGSD)
- DOC Reserve



SCALE BAR:



EXPLANATION:

Background shade model derived from a LiDAR based Digital Elevation Model (1m ground resolution) which was resampled to 3 m for the analysis

PROJECTION: New Zealand Transverse Mercator 2000

DRW:  
BL  
CHK:  
CM, SDV



## LANDSLIDE HAZARD FOOTPRINTS

### Cape Kidnappers

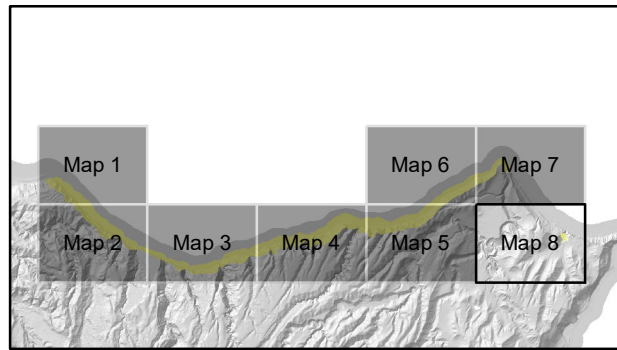
**FIGURE 3.7**

Map 7

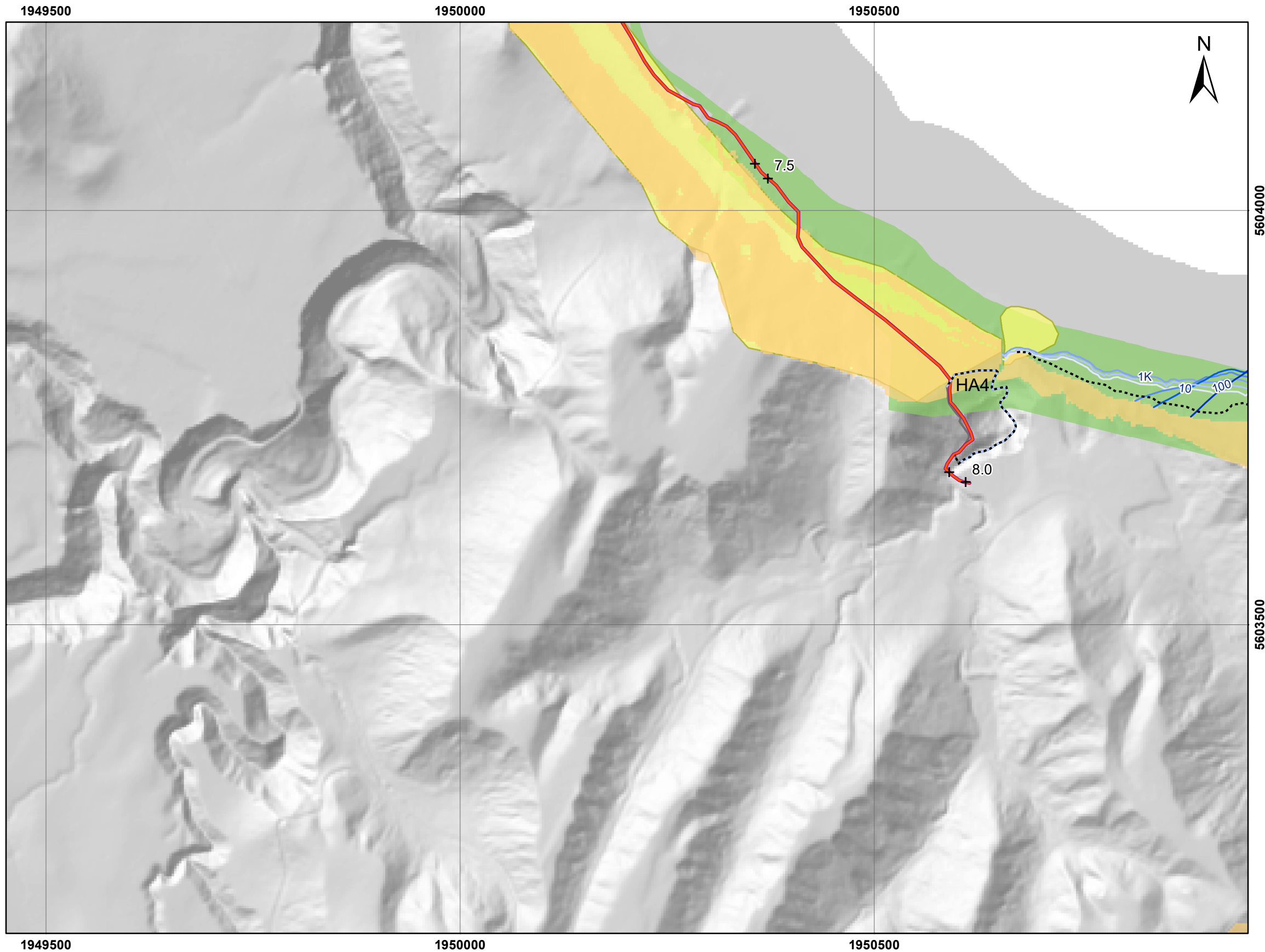
**FINAL**

REPORT:  
CR2020/28

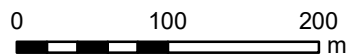
DATE:  
May 2020



- Simulated landslide source area (slopes  $\geq 30^\circ$ )
- Landslide runout extent (F-angles)**  
(Landslide volume class  $m^3$ )
- 10
- 100
- 1000
- 10000
- 25000
- 50000 & 100000
- Rockfall limit line
- Spring tide route
- Neap tide route
- + Distance along the route (km)
- Hazard area
- Risk exclusion zone**
- Debris flow
- Deep-seated gravitational slope deformation (DSGSD)
- DOC Reserve



SCALE BAR:



EXPLANATION:

Background shade model derived from a LiDAR based Digital Elevation Model (1m ground resolution) which was resampled to 3 m for the analysis

PROJECTION: New Zealand Transverse Mercator 2000

DRW:  
BL

CHK:  
CM, SDV



## LANDSLIDE HAZARD FOOTPRINTS

### Cape Kidnappers

**FIGURE 3.7**

Map 8

**FINAL**

REPORT:  
CR2020/28

DATE:  
May 2020

### **Physics-Based Relationship: Rockfalls**

Landslides with source volumes  $\leq 1 \text{ m}^3$  are assumed to be rockfalls, and it has been assumed that they could source from anywhere within the hazard areas from slopes  $\geq 45^\circ$ . The distance and path that a rock block travels downslope from a source area, and the number of simulated rocks passing through a grid cell, was assessed numerically using the Rapid Mass Movements (RAMMS) Rockfall software (RAMMS 2016), using the 3 m resolution DEM for the area. This software simulates the rigid body motion of falling rocks. The model predicts rock trajectories in general three-dimensional terrain. Rock trajectories are governed by the interaction between the rock and ground. The results from the simulations comprise: kinetic energy, runout distance, jump heights and the number of simulated trajectories passing through a given grid cell. Generalised rock shapes are simulated, and rock block orientation and rotational speed are included in the rock/ground interaction. The shape of the rock block can influence the runout, and the nature of the material forming the substrate, along which the rock block travels by bouncing, sliding and rolling, also influences the runout. For example, a soft substrate, such as sand and gravel, will remove or 'damp' much of the energy from the block as it hits the ground. Conversely, a hard substrate, such as rock, will not remove much energy from the rock block. Therefore, rock blocks falling onto rock tend to travel further than rock blocks falling onto sand and gravel.

The simulation parameters used for forecasting were derived from the back analysis of fallen rocks within the study area where the source areas, boulder shapes and rockfall trails could be inferred; an example is shown in Figure 3.8. The RAMMS Rockfall forecast parameters adopted from back analysis are shown in Table 3.8, along with descriptions of the parameters and the data sources used to derive them.

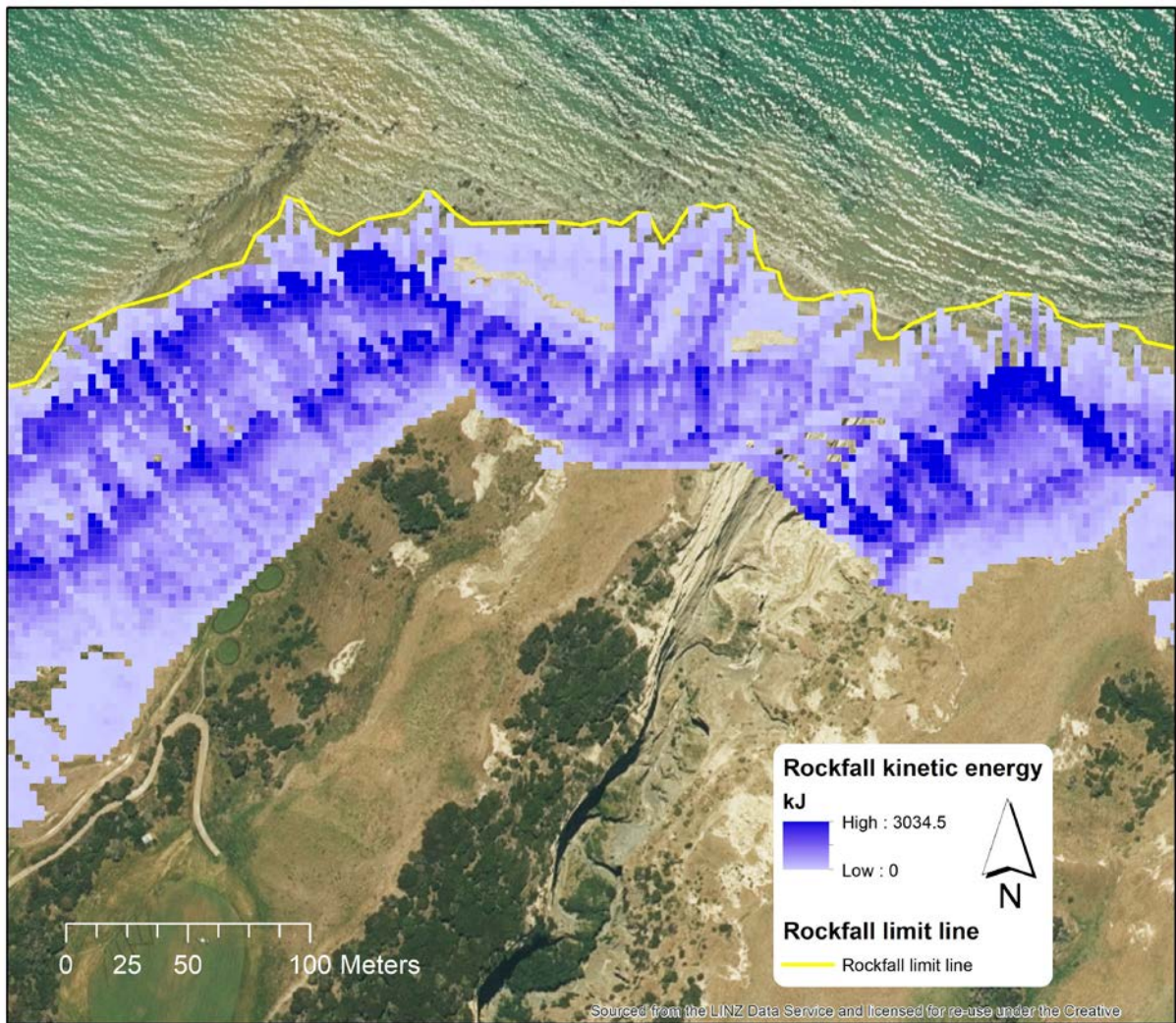


Figure 3.8 Rockfall simulations showing the simulated rockfall trajectories and runout distances for the mean boulder size of 1 m<sup>3</sup>. The grid cells (3 m by 3 m squares) show the maximum kinetic energy (KE; measured in kilojoules) of the simulated rockfalls that pass through each cell. The falling, bouncing, rolling and sliding of each rockfall is simulated down the slope from the source areas (the cliffs) to the rockfall limit of runout. The thick yellow line represents a line drawn around the simulated limit of rockfall runout. Only the maximum KE of a boulder passing through a given cell is shown. The KE is a function of the simulated rock block mass and its angular and rotational velocity.



Table 3.8 RAMMS Rockfall model parameters used for forecasting rockfalls.

Simulation Variable	Description	RAMMS Parameter	Data Source
Substrate material	Beach: sand	Terrain parameter: Extra soft	Material polygons were defined using slope angle, where $<30^\circ$ = sand and $\geq 30^\circ$ = rock
	Rock, rock at/near surface	Terrain parameter: Extra soft	
Vegetation	Bare	N/A	N/A
Rock shape	The shape of the boulders used in the simulations	Rock parameter: 'Real long' dimensions (1.5 by 1.0 by 1.0 m). Rock volume = 1 m <sup>3</sup> (assumes rounded edges). Mass = 2000 kg	Field mapping and measurements of rockfalls
Topography	The DEM used in the simulations	Terrain = 3 m by 3 m grid-cell resolution	DEM (bare earth) derived from the LiDAR surveys of both study areas
Release	Number of random orientations of the rock blocks at source	One random orientation was selected	N/A
	Source area locations	Rock positions: from 3 m by 3 m grid cells, with slope angles $\geq 45^\circ$	From the LiDAR DEMs
	Initial velocities of the rock blocks	Initial velocities of X = 1.5 m/s, Y = 1.5 m/s and Z = 1.0 m/s were assumed in order for the rockfalls to start moving	N/A

The results from the simulations, comprising the number of simulated rockfalls (individual rock blocks) passing through each grid cell were exported as grids. A rockfall limit line was then drawn using the simulation results as a guide, along with any other field-mapped, historical and geomorphological data relating to rockfalls. The rockfall limit line marks the simulated runout limit of boulders 1 m<sup>3</sup> in volume. The line does not represent the probability of a boulder reaching the line. In some cases, rockfalls that are larger (in mass) than those simulated may travel further than the limit line and, conversely, smaller boulders may stop short. Therefore, it should not be assumed that all boulders will reach or stop at the limit line.

### 3.2.3.2 Step 2: Probability of a Person being in the Path of One Landslide

$P_{(S:H)}$  is the probability of the debris from a landslide reaching or passing a given location on the slope (in this case the cliff bottom, the rockfall limit line and the F-angle lines) as it travels downhill from the source area. The probability of a person being in the path of one rockfall or debris avalanche when it passes through the cliff bottom upon reaching the F-angle line, perpendicular to the debris path, is expressed as:

$$P_{Vol(S:H)} = \frac{W+d}{L} \quad \text{Equation 3.3}$$

where  $W$  is the width of the debris at the cliff toe, rockfall limit line or F-angle line that travels along a path either side of  $d$ , within which the debris cannot miss;  $d$  is the diameter of an object, such as a person or width of a building; and  $L$  is the unit length of the cliff toe, rockfall limit line or F-angle line perpendicular to the runout path along the entire study area.  $L$  will vary for each

rockfall limit line and F-angle line, as it depends on where the various landslide sources of a given volume can occur from the sources and the shape of the slopes. For rockfalls,  $W$  is assumed to be 1 m. For debris avalanches,  $W$  is assumed to be 1.5 times the representative landslide source area width (Table 3.3) at the cliff bottom, and 1.8 times the representative landslide source area width when the debris reaches the F-angle line. This assumes that the debris fans out upon impacting the beach and is based on measurements taken from recent landslides that have occurred within the study area (Figure 3.9).

Not all debris will inundate the entire area from the cliff bottom to the F-angle line, and not every rockfall will reach the rockfall limit line. For rockfalls (landslide volume classes of  $1 \text{ m}^3$ ), the RAMMS simulations indicate that only about 40–50% of the simulated rockfalls reach the limit line. For the calculations of the probability of being in the path of landslide debris (rockfalls), it was assumed that 50% of the rockfalls reach the rockfall limit line. To take this into account, we have multiplied  $P_{1(S:H)}$  by 0.5.

For debris avalanches, the F-angles projected from grid cells located on the lower- and mid-slope areas do not extend as far out to sea as the those located on the upper slope areas. For the modelling, we have drawn the F-angle lines where they project the furthest out from the cliff bottom; therefore, in most cases, these are projected from grid cells on the upper part of the slopes. As a result, not all of the area between the cliff bottom and the F-angle line is likely to be inundated by debris. To take this into account, we have multiplied  $P_{VOL(S:H)}$  by 0.5 for each volume class, which assumes only 50% of the area could be inundated by debris.

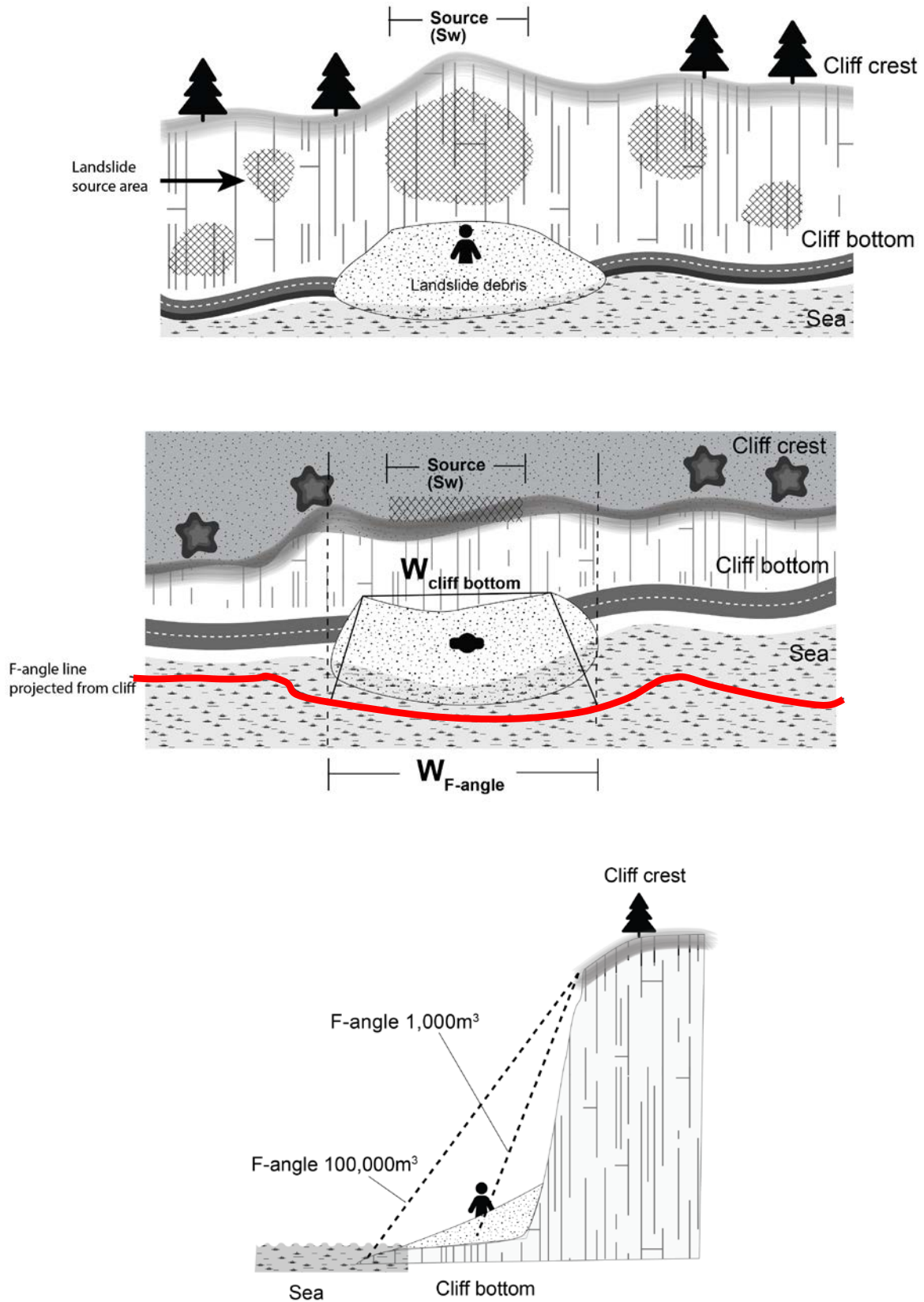


Figure 3.9 Schematic diagram showing how the probability of a person being in the path of one landslide is calculated in the risk analysis.

### 3.2.3.3 Step 3: Probability of being in the Path of Multiple Landslides

For earthquake-induced landslides, it is assumed that multiple landslides of varying source volumes may be triggered simultaneously. Therefore, it is important in the risk calculations to ensure that a person is not killed more than once, if they are present in a grid cell and hit by debris. For example, a person present in a given grid cell at the time of an earthquake could be hit and killed by debris from one source area or from multiple source areas combined. However, although the probability of death increases with the increasing volume of debris passing through a given portion of slope, it cannot exceed 1.

For non-earthquake-induced landslides, it is assumed that a landslide within each volume class is independent of those that may occur in other landslide volume classes. This is because the generation of a landslide of one volume class from a given source area precludes the simultaneous generation of another landslide of a different volume class from that same source area. Also, a person, if present in a grid cell where they are killed by debris from a landslide of a given volume class, cannot be killed at the same time by debris sourcing from another landslide within the same volume class.

Therefore, Equation 3.3 is fine for individual landslides that occur independently of each other, for example, those that are triggered by non-earthquake events. However, for earthquake-induced landslides, it is possible that many landslides are triggered at the same time. To take this into account in the risk analysis, the probability of being in the path of a number of landslides ( $N$ ) of a given volume class, triggered by each earthquake band, is given by:

$$P_{VOL\_N(S:H)} = 1 - (1 - P_{VOL(S:H)})^{N\_EQ\_Band \ x} \quad \text{Equation 3.4}$$

Where  $N\_EQ\_Band \ x$  is the number of landslides within the given volume class that are triggered by the given earthquake band (Appendix 1).

### 3.2.4 Vulnerability: Probability that a Person is Killed, if Present and in the Path of Landslide Debris

The vulnerability ( $V$ ) is the probability of a person being killed, if present and in the path of a landslide, considering both: a) the likelihood of being killed if struck and b) the possibility of being able to take evasive action and avoid being struck. Physical vulnerability ( $V$ ) depends on the landslide intensity, the characteristics of the elements at risk and the impact of the landslide (Du et al. 2013).

This probability is expressed as vulnerability, the term used to describe the amount of damage that results from a particular degree of hazard. Vulnerability ranges between 0 and 1 and, for fatality risk, combines the likelihood of an injury sustained by the individual (if struck) being fatal (1) and the possibility of getting out of the way to avoid being struck.

Studies from Hong Kong (e.g. Finlay et al. 1999) summarised the vulnerability ranges and recommended likelihood of death 'if struck by rockfall'. The vulnerability of an individual in open space, if struck by a rockfall, is given as 0.1–0.7, with a recommended value of 0.5, assuming that it may be possible to get out of the way. There have been five known instances in the study area where people have been hit and injured by landslide debris, but nobody has died. During these near misses, it appears that the people heard the debris moving down the slope and had time to run away from the steeper cliffs towards the sea. Stantec (2020) describe the injuries from these impacts as all being confined to the lower body. From media accounts at the time, it appears the tourists that were hit by debris in 1988 and 2019 were on

the beach during Spring low tides, when the beach is wider, when trying to take evasive action by running away from the cliffs. At Neap tides, there is very little beach exposed, even at low tide, and so running away is not as easy.

Field observations of the landslides, coupled with newspaper accounts from the injured people, suggest that the landslide debris, upon hitting the cliff bottom, transitions into more of a flow (Stantec 2020), which, if entering the sea, could also create a pressure wave ahead of the moving debris. This pressure wave may account for why some of the injured people report being swept out to sea, and it may also account for why they were not killed by the large volumes of debris. If located at the cliff bottom, it is unlikely a person could take evasive action even if they were alerted to a landslide, especially if the landslide is large. This appears to have happened to the three workers in 1973, as one was partially buried (and the tractor and trailer were damaged), although the other two people managed to escape. The landslide was reported as being relatively large (Stantec 2020).

The ability of people to take evasive action depends mainly on the intensity of the landslide. Landslide intensity is a function of the volume of debris passing through a given location and its velocity. For this assessment, variable physical vulnerability values have been adopted to account for landslide intensity. These are listed in Table 3.9, which are linked to the size of the landslide and location on the beach.

Table 3.9 Physical vulnerability values used in the study.

Representative Landslide Volume (m <sup>3</sup> )	Vulnerability: Cliff Bottom	Vulnerability: Rockfall Limit and F-Angle Lines	Description
1	0.15	0.05	Debris limited in impact area. In the past, people have had time to observe and then take evasive action.
10	0.15	0.1	
100	0.3	0.15	Debris confined to the toe of steep slopes. In the past, people have had time to observe and then take evasive action, but it becomes increasingly more difficult to take evasive action given the volumes of boulders involved.
1000	0.3	0.2	
10,000	0.4	0.3	Debris starts to cover a large enough area to make it difficult to take evasive action.
25,000	0.5	0.5	
50,000	0.5	0.5	Given the large volume of debris, it is very unlikely that evasive action could be taken.
100,000	1.0	0.7	

To assess the sensitivity of the risk analysis results to changes in the vulnerability, we have also estimated the vulnerability using an event tree approach for a walker and group member on a tractor, separately. Adopting the formula:

$$V_{OVERALL} = [(1 - V1) + V1 \times V2] \times V3 \times V4 \quad \text{Equation 3.5}$$

The values were used for walkers and GBA group members irrespective of where they are located on the beach (Table 3.10 and Table 3.11).

Table 3.10 Physical vulnerability values for a walker on their own.

Representative Landslide Volume (m <sup>3</sup> )	Walker on Their Own				
	V1 Aware the landslide is moving before it reaches the beach	V2 Unable to get out of the way, given aware	V3 Hit if debris passes while in the way	V4 Killed if hit	OVERALL V Killed if would have been in path
1	0.50	0.20	1.00	0.25	0.15
10	0.60	0.30	1.00	0.40	0.23
100	0.70	0.40	1.00	0.60	0.35
1000	0.80	0.50	1.00	0.70	0.42
10,000	0.90	0.60	1.00	0.80	0.51
25,000	1.00	0.70	1.00	0.90	0.63
50,000	1.00	0.80	1.00	0.90	0.72
100,000	1.00	0.80	1.00	0.90	0.72

Table 3.11 Physical vulnerability values for a group member on a GBA tour.

Representative Landslide Volume (m <sup>3</sup> )	Group Member on a GBA Tour				
	V1 Aware the landslide is moving before it reaches the beach	V2 Unable to get out of the way, given aware	V3 Hit if debris passes while in the way	V4 Killed if hit	OVERALL V Killed if would have been in path
1	0.10	0.20	0.50	0.25	0.12
10	0.20	0.30	0.50	0.40	0.17
100	0.40	0.40	0.60	0.60	0.27
1000	0.60	0.50	0.70	0.70	0.34
10,000	0.80	0.60	0.80	0.80	0.44
25,000	1.00	0.70	0.90	0.90	0.57
50,000	1.00	0.80	0.90	0.90	0.65
100,000	1.00	0.80	0.90	0.90	0.65

V1: Accounts for diminished awareness. For example, a passenger on a tractor may not be able to hear the smaller landslides due to the noise of the engine or surf. However, this is potentially mitigated by the height of the trailer (V3). However, a passenger on a GBA tour will be with an experienced guide, who knows the area well and what to look for. A walker on their own, who may only visit the site once in a lifetime, will not have such awareness or local knowledge.

V2: This would vary for Neap and Spring tides, as there is more beach to run down before hitting the sea, away from any landslide.

V3: It is less likely a person on a tractor would be hit by smaller landslides, as they are elevated above them. The tractor operators do drive out into the sea if they notice something falling from the cliffs. These values allow for some protective effect of the tractor or trailer.

V4: Is linked to increasing landslide intensity associated with increasing landslide volume.

### 3.2.5 Local Personal Risk

The LPR is calculated by assuming a person is present in every grid cell 100% of the time, and it is calculated for each grid cell using the following steps:

#### 3.2.5.1 For Earthquake-Induced Landslides

- **Step 1:** This is calculated for landslides in each volume class and within each earthquake band, from Equation 3.4. The probability of death ( $P_{DEATH}$ ) for a given landslide volume within a given earthquake band is then multiplied by the vulnerability ( $V$ ) value (Tables 3.9–3.11) for  $P_{VOL\_N(S:H)}$  values calculated at the cliff bottom, rockfall limit line and F-angle line, where:

$$P_{DEATH:VOL\_N\_Band\ x} = P_{VOL\_N(S:H)} \times V \quad \text{Equation 3.6}$$

- **Step 2:** These values are then attached in ArcGIS to the relevant cliff bottom, rockfall limit line and F-angle lines for each landslide volume class within each earthquake band.  $P_{DEATH}$  is then modelled (interpolated) between the lines, using the ArcGIS natural neighbour function, to produce grids of  $P_{DEATH}$  for each volume class of landslide for each earthquake band.
- **Step 3:** To account for the possibility that multiple landslides of different volumes could be triggered at the same time by an earthquake, the probability of being in the path of any landslide within the earthquake band is therefore given by:

$$P_{DEATH:ALL\_Band\ x} = 1 - (1 - P_{DEATH:VOL\_1}) \times (1 - P_{DEATH:VOL\_10}) \times (1 - P_{DEATH:VOL\_100}) \times (1 - P_{DEATH:VOL\_n...}) \quad \text{Equation 3.7}$$

$P_{DEATH:ALL\_Band\ x}$  is calculated in ArcGIS per earthquake band by overlaying the  $P_{DEATH:VOL\_N\_Band\ x}$  grids for each landslide volume class within each band and sampling the values for all landslide volume classes within the given grid cell.

- **Step 4:**  $P_{DEATH:ALL\_Band\ x}$  is then multiplied by the annual frequency ( $Af$ ) of the representative earthquake PGA for the given band (Table 3.4) to calculate the LPR at each grid cell for each band, where:

$$LPR_{Band\ x} = P_{DEATH:ALL\_Band\ x} \times Af_{Band\ x} \quad \text{Equation 3.8}$$

- **Step 5:** The  $LPR_{Band\ x}$  values are added together for each grid cell to create a grid of  $LPR_{Total}$  for the lower and upper estimates of the number of landslides of a given volume occurring within each earthquake band.

#### 3.2.5.2 For Non-Earthquake-Induced Landslides

- **Step 1:** Calculate the annual frequency ( $Af_{Vol\ x}$ ) of being in the path of a landslide of a given volume at the cliff bottom, rockfall limit line and F-angle line within each hazard area using Equation 3.3. Multiply  $P_{VOL(S:H)}$  by the annual frequencies in Table 3.5 to derive  $Af_{Vol\ x}$ .
- **Step 2:** Multiply  $Af_{Vol\ x}$  by the relevant vulnerability factor from Tables 3.9–3.11 to calculate the LPR at the cliff bottom, rockfall limit line and F-angle line for the given volume class, within the given hazard area.

- **Step 3:** These values are then attached in ArcGIS to the relevant cliff bottom, rockfall limit line and F-angle lines for each landslide volume class. The  $LPR_{VOL:x}$  is then modelled (interpolated) between the lines, using the ArcGIS natural neighbour function, to produce grids of  $LPR_{VOL:x}$  for each volume class of landslide.
- **Step 4:** The  $LPR_{VOL:x}$  values are added together for each grid cell to create a grid of  $LPR_{Total}$  for the lower and upper estimates of landslide annual frequency.

### 3.2.6 Probability that a Person is Present

$P_{(T:S)}$  is the probability an individual is present in the portion of the slope when a landslide moves through it. It is a function of the proportion of time spent by a person at a location each day and can range from 0%, if the person is not present, to 100%, if the person is present all of the time.

For planning and regulatory purposes, it is established practice to consider individual risk to a 'critical group' of people that are more highly exposed to risk. For example, GBA and DOC staff carry out more trips per year than a visitor who may only do one trip a year or, more likely, one trip per lifetime. Therefore, the amount of time that GBA and DOC staff and visitors spend in the study area, and therefore are exposed to landslide hazards, will vary greatly. For this assessment, information on the time visitors and DOC and GBA staff spend in the study area was taken from Stantec (2020). While it is acknowledged that people could walk anywhere within the narrow confines of the beach, for this analysis, two main routes to travel from the start of the beach to the gannet colony were digitised, one at Neap tide and one at Spring tide. The Neap tide route was walked and driven (by the GBA operator) by several of the authors in 2020. The Spring tide route is assumed to be 20 m further out to sea from the Neap tide route (Figure 3.7). Both routes are thought to be representative of the typical route people may take along the beach.

The sensitivity of the risk analysis results has been assessed to a range of values representing the most exposed (upper) and average (lower) exposure to a person on a route, for visitors and GBA and DOC staff, based on the information in Stantec (2020) and assumptions about how long a person takes to walk or drive a given route (Table 3.12).

When a person is on the beach, they will spend time walking or driving along a given route, and the length of each route will vary slightly per trip depending on local conditions at the time. The representative routes were overlain on the LPR scenarios (based on the 3 m by 3 m grid cells), and the LPRs from each scenario per 3 m sections along each track/road were then sampled.

The probability that a person will be occupying a given grid cell along one of the routes if they spend a number of hours ( $N_{HRS}$ ) walking or driving that route can be expressed as:

$$P_{(T:S)} = \frac{(N_{HRS})}{(N_C)} \quad \text{Equation 3.9}$$

Where ( $N_C$ ) is the number of cells visited along the route.



Table 3.12 Exposure data.

Name	Lower	Upper	Units	Comments
<b>GBA Operator</b>				
Operates	7	8	Months per year	
April and October	15	20	Trips per month	
Other months	20	25	Trips per month	
Person most exposed	130	150	Trips per year	Exposed on the beach
Time per trip	1.75	2.1	Hours per trip	Staff and tourists
Number of trips	1	2	Trips per day	
GBA passengers	7000	11,000	Passengers per year	Based on GBA data and DOC track counter data
GBA passengers	1.75	2.1	Hours per trip	Exposed on the beach
Length of time operating	67		Years	
GBA passengers	27	200	Per tour	Average and maximum
GBA total estimate of passengers over the years	400,000	500,000	Total trips made	Loose estimate
<b>Walkers</b>				
Annual walkers during season	1200	2000	Per year	Based on GBA data and DOC track counter data
Walkers during season	12	26	Walks per day	
Walkers during season	107	179	Walks per week	
Walkers during season	2	10	Walkers per group	
Walkers during season	3.5	4	Hours per trip	Exposed on the beach
Local walker	1	2	Hours per trip	
Local walker	20	30	Trips per year	Possibly an overestimate
Total number of walkers	100,000		Past 50 years	Loose estimate
<b>DOC Worker (Including HDC Staff and HDC and DOC Contractors)</b>				
Person most exposed	2	4	Hours per trip	From DOC data
Person most exposed	4	6	Trips per year	From DOC data

## 4.0 RISK ANALYSIS RESULTS

The results are presented in terms of LPR (Section 4.1), AIFR (Section 4.2) and societal risk (Section 4.3). Commentary on the consistency of these results with actual experience in the study area is provided in Section 4.4.

The risk metrics calculated in this study are generally very small numbers, with large uncertainties. This report makes extensive use of the scientific number format of expressing risk in terms of powers of ten. For example, the number  $10^{-4}$  (10 to the power of minus 4) is the fraction 1/10,000, and the decimal number 0.0001; it may also be expressed as 0.01%. The units of risk are a dimensionless probability of a given outcome (e.g. death) per unit of activity or time. The units of AIFR are probability of fatality (death or loss of life, but in this report also include life-threatening injury) per year.

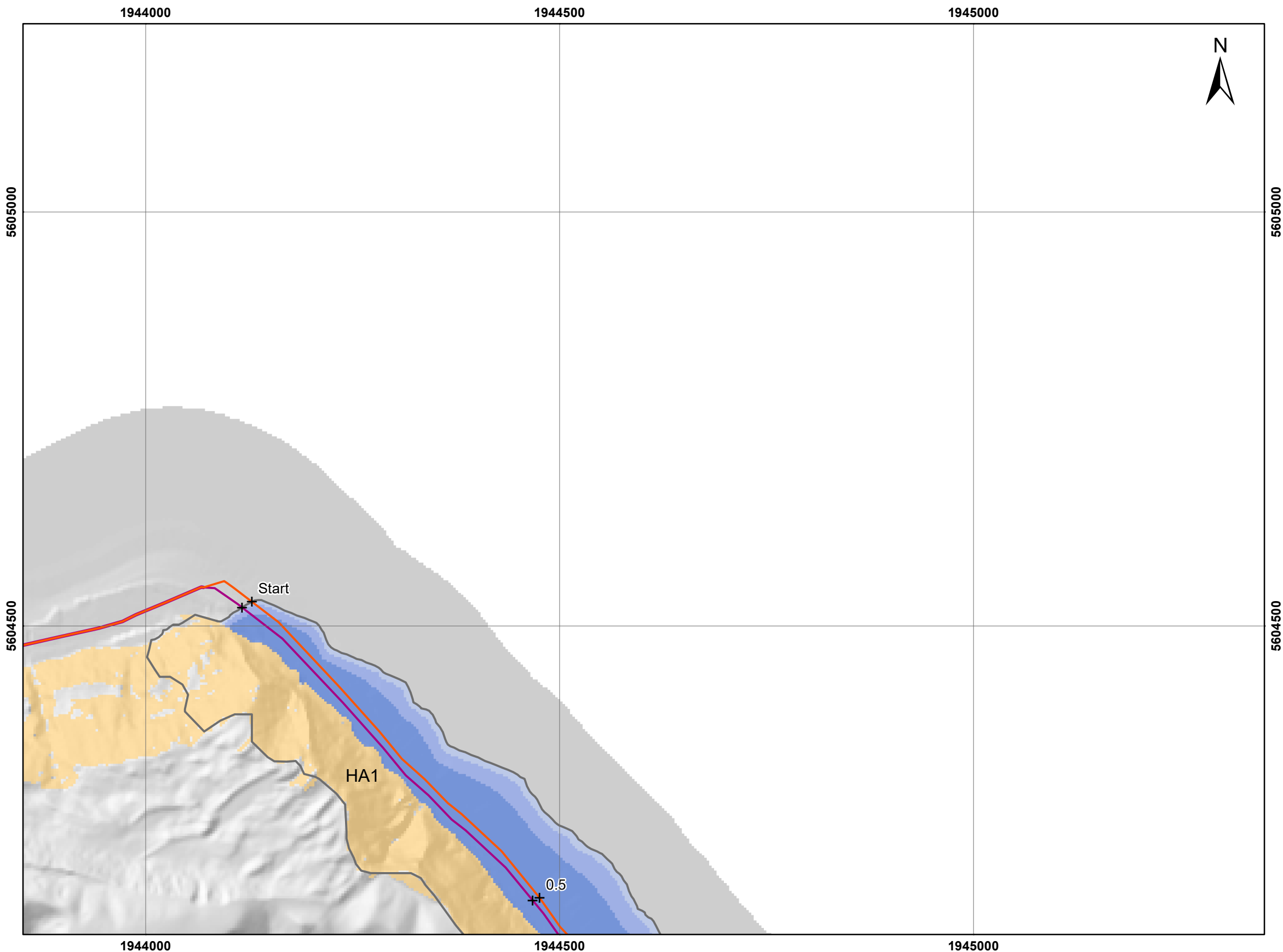
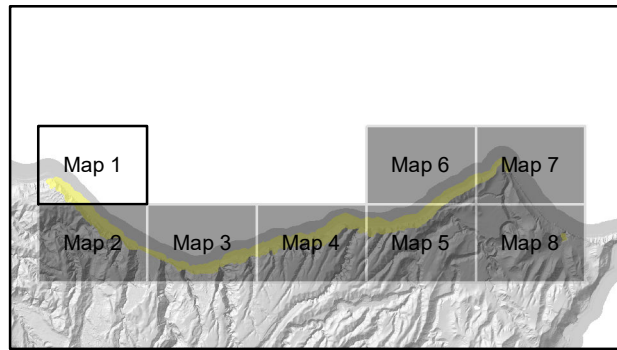
The risks presented in this section of the report do not include any consideration of the potential reduction in risk caused by the control measures that are currently in place.

### 4.1 The Local Personal Risk

Maps showing the LPR, which represents the annual probability of death for an imaginary person present in a particular grid cell within the study area (24 hours a day and 365 days of the year), are shown for the study area in Figure 4.1. These figures show the LPR for:

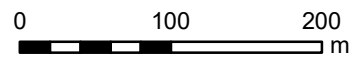
- A) Earthquake-induced landslides only.
- B) Non-earthquake-induced landslides only.
- C) Both earthquake- and non-earthquake-induced landslides.

The contribution to the LPR from earthquake- and non-earthquake-induced landslides is shown in Figure 4.1 (a–c) as the lower and upper estimates of the annual frequency (number of landslides per year) of landslides of a given volume being generated by earthquake and non-earthquake triggers.



- Simulated landslide source area  
(slopes  $\geq 30^\circ$ )
- Local personal risk**
- $10^{-1}$  to  $10^{-2}$
- $10^{-2}$  to  $10^{-3}$
- $10^{-3}$  to  $10^{-4}$
- $10^{-4}$  to  $10^{-5}$
- Less than  $10^{-5}$
- Spring tide route
- Neap tide route
- + Distance along the route (km)
- Hazard area
- DOC Reserve

SCALE BAR:



EXPLANATION:

Background shade model derived from a LiDAR based Digital Elevation Model (1m ground resolution) which was resampled to 3 m for the analysis

PROJECTION: New Zealand Transverse Mercator 2000

DRW:  
BL  
CHK:  
CM, SDV



**LOCAL PERSONAL RISK**  
**from earthquake induced landslides only**

**Cape Kidnappers**

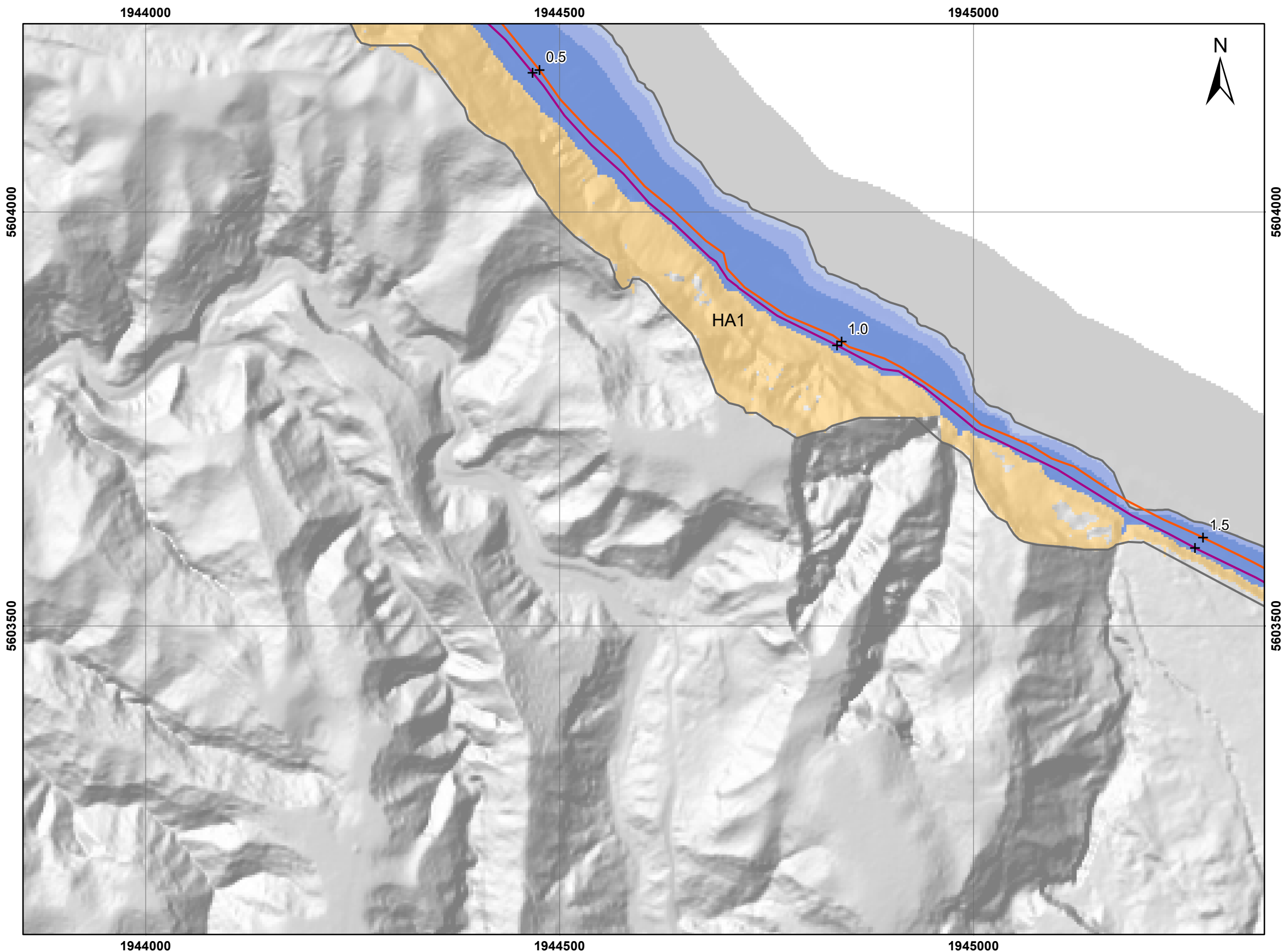
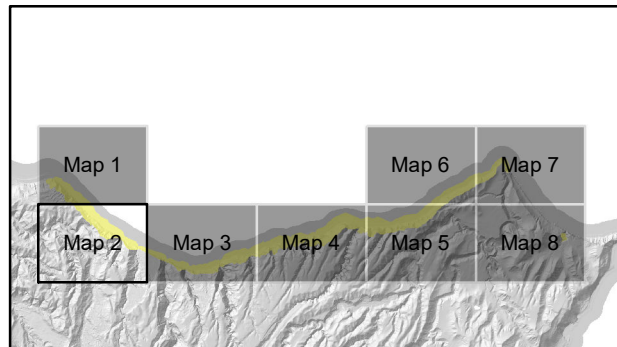
**FIGURE 4.1a**


Map 1

**FINAL**






REPORT:  
CR2020/28

DATE:  
May 2020



 Simulated landslide source area  
(slopes  $\geq 30^\circ$ )

**Local personal risk**

-   $10^{-1}$  to  $10^{-2}$
-   $10^{-2}$  to  $10^{-3}$
-   $10^{-3}$  to  $10^{-4}$
-   $10^{-4}$  to  $10^{-5}$
-  Less than  $10^{-5}$

 Spring tide route

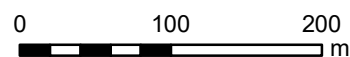
 Neap tide route

 Distance along the route (km)

 Hazard area

 DOC Reserve

SCALE BAR:



EXPLANATION:

Background shade model derived from a LiDAR based Digital Elevation Model (1m ground resolution) which was resampled to 3 m for the analysis

PROJECTION: New Zealand Transverse Mercator 2000

DRW:  
BL  
CHK:  
CM, SDV



**LOCAL PERSONAL RISK**  
**from earthquake induced landslides only**

**Cape Kidnappers**

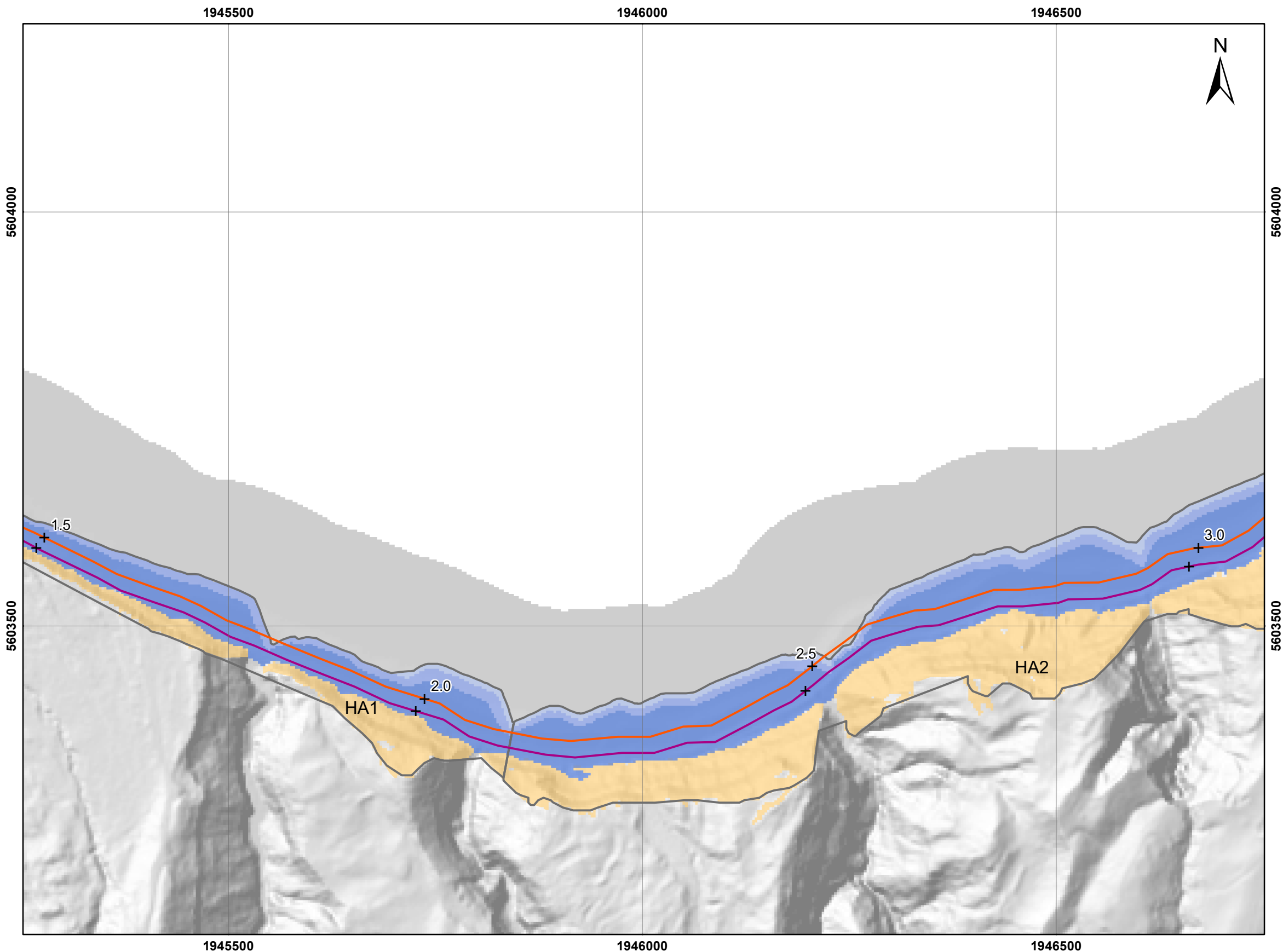
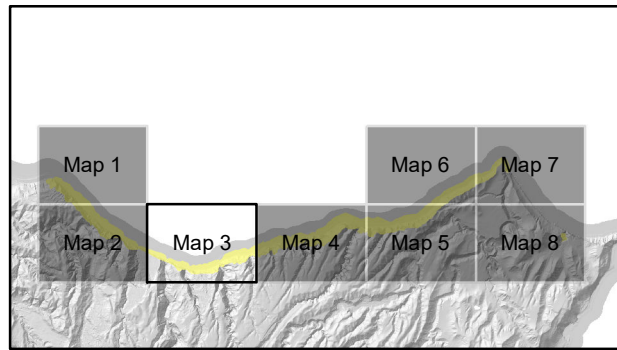
**FIGURE 4.1a**

Map 2

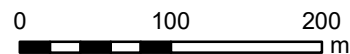
**FINAL**

REPORT:  
CR2020/28

DATE:  
May 2020



SCALE BAR:



EXPLANATION:

Background shade model derived from a LiDAR based Digital Elevation Model (1m ground resolution) which was resampled to 3 m for the analysis

PROJECTION: New Zealand Transverse Mercator 2000

DRW:  
BL  
CHK:  
CM, SDV



**LOCAL PERSONAL RISK**  
**from earthquake induced landslides only**

**Cape Kidnappers**

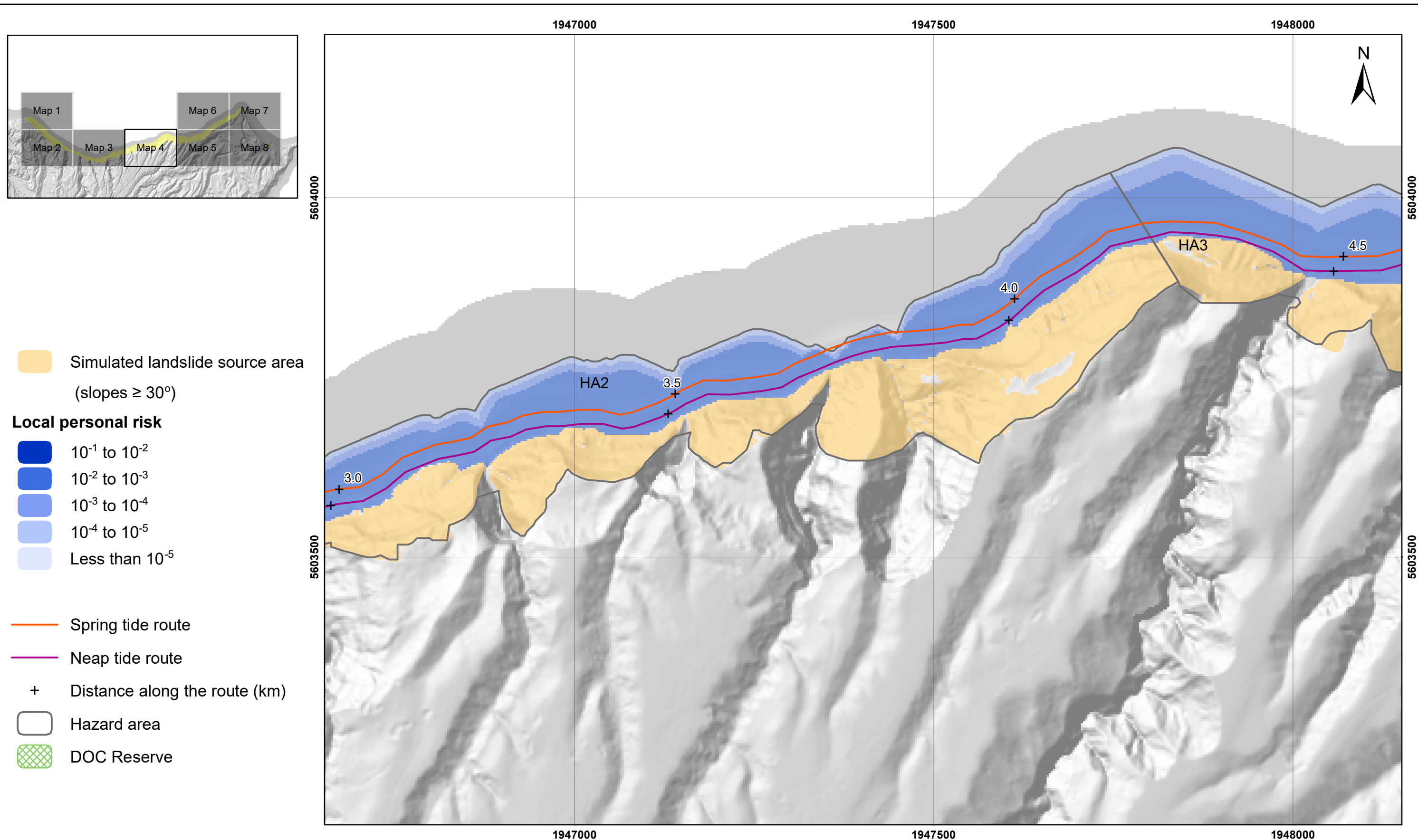
**FIGURE 4.1a**

Map 3

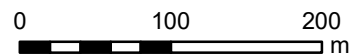
**FINAL**

REPORT:  
CR2020/28

DATE:  
May 2020



SCALE BAR:



EXPLANATION:

Background shade model derived from a LiDAR based Digital Elevation Model (1m ground resolution) which was resampled to 3 m for the analysis

PROJECTION: New Zealand Transverse Mercator 2000

DRW:  
BL  
CHK:  
CM, SDV



**LOCAL PERSONAL RISK**  
**from earthquake induced landslides only**

**Cape Kidnappers**

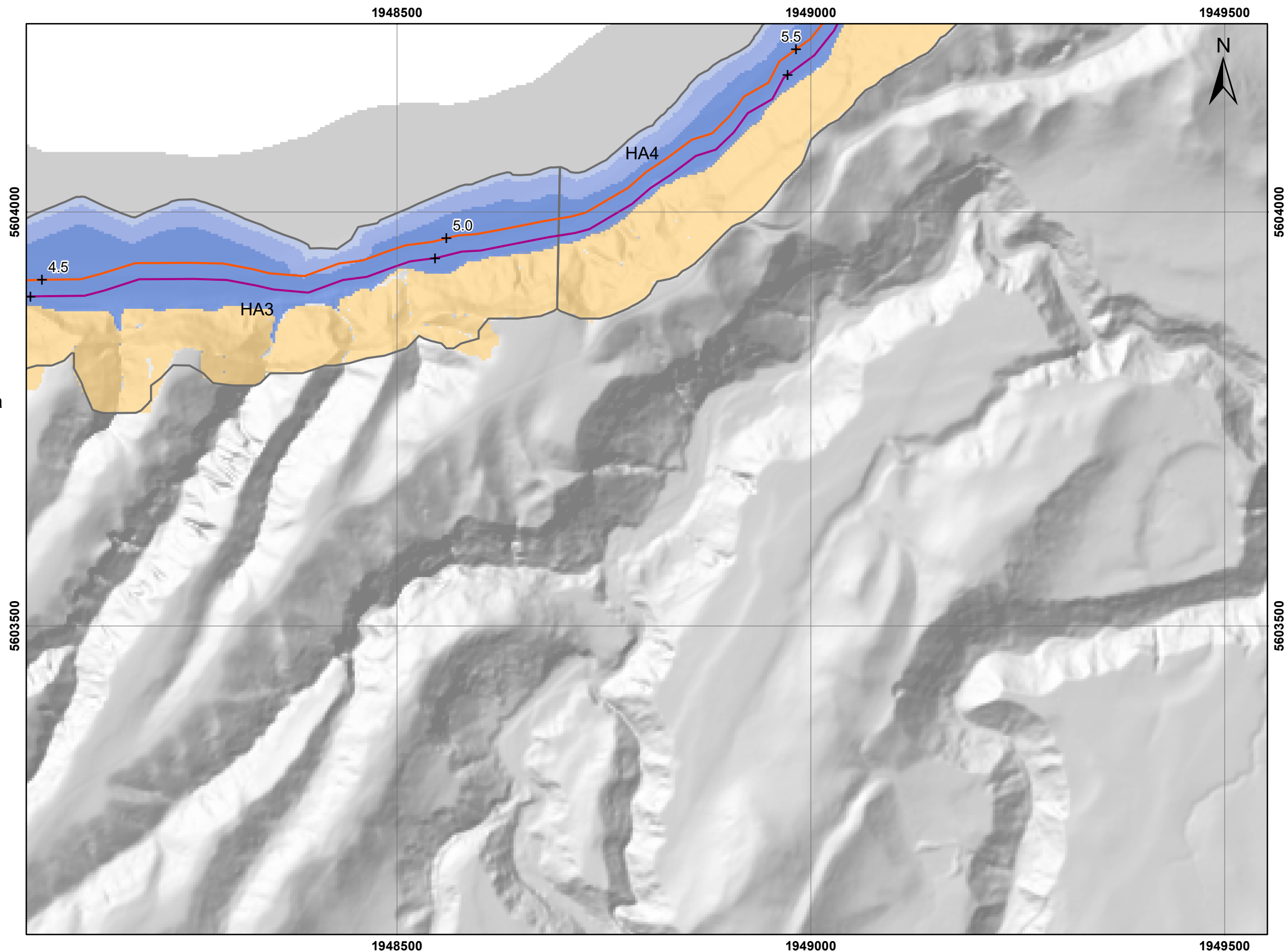
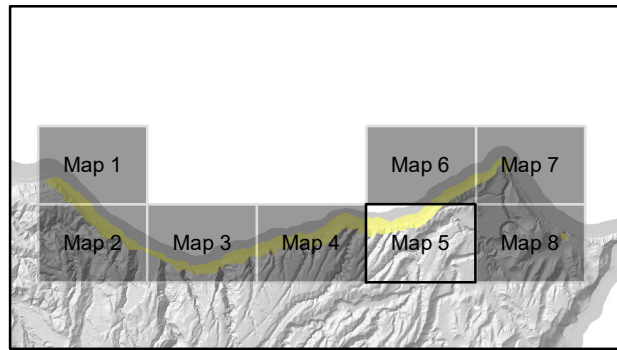
**FIGURE 4.1a**


Map 4

**FINAL**






REPORT:  
CR2020/28


DATE:  
May 2020



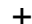
 Simulated landslide source area  
(slopes  $\geq 30^\circ$ )

**Local personal risk**

-   $10^{-1}$  to  $10^{-2}$
-   $10^{-2}$  to  $10^{-3}$
-   $10^{-3}$  to  $10^{-4}$
-   $10^{-4}$  to  $10^{-5}$
-  Less than  $10^{-5}$

 Spring tide route

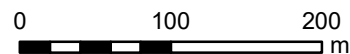
 Neap tide route

 Distance along the route (km)

 Hazard area

 DOC Reserve

SCALE BAR:



EXPLANATION:

Background shade model derived from a LiDAR based Digital Elevation Model (1m ground resolution) which was resampled to 3 m for the analysis

PROJECTION: New Zealand Transverse Mercator 2000

DRW:  
BL  
CHK:  
CM, SDV



**LOCAL PERSONAL RISK**  
**from earthquake induced landslides only**

**Cape Kidnappers**

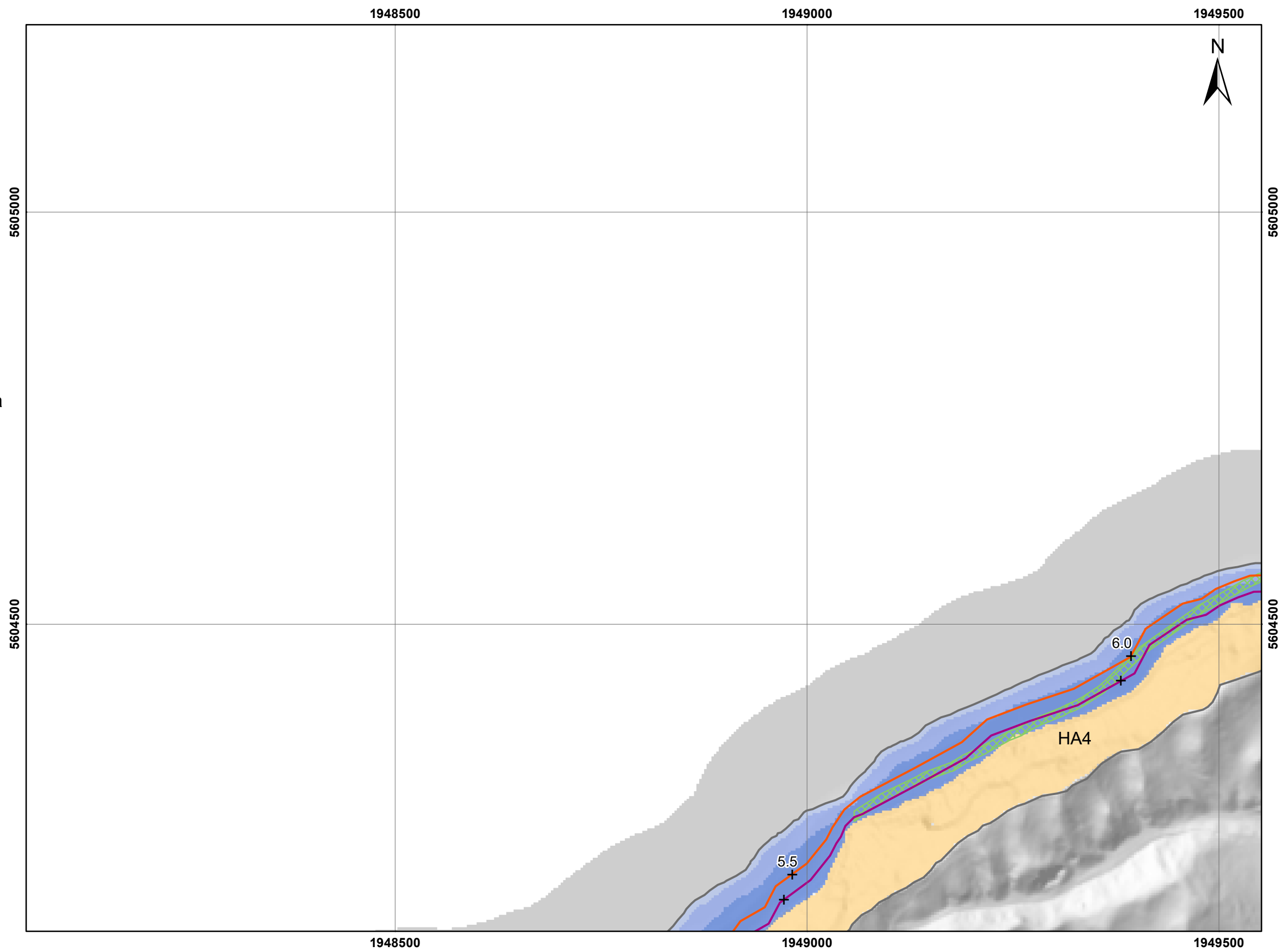
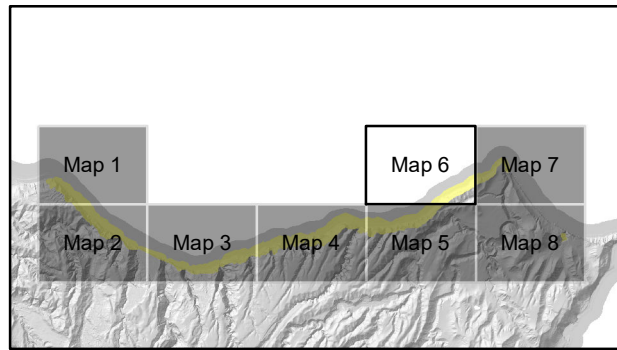
**FIGURE 4.1a**

Map 5

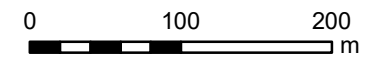
**FINAL**

REPORT:  
CR2020/28

DATE:  
May 2020



- Simulated landslide source area  
(slopes  $\geq 30^\circ$ )
- Local personal risk**
- $10^{-1}$  to  $10^{-2}$
- $10^{-2}$  to  $10^{-3}$
- $10^{-3}$  to  $10^{-4}$
- $10^{-4}$  to  $10^{-5}$
- Less than  $10^{-5}$
- Spring tide route
- Neap tide route
- + Distance along the route (km)
- Hazard area
- DOC Reserve



DRW:  
BL

CHK:  
CM, SDV



**LOCAL PERSONAL RISK**  
**from earthquake induced landslides only**

**Cape Kidnappers**

**FIGURE 4.1a**

Map 6

**FINAL**

REPORT: CR2020/28      DATE: May 2020

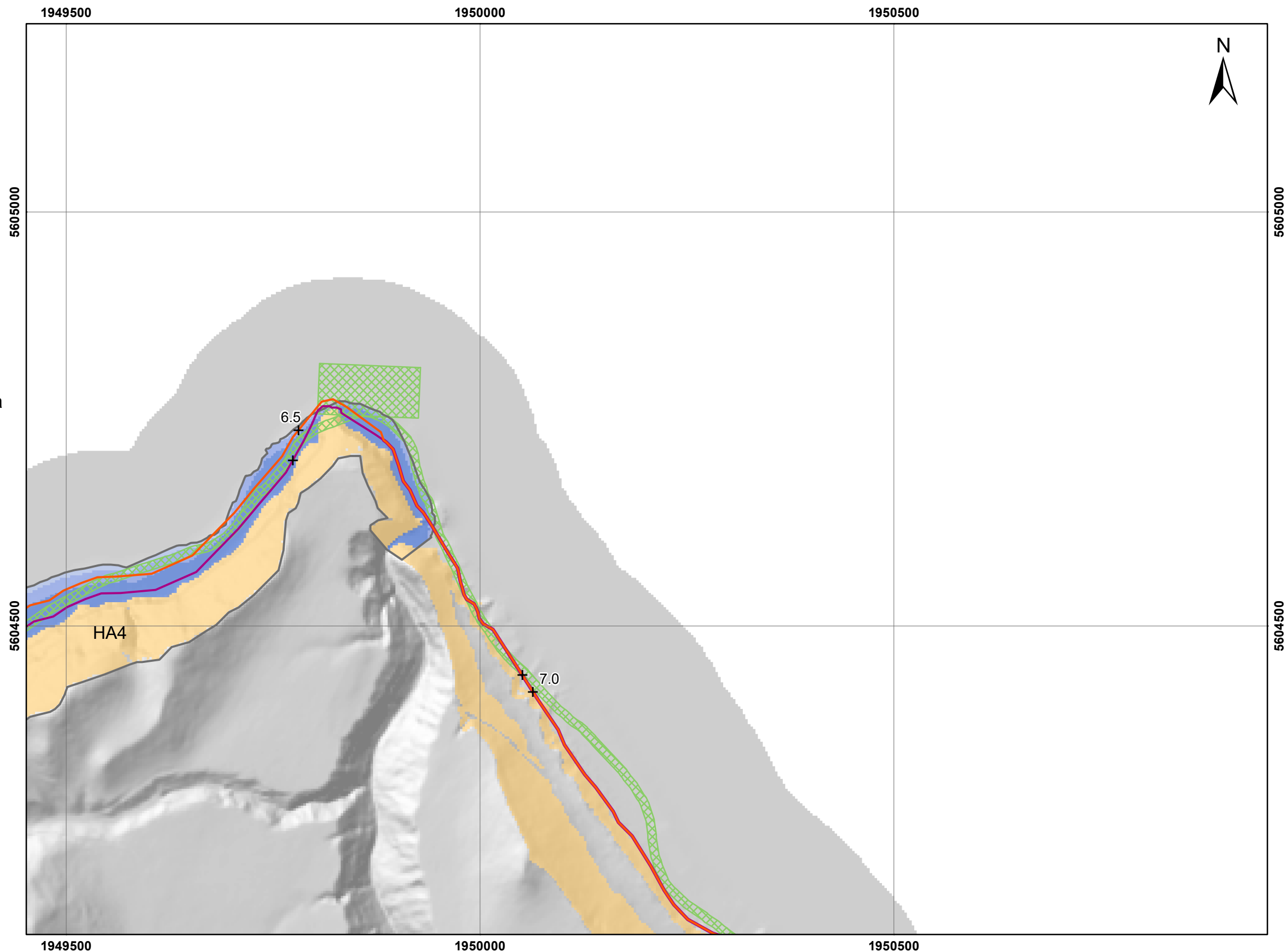
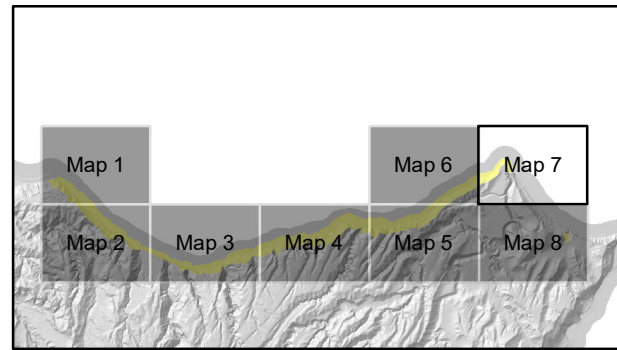
SCALE BAR:

EXPLANATION:

Background shade model derived from a LiDAR based Digital Elevation Model (1m ground resolution) which was resampled to 3 m for the analysis

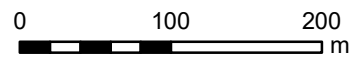
PROJECTION: New Zealand Transverse Mercator 2000





- Simulated landslide source area  
(slopes  $\geq 30^\circ$ )
- Local personal risk**
- $10^{-1}$  to  $10^{-2}$
- $10^{-2}$  to  $10^{-3}$
- $10^{-3}$  to  $10^{-4}$
- $10^{-4}$  to  $10^{-5}$
- Less than  $10^{-5}$
- Spring tide route
- Neap tide route
- + Distance along the route (km)
- Hazard area
- DOC Reserve

SCALE BAR:



EXPLANATION:

Background shade model derived from a LiDAR based Digital Elevation Model (1m ground resolution) which was resampled to 3 m for the analysis

PROJECTION: New Zealand Transverse Mercator 2000

DRW:  
BL  
CHK:  
CM, SDV



**LOCAL PERSONAL RISK  
from earthquake induced landslides only**

**Cape Kidnappers**

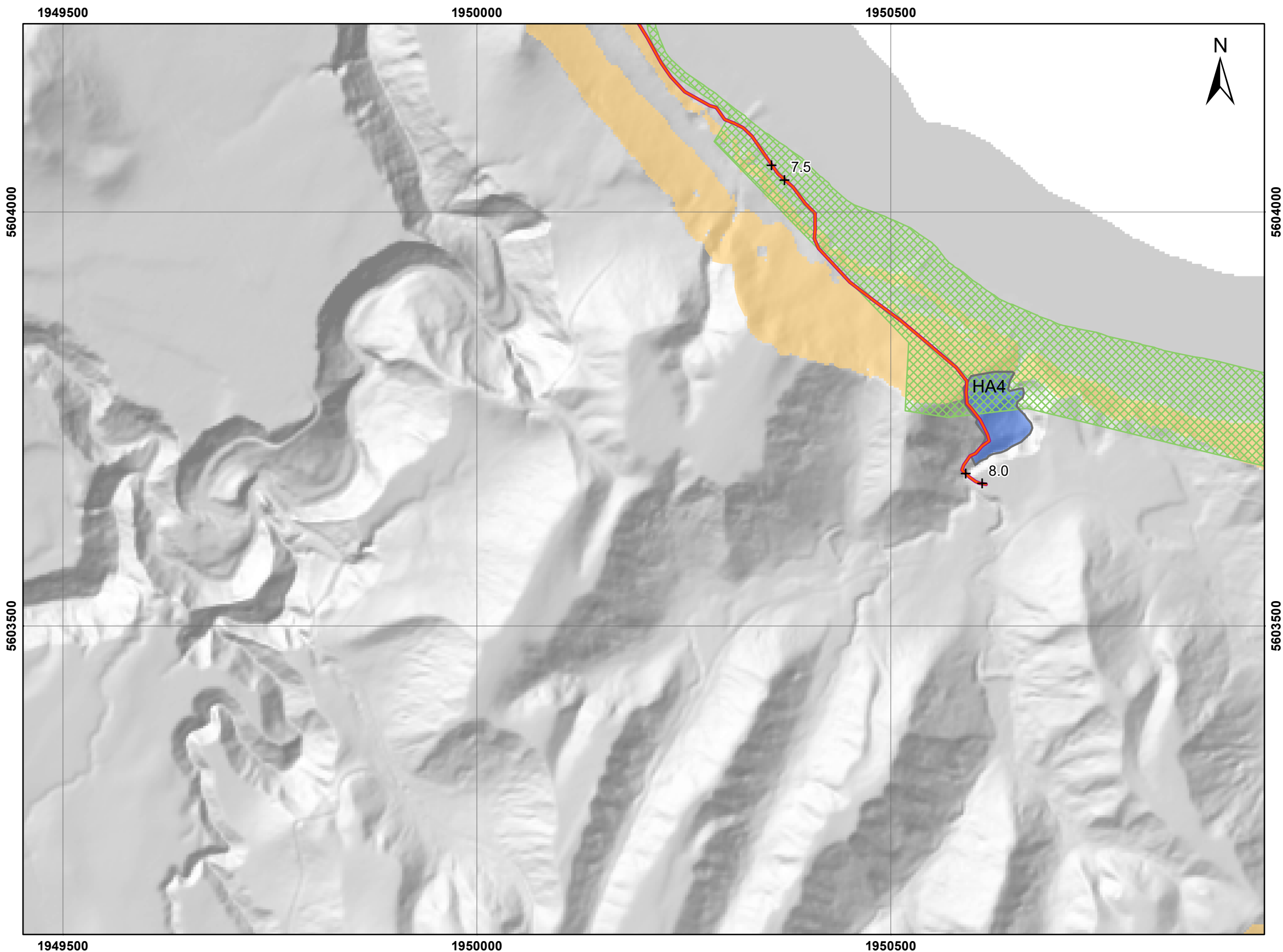
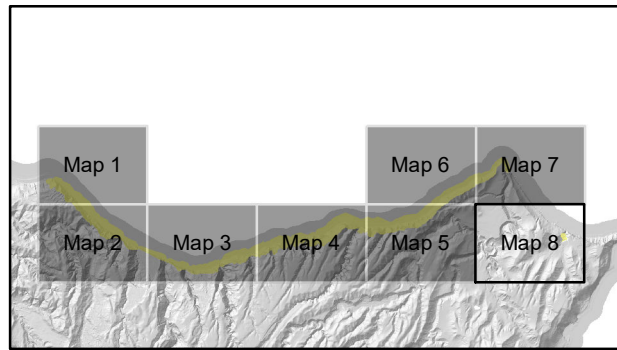
**FIGURE 4.1a**

Map 7

**FINAL**

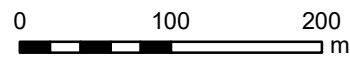
REPORT:  
CR2020/28

DATE:  
May 2020



- Simulated landslide source area (slopes  $\geq 30^\circ$ )
- Local personal risk**
- $10^{-1}$  to  $10^{-2}$
- $10^{-2}$  to  $10^{-3}$
- $10^{-3}$  to  $10^{-4}$
- $10^{-4}$  to  $10^{-5}$
- Less than  $10^{-5}$
- Spring tide route
- Neap tide route
- + Distance along the route (km)
- Hazard area
- DOC Reserve

SCALE BAR:



EXPLANATION:

Background shade model derived from a LiDAR based Digital Elevation Model (1m ground resolution) which was resampled to 3 m for the analysis

PROJECTION: New Zealand Transverse Mercator 2000

DRW:  
BL  
CHK:  
CM, SDV



**LOCAL PERSONAL RISK**  
**from earthquake induced landslides only**

**Cape Kidnappers**

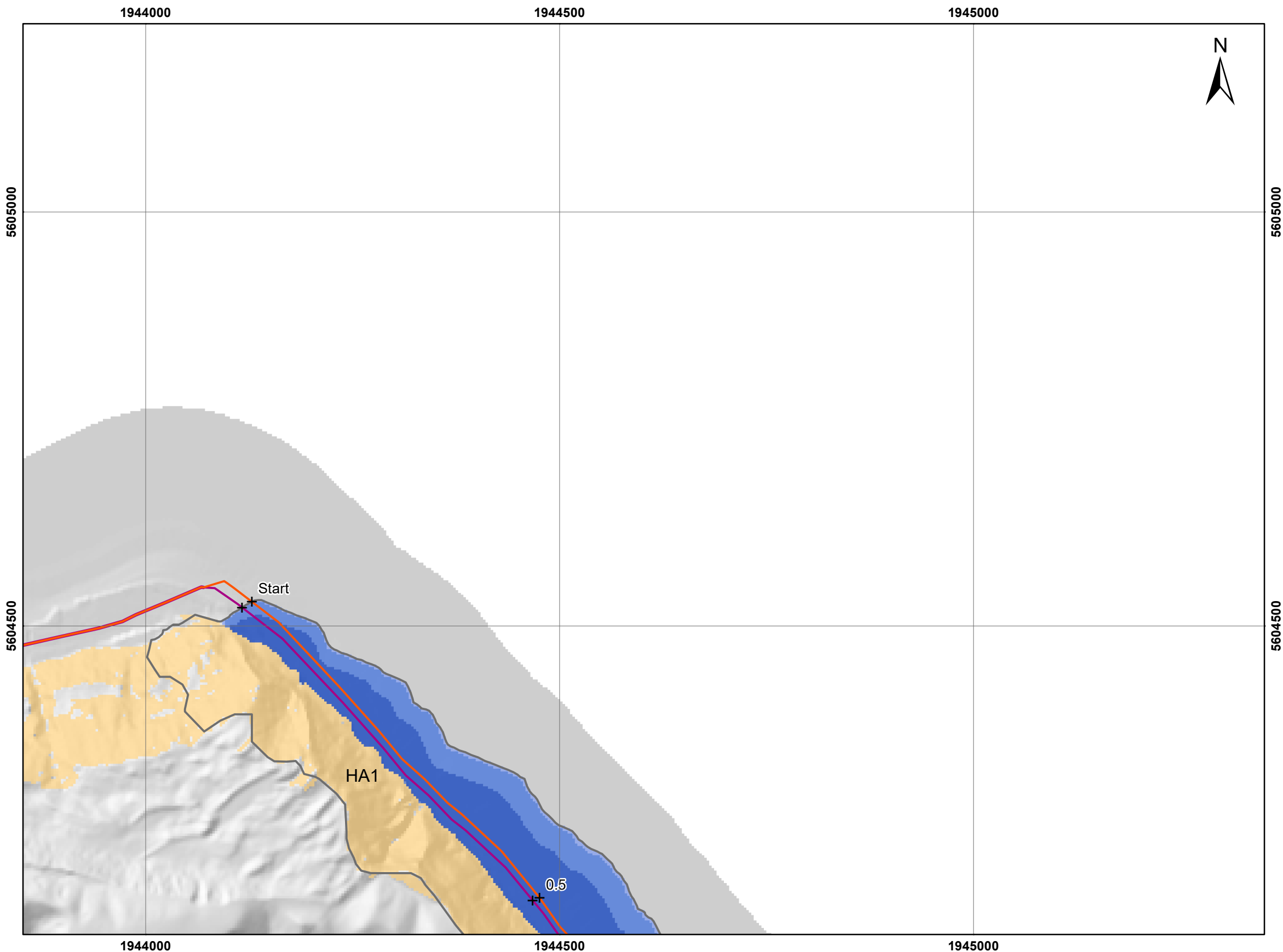
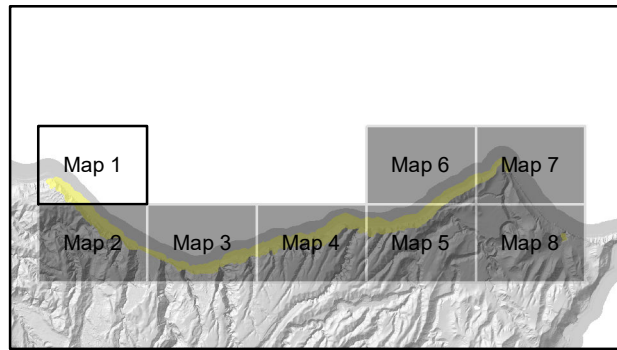
**FIGURE 4.1a**

Map 8

**FINAL**

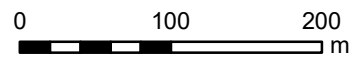
REPORT:  
CR2020/28

DATE:  
May 2020



- Simulated landslide source area  
(slopes  $\geq 30^\circ$ )
- Local personal risk**
- $10^{-1}$  to  $10^{-2}$
- $10^{-2}$  to  $10^{-3}$
- $10^{-3}$  to  $10^{-4}$
- $10^{-4}$  to  $10^{-5}$
- Less than  $10^{-5}$
- Spring tide route
- Neap tide route
- + Distance along the route (km)
- Hazard area
- DOC Reserve

SCALE BAR:



EXPLANATION:

Background shade model derived from a LiDAR based Digital Elevation Model (1m ground resolution) which was resampled to 3 m for the analysis

PROJECTION: New Zealand Transverse Mercator 2000

DRW:  
BL  
CHK:  
CM, SDV



**LOCAL PERSONAL RISK**  
from non-earthquake induced landslides only

**Cape Kidnappers**

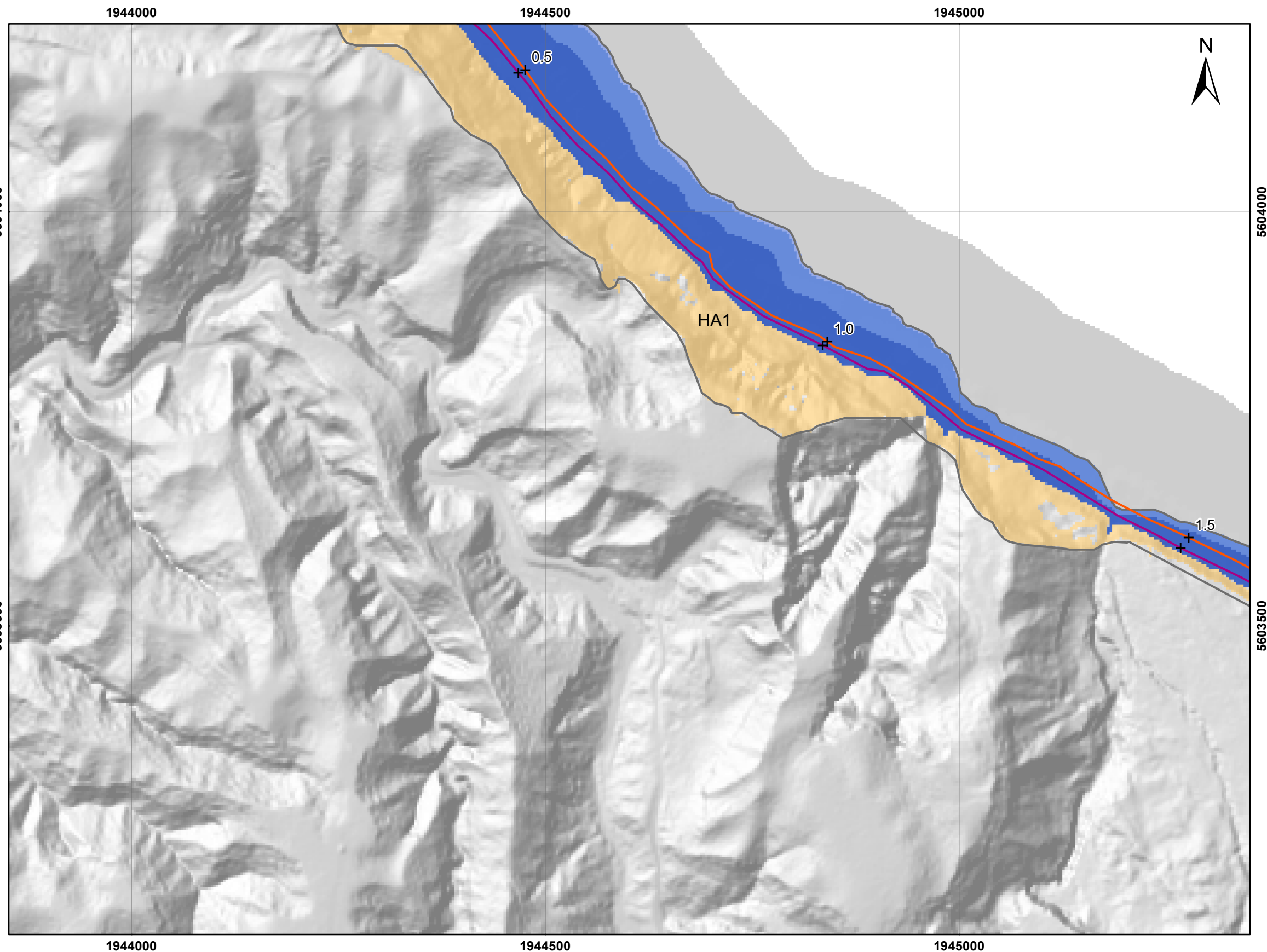
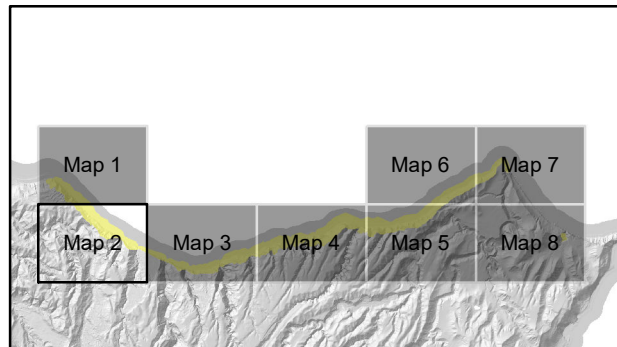
**FIGURE 4.1b**


Map 1

**FINAL**






REPORT:  
CR2020/28

DATE:  
May 2020



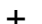
 Simulated landslide source area  
(slopes  $\geq 30^\circ$ )

**Local personal risk**

-   $10^{-1}$  to  $10^{-2}$
-   $10^{-2}$  to  $10^{-3}$
-   $10^{-3}$  to  $10^{-4}$
-   $10^{-4}$  to  $10^{-5}$
-  Less than  $10^{-5}$

 Spring tide route

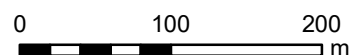
 Neap tide route

 Distance along the route (km)

 Hazard area

 DOC Reserve

SCALE BAR:



EXPLANATION:

Background shade model derived from a LiDAR based Digital Elevation Model (1m ground resolution) which was resampled to 3 m for the analysis

PROJECTION: New Zealand Transverse Mercator 2000

DRW:  
BL

CHK:  
CM, SDV



**LOCAL PERSONAL RISK**  
**from non-earthquake induced landslides only**

**Cape Kidnappers**

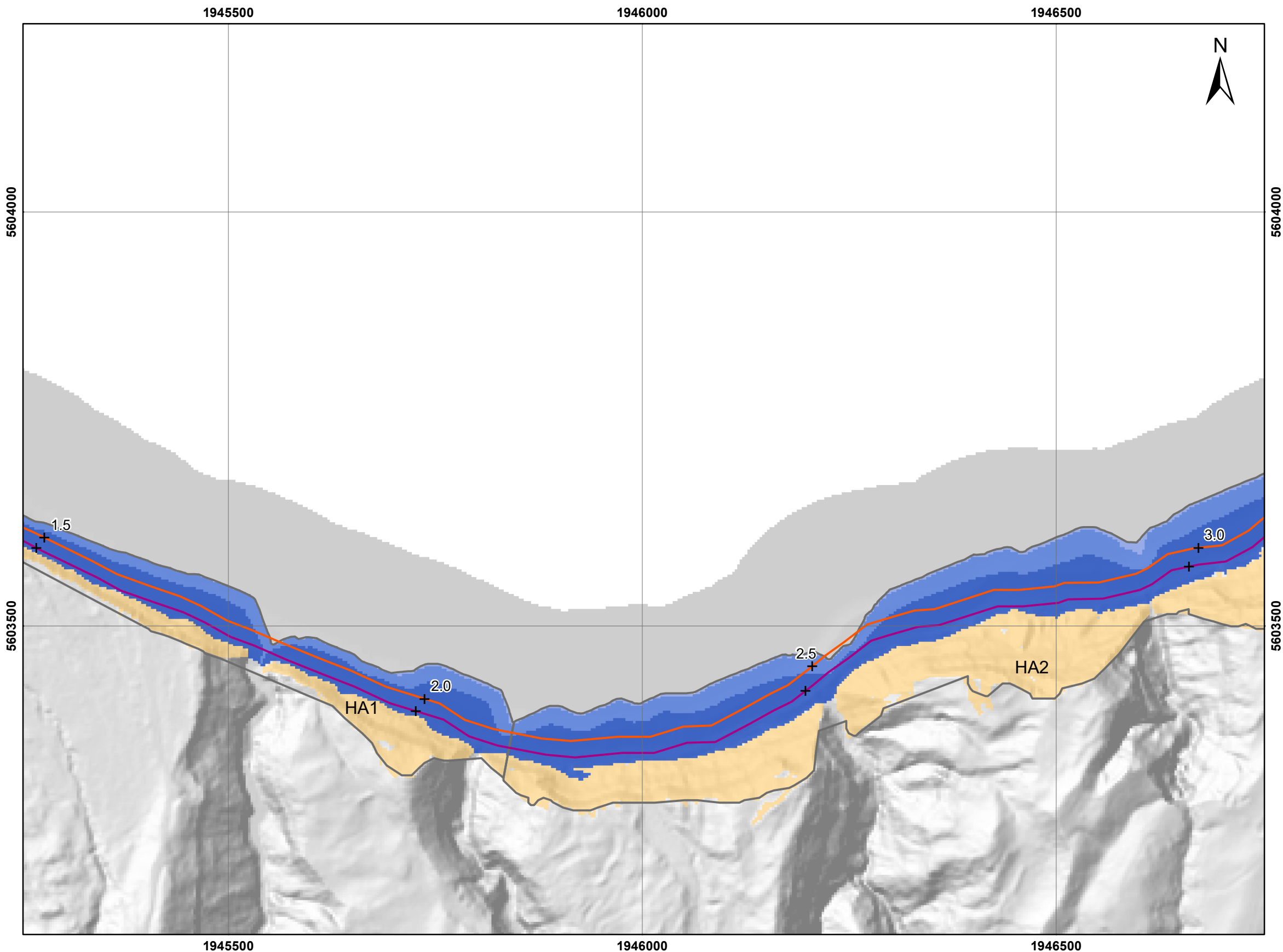
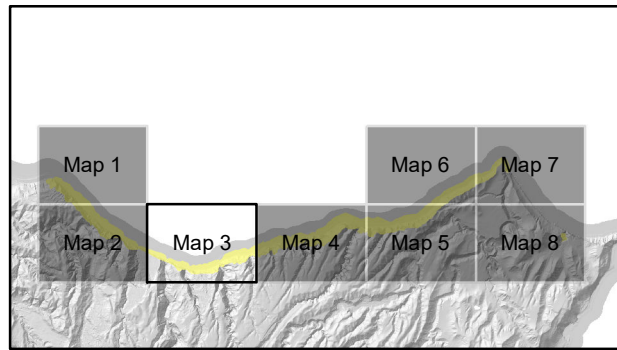
**FIGURE 4.1b**

Map 2

**FINAL**

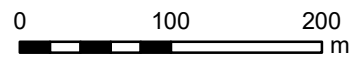
REPORT:  
CR2020/28

DATE:  
May 2020



- Simulated landslide source area (slopes  $\geq 30^\circ$ )
- Local personal risk**
- $10^{-1}$  to  $10^{-2}$
- $10^{-2}$  to  $10^{-3}$
- $10^{-3}$  to  $10^{-4}$
- $10^{-4}$  to  $10^{-5}$
- Less than  $10^{-5}$
- Spring tide route
- Neap tide route
- + Distance along the route (km)
- Hazard area
- DOC Reserve

SCALE BAR:



EXPLANATION:

Background shade model derived from a LiDAR based Digital Elevation Model (1m ground resolution) which was resampled to 3 m for the analysis

PROJECTION: New Zealand Transverse Mercator 2000

DRW:  
BL  
CHK:  
CM, SDV



**LOCAL PERSONAL RISK**  
**from non-earthquake induced landslides only**

**Cape Kidnappers**

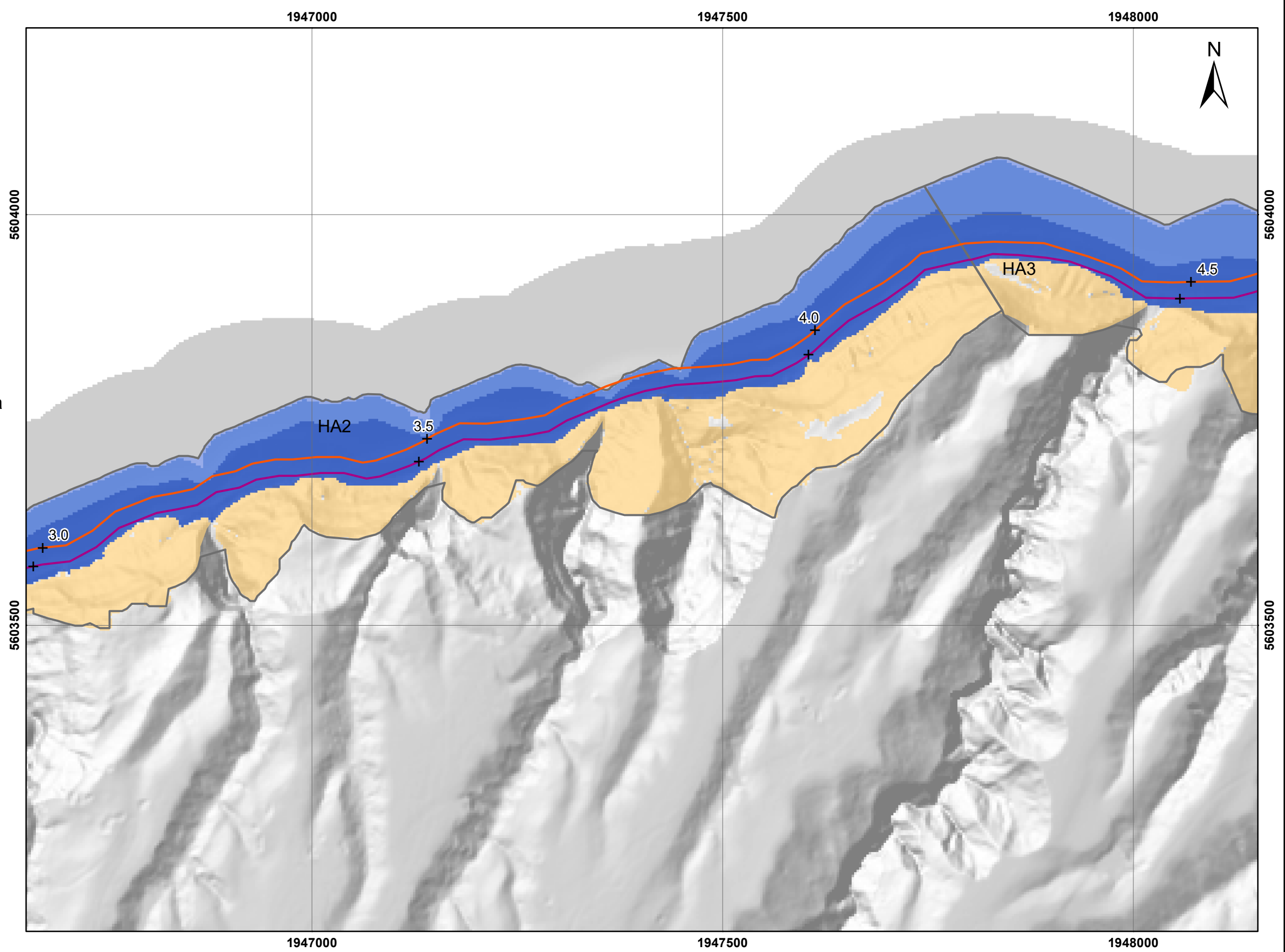
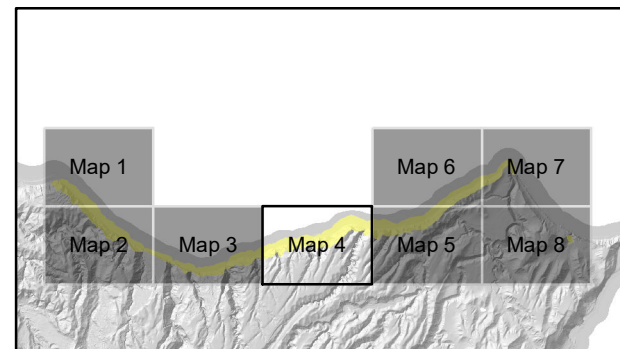
**FIGURE 4.1b**

Map 3

**FINAL**

REPORT:  
CR2020/28

DATE:  
May 2020



- Simulated landslide source area (slopes  $\geq 30^\circ$ )
- Local personal risk**
- $10^{-1}$  to  $10^{-2}$
- $10^{-2}$  to  $10^{-3}$
- $10^{-3}$  to  $10^{-4}$
- $10^{-4}$  to  $10^{-5}$
- Less than  $10^{-5}$
- Spring tide route
- Neap tide route
- + Distance along the route (km)
- Hazard area
- DOC Reserve

SCALE BAR:

EXPLANATION:

Background shade model derived from a LiDAR based Digital Elevation Model (1m ground resolution) which was resampled to 3 m for the analysis

PROJECTION: New Zealand Transverse Mercator 2000

DRW:  
BL

CHK:  
CM, SDV



**LOCAL PERSONAL RISK**  
from non-earthquake induced landslides only

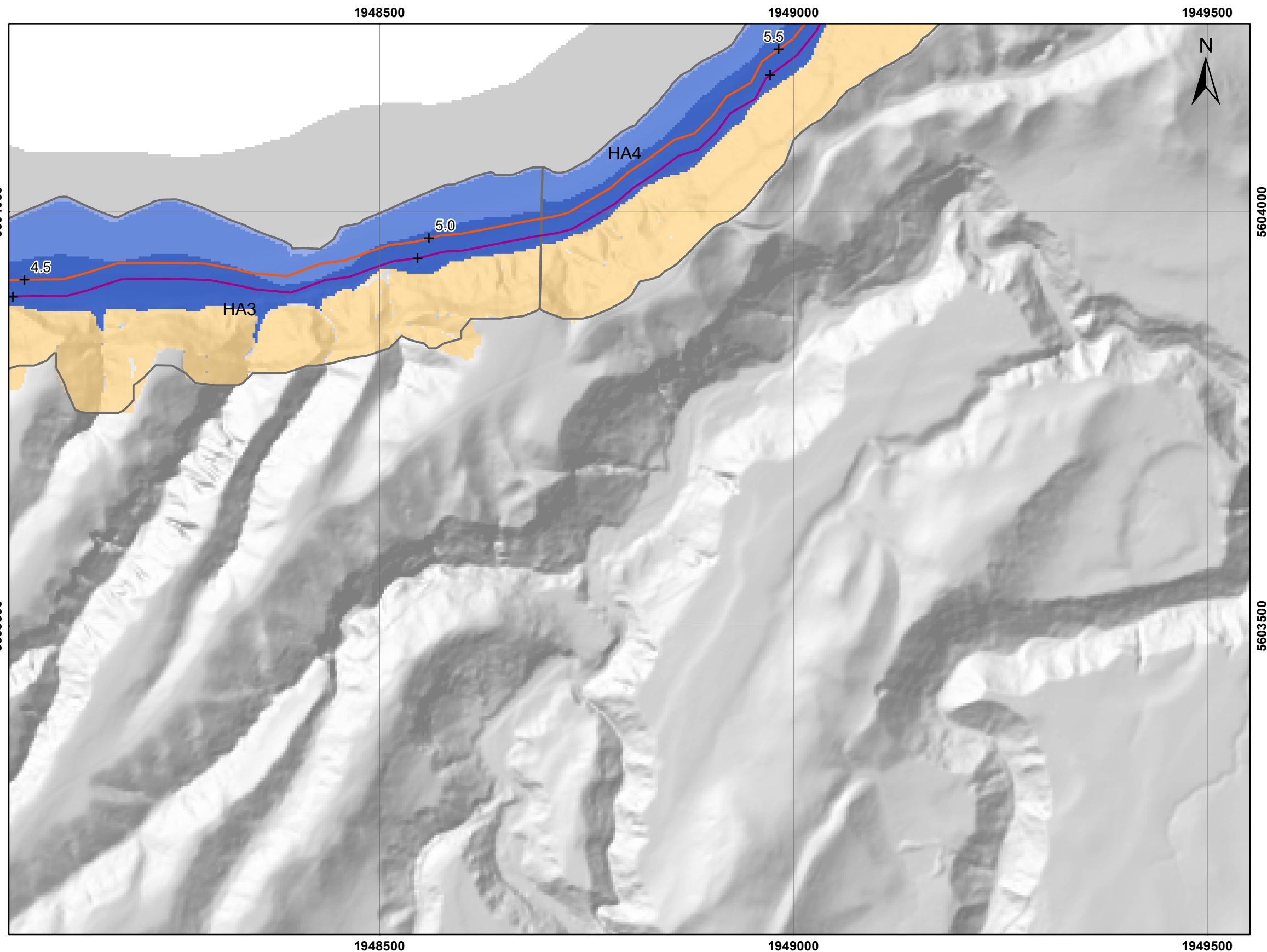
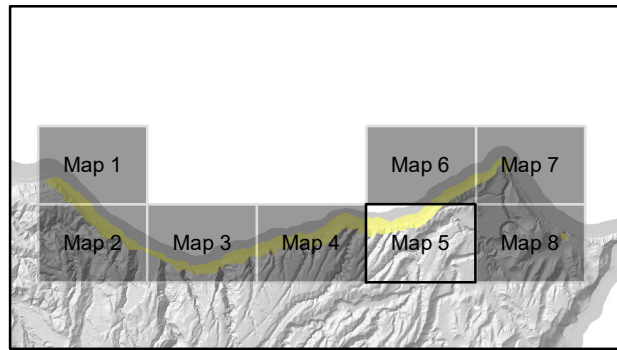
**Cape Kidnappers**


**FIGURE 4.1b**

Map 4






**FINAL**

REPORT: CR2020/28	DATE: May 2020
----------------------	-------------------



 Simulated landslide source area  
(slopes  $\geq 30^\circ$ )

**Local personal risk**

-   $10^{-1}$  to  $10^{-2}$
-   $10^{-2}$  to  $10^{-3}$
-   $10^{-3}$  to  $10^{-4}$
-   $10^{-4}$  to  $10^{-5}$
-  Less than  $10^{-5}$

 Spring tide route

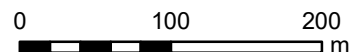
 Neap tide route

 Distance along the route (km)

 Hazard area

 DOC Reserve

SCALE BAR:



EXPLANATION:

Background shade model derived from a LiDAR based Digital Elevation Model (1m ground resolution) which was resampled to 3 m for the analysis

PROJECTION: New Zealand Transverse Mercator 2000

DRW:  
BL  
CHK:  
CM, SDV



**LOCAL PERSONAL RISK**  
from non-earthquake induced landslides only

**Cape Kidnappers**

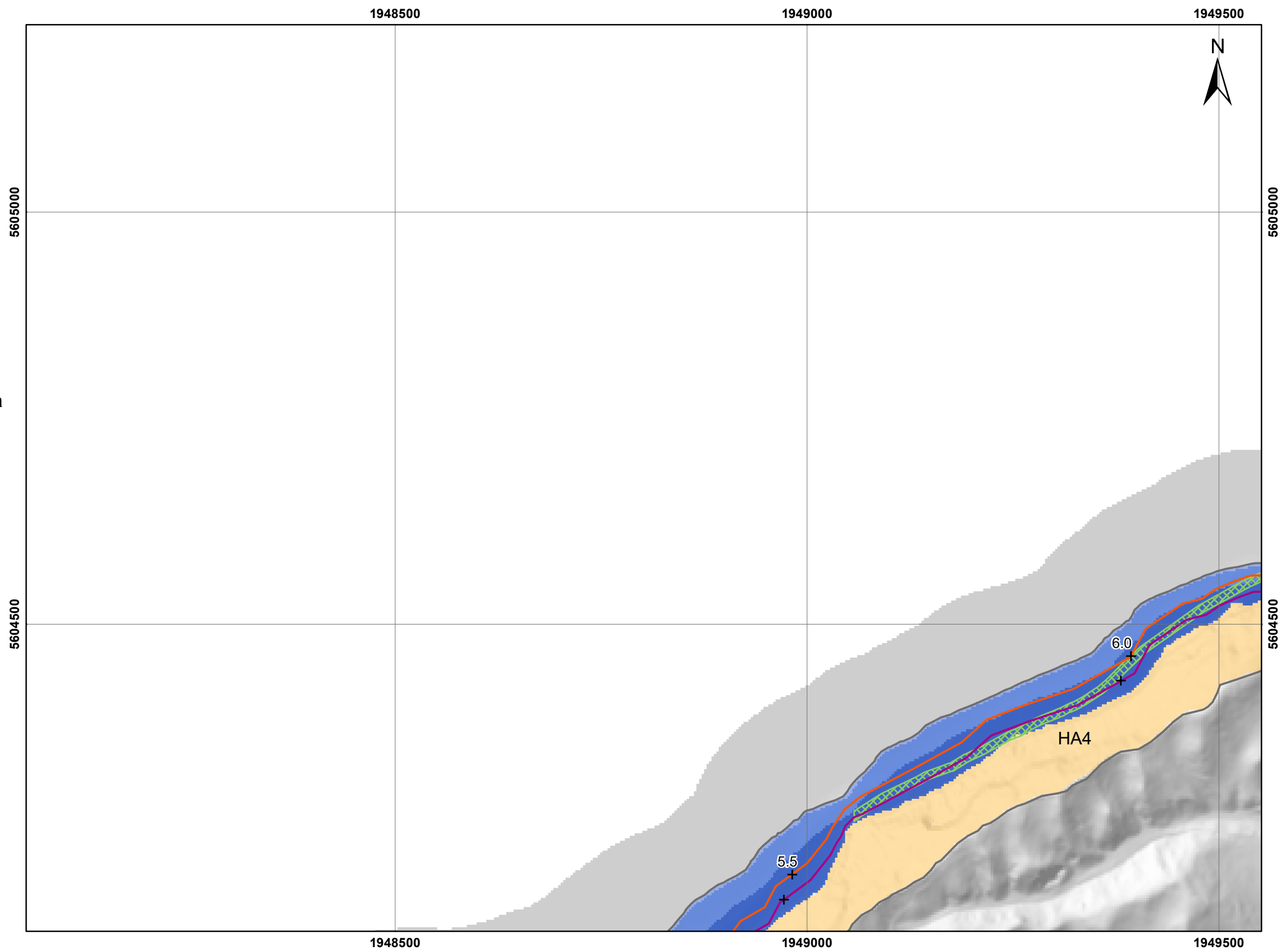
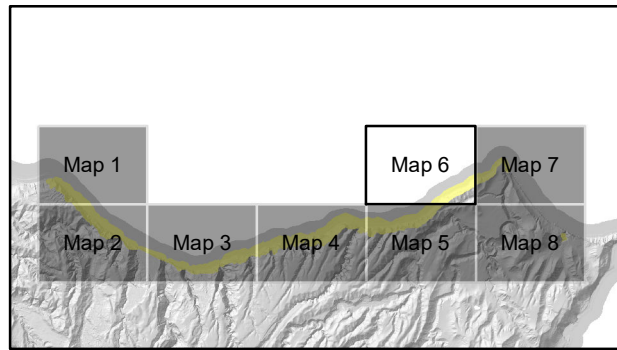
**FIGURE 4.1b**

Map 5

**FINAL**

REPORT:  
CR2020/28

DATE:  
May 2020



- Simulated landslide source area  
(slopes  $\geq 30^\circ$ )
- Local personal risk**
- $10^{-1}$  to  $10^{-2}$
- $10^{-2}$  to  $10^{-3}$
- $10^{-3}$  to  $10^{-4}$
- $10^{-4}$  to  $10^{-5}$
- Less than  $10^{-5}$
- Spring tide route
- Neap tide route
- + Distance along the route (km)
- Hazard area
- DOC Reserve

SCALE BAR: 
0
100
200
m

EXPLANATION:  
 Background shade model derived from a LiDAR based Digital Elevation Model (1m ground resolution) which was resampled to 3 m for the analysis  
 PROJECTION: New Zealand Transverse Mercator 2000

DRW:  
BL  
 CHK:  
CM, SDV



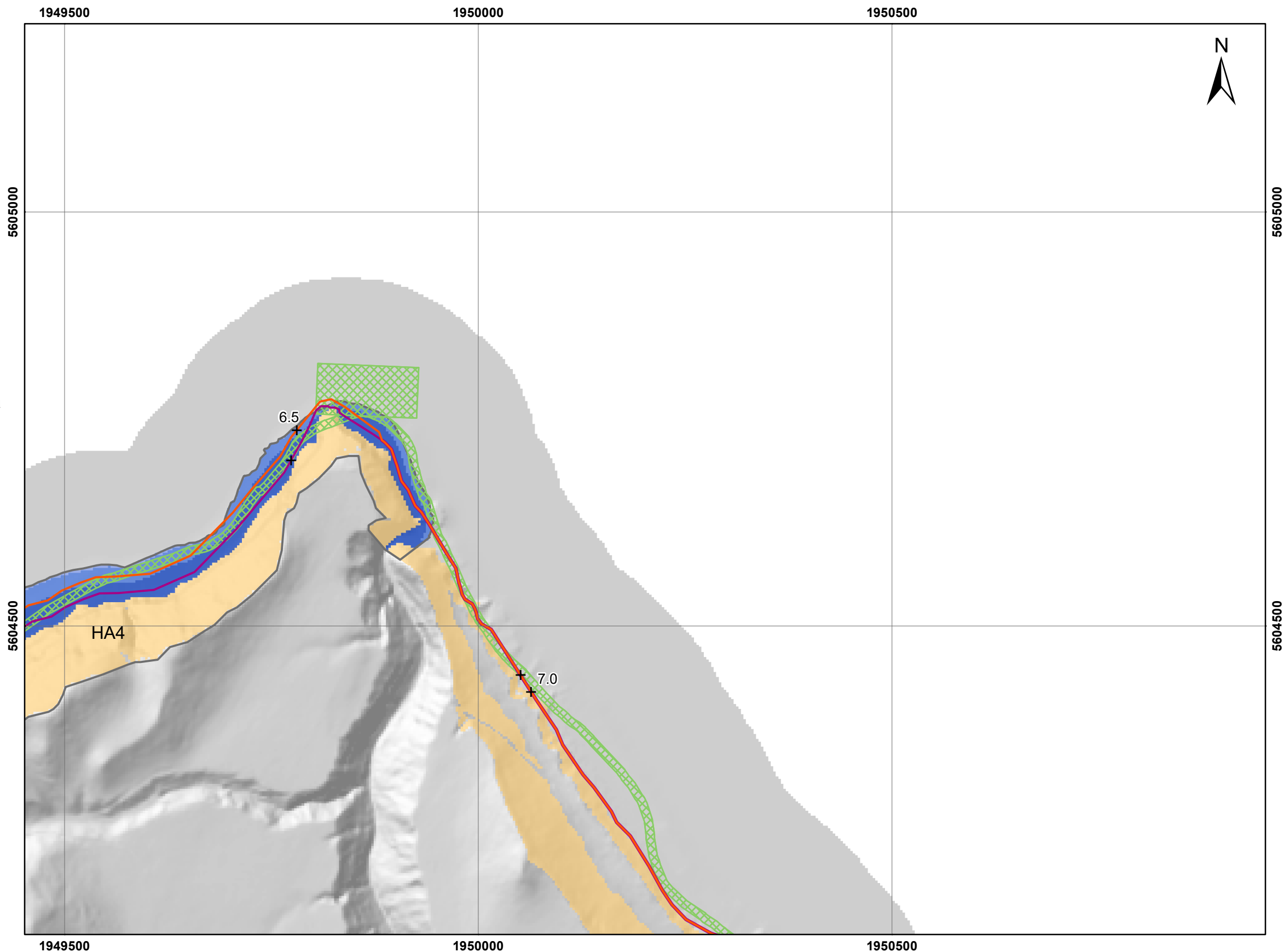
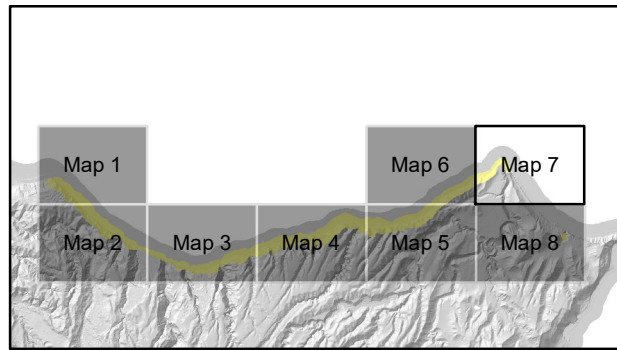
**LOCAL PERSONAL RISK**  
**from non-earthquake induced landslides only**

**Cape Kidnappers**

**FIGURE 4.1b**  
 Map 6  
**FINAL**

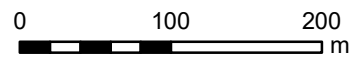
REPORT: CR2020/28      DATE: May 2020





- Simulated landslide source area  
(slopes  $\geq 30^\circ$ )
- Local personal risk**
- $10^{-1}$  to  $10^{-2}$
- $10^{-2}$  to  $10^{-3}$
- $10^{-3}$  to  $10^{-4}$
- $10^{-4}$  to  $10^{-5}$
- Less than  $10^{-5}$
- Spring tide route
- Neap tide route
- + Distance along the route (km)
- Hazard area
- DOC Reserve

SCALE BAR:



EXPLANATION:

Background shade model derived from a LiDAR based Digital Elevation Model (1m ground resolution) which was resampled to 3 m for the analysis

PROJECTION: New Zealand Transverse Mercator 2000

DRW:  
BL  
CHK:  
CM, SDV



**LOCAL PERSONAL RISK**  
from non-earthquake induced landslides only

**Cape Kidnappers**

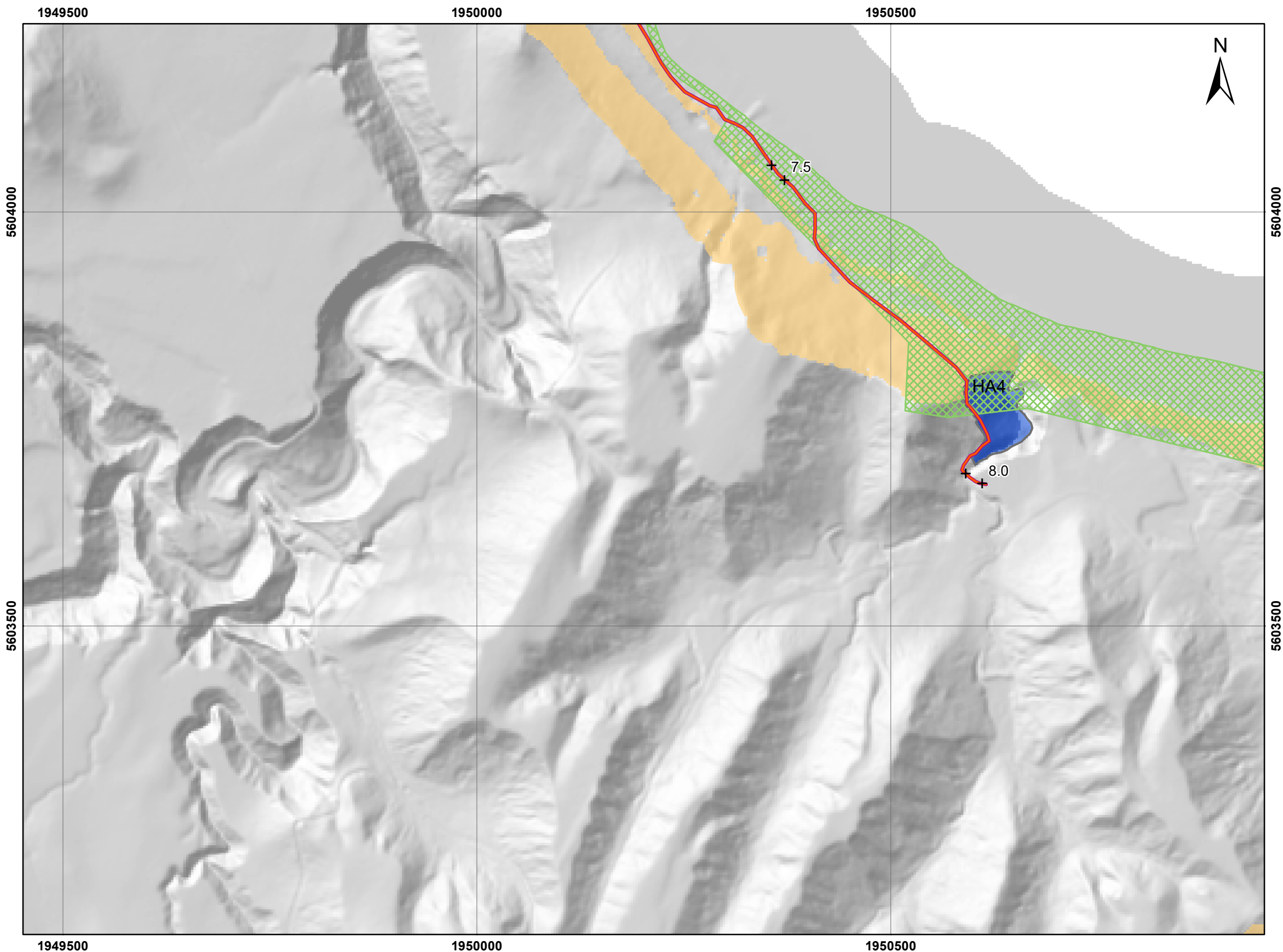
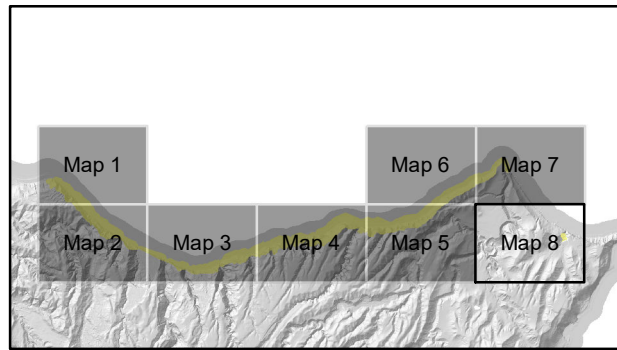
**FIGURE 4.1b**

Map 7

**FINAL**

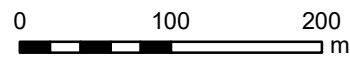
REPORT:  
CR2020/28

DATE:  
May 2020



- Simulated landslide source area (slopes  $\geq 30^\circ$ )
- Local personal risk**
- $10^{-1}$  to  $10^{-2}$
- $10^{-2}$  to  $10^{-3}$
- $10^{-3}$  to  $10^{-4}$
- $10^{-4}$  to  $10^{-5}$
- Less than  $10^{-5}$
- Spring tide route
- Neap tide route
- + Distance along the route (km)
- Hazard area
- DOC Reserve

SCALE BAR:



EXPLANATION:

Background shade model derived from a LiDAR based Digital Elevation Model (1m ground resolution) which was resampled to 3 m for the analysis

PROJECTION: New Zealand Transverse Mercator 2000

DRW:  
BL  
CHK:  
CM, SDV



**LOCAL PERSONAL RISK**  
from non-earthquake induced landslides only

**Cape Kidnappers**

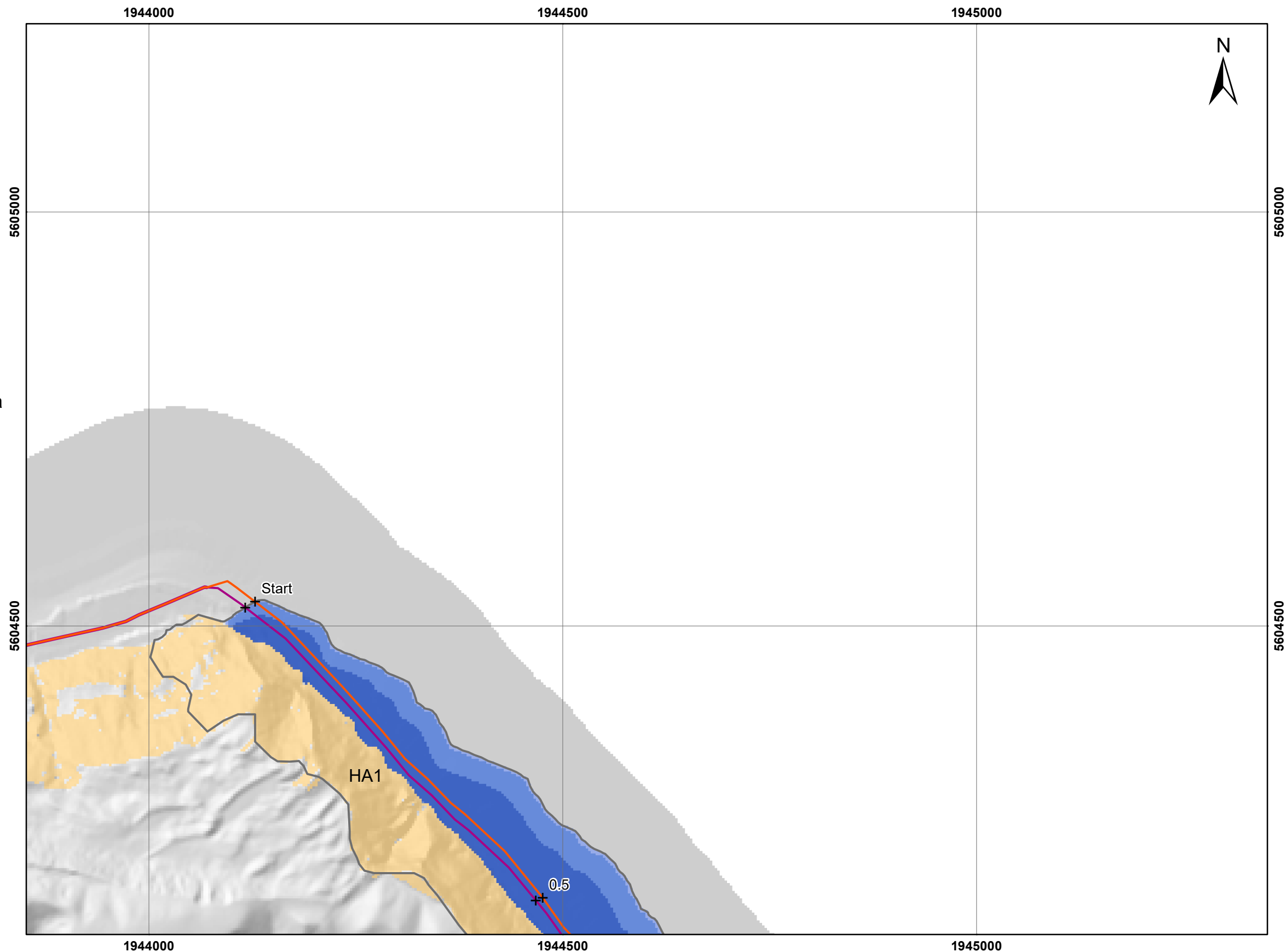
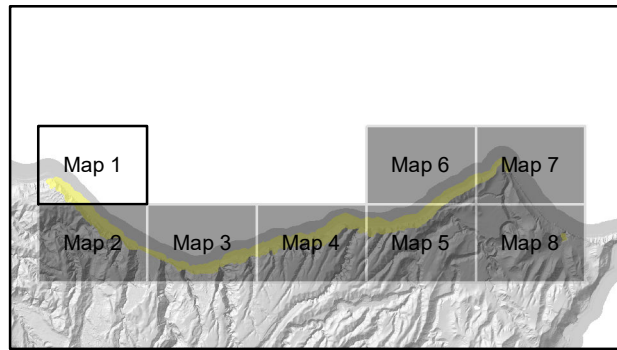
**FIGURE 4.1b**

Map 8

**FINAL**

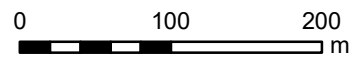
REPORT:  
CR2020/28

DATE:  
May 2020



- Simulated landslide source area  
(slopes  $\geq 30^\circ$ )
- Local personal risk**
- $10^{-1}$  to  $10^{-2}$
- $10^{-2}$  to  $10^{-3}$
- $10^{-3}$  to  $10^{-4}$
- $10^{-4}$  to  $10^{-5}$
- Less than  $10^{-5}$
- Spring tide route
- Neap tide route
- + Distance along the route (km)
- Hazard area
- DOC Reserve

SCALE BAR:



EXPLANATION:

Background shade model derived from a LiDAR based Digital Elevation Model (1m ground resolution) which was resampled to 3 m for the analysis

PROJECTION: New Zealand Transverse Mercator 2000

DRW:  
BL  
CHK:  
CM, SDV



**LOCAL PERSONAL RISK**  
**from earthquake and non-earthquake induced landslides**

**Cape Kidnappers**

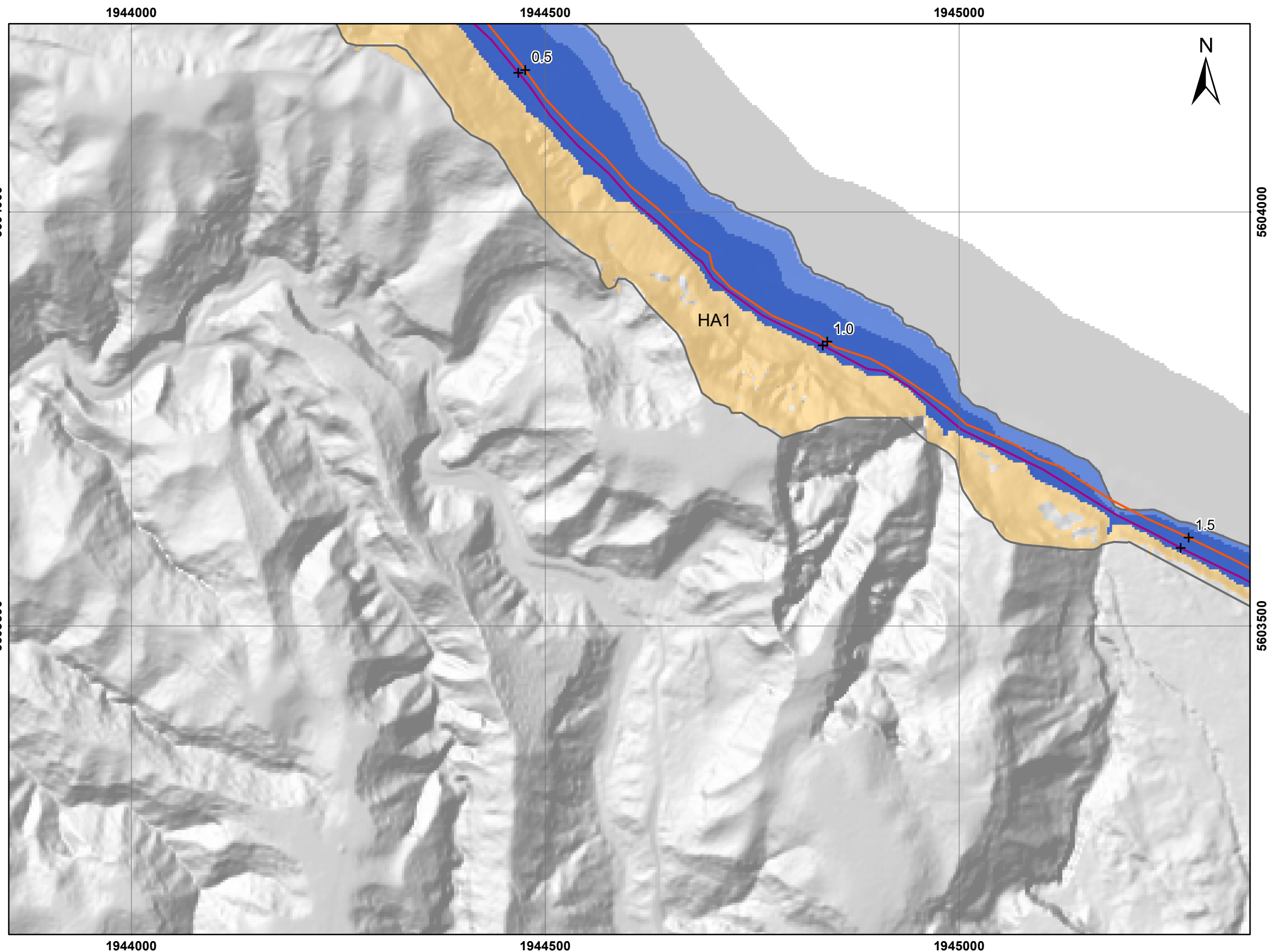
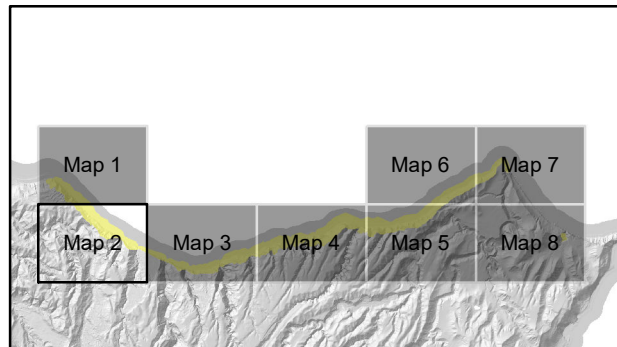
**FIGURE 4.1c**


Map 1

**FINAL**






REPORT:  
CR2020/28

DATE:  
May 2020



 Simulated landslide source area  
(slopes  $\geq 30^\circ$ )

**Local personal risk**

-   $10^{-1}$  to  $10^{-2}$
-   $10^{-2}$  to  $10^{-3}$
-   $10^{-3}$  to  $10^{-4}$
-   $10^{-4}$  to  $10^{-5}$
-  Less than  $10^{-5}$

 Spring tide route

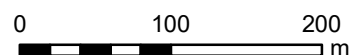
 Neap tide route

 Distance along the route (km)

 Hazard area

 DOC Reserve

SCALE BAR:



EXPLANATION:

Background shade model derived from a LiDAR based Digital Elevation Model (1m ground resolution) which was resampled to 3 m for the analysis

PROJECTION: New Zealand Transverse Mercator 2000

DRW:  
BL  
CHK:  
CM, SDV



**LOCAL PERSONAL RISK**  
**from earthquake and non-earthquake induced landslides**

**Cape Kidnappers**

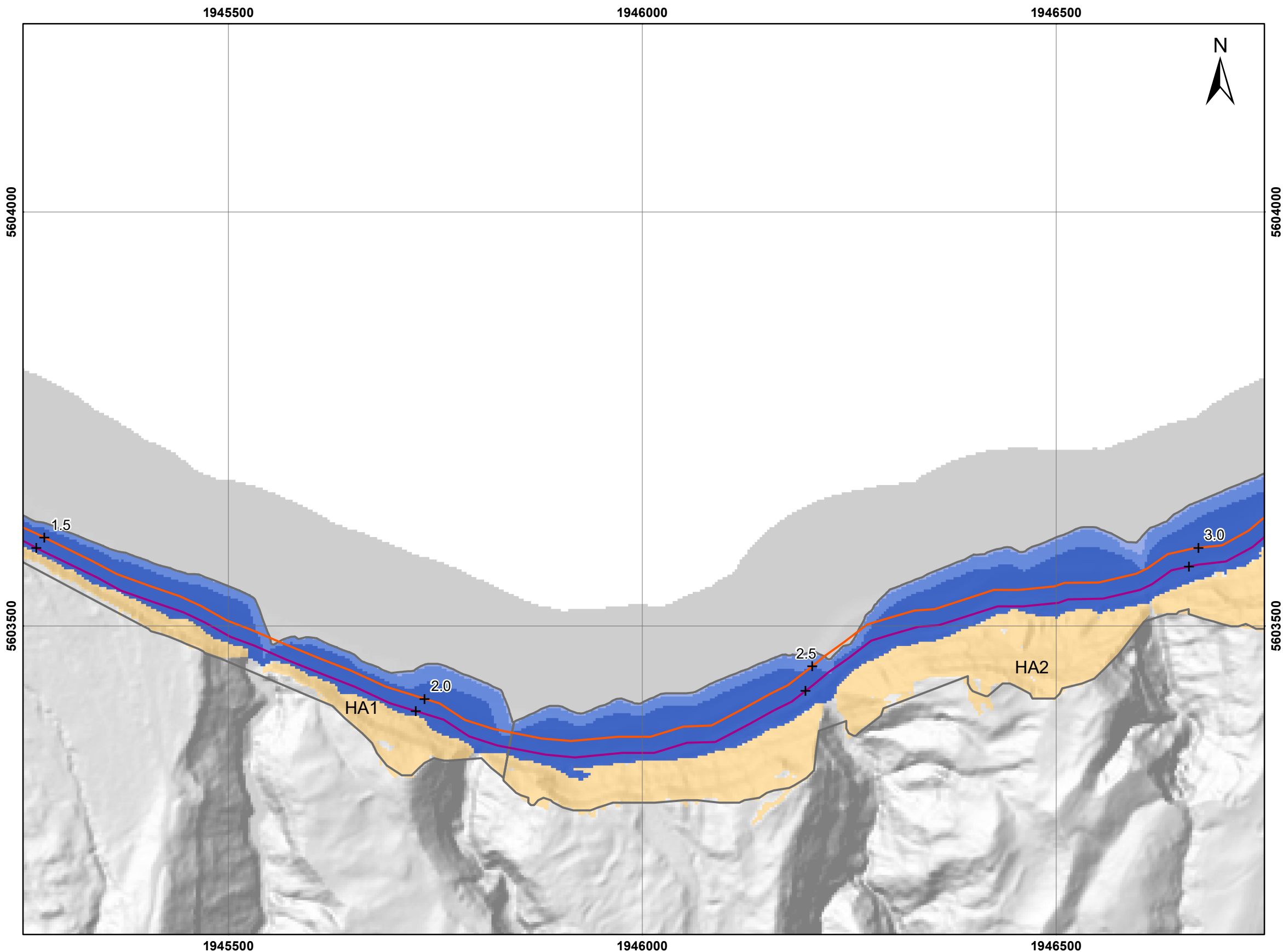
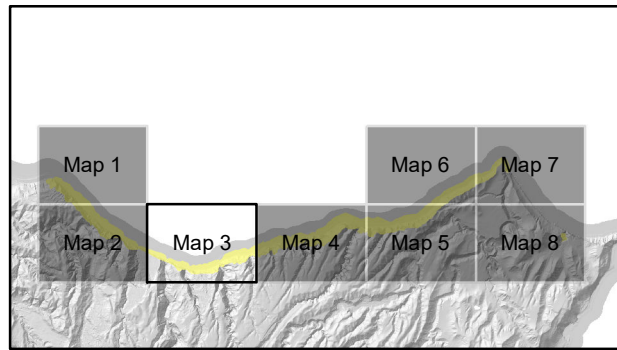
**FIGURE 4.1c**

Map 2

**FINAL**

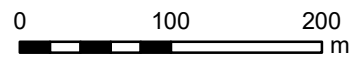
REPORT:  
CR2020/28

DATE:  
May 2020



- Simulated landslide source area (slopes  $\geq 30^\circ$ )
- Local personal risk**
- $10^{-1}$  to  $10^{-2}$
- $10^{-2}$  to  $10^{-3}$
- $10^{-3}$  to  $10^{-4}$
- $10^{-4}$  to  $10^{-5}$
- Less than  $10^{-5}$
- Spring tide route
- Neap tide route
- + Distance along the route (km)
- Hazard area
- DOC Reserve

SCALE BAR:



EXPLANATION:

Background shade model derived from a LiDAR based Digital Elevation Model (1m ground resolution) which was resampled to 3 m for the analysis

PROJECTION: New Zealand Transverse Mercator 2000

DRW:  
BL  
CHK:  
CM, SDV



**LOCAL PERSONAL RISK  
from earthquake and non-earthquake induced landslides**

**Cape Kidnappers**

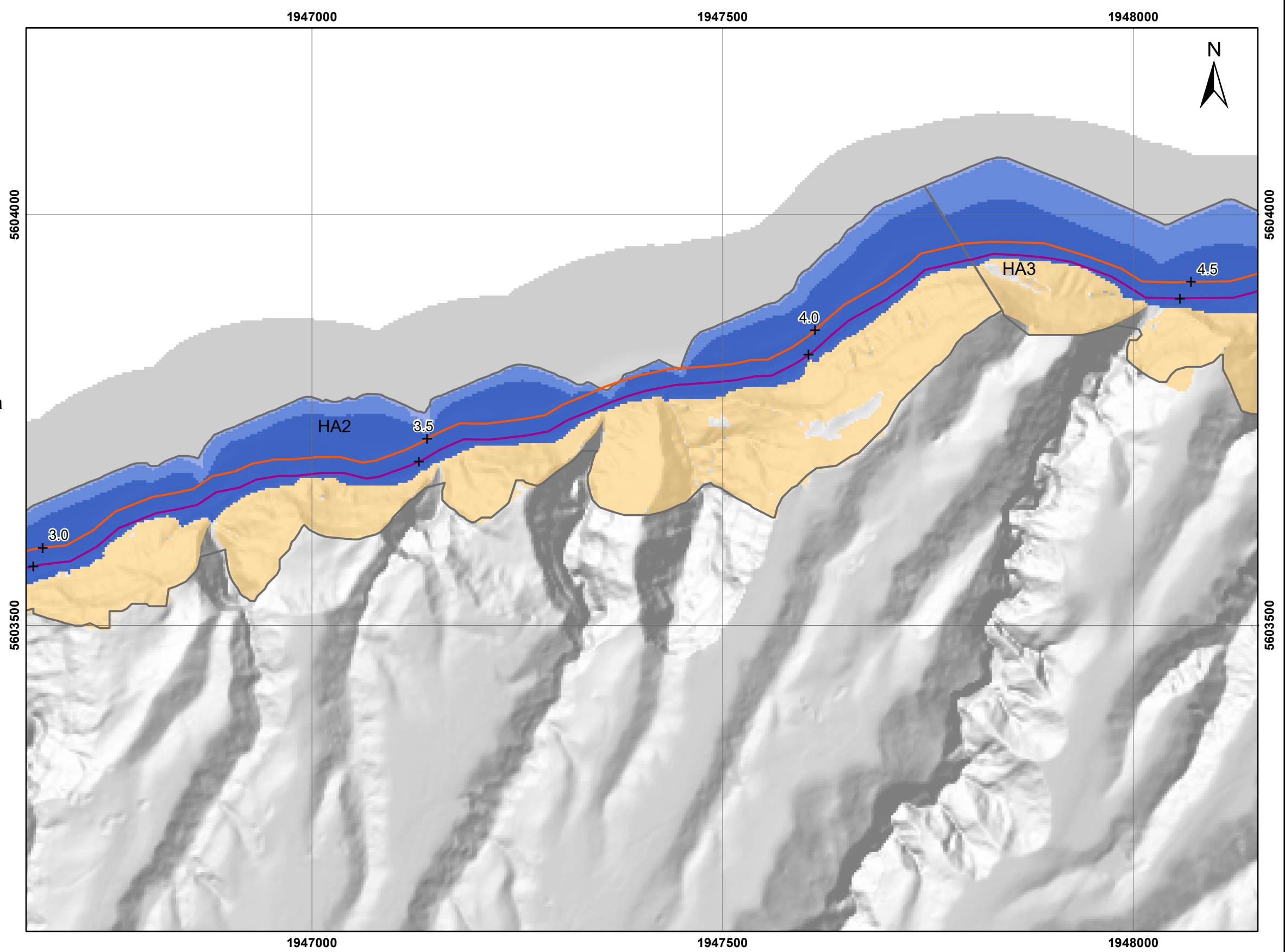
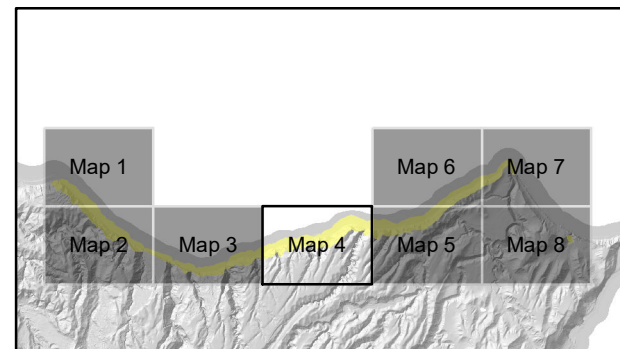
**FIGURE 4.1c**

Map 3

**FINAL**

REPORT:  
CR2020/28

DATE:  
May 2020



- Simulated landslide source area (slopes  $\geq 30^\circ$ )
- Local personal risk**
- $10^{-1}$  to  $10^{-2}$
- $10^{-2}$  to  $10^{-3}$
- $10^{-3}$  to  $10^{-4}$
- $10^{-4}$  to  $10^{-5}$
- Less than  $10^{-5}$
- Spring tide route
- Neap tide route
- + Distance along the route (km)
- Hazard area
- DOC Reserve

SCALE BAR:

EXPLANATION:

Background shade model derived from a LiDAR based Digital Elevation Model (1m ground resolution) which was resampled to 3 m for the analysis

PROJECTION: New Zealand Transverse Mercator 2000

DRW:  
BL

CHK:  
CM, SDV



**LOCAL PERSONAL RISK**  
from earthquake and non-earthquake induced landslides

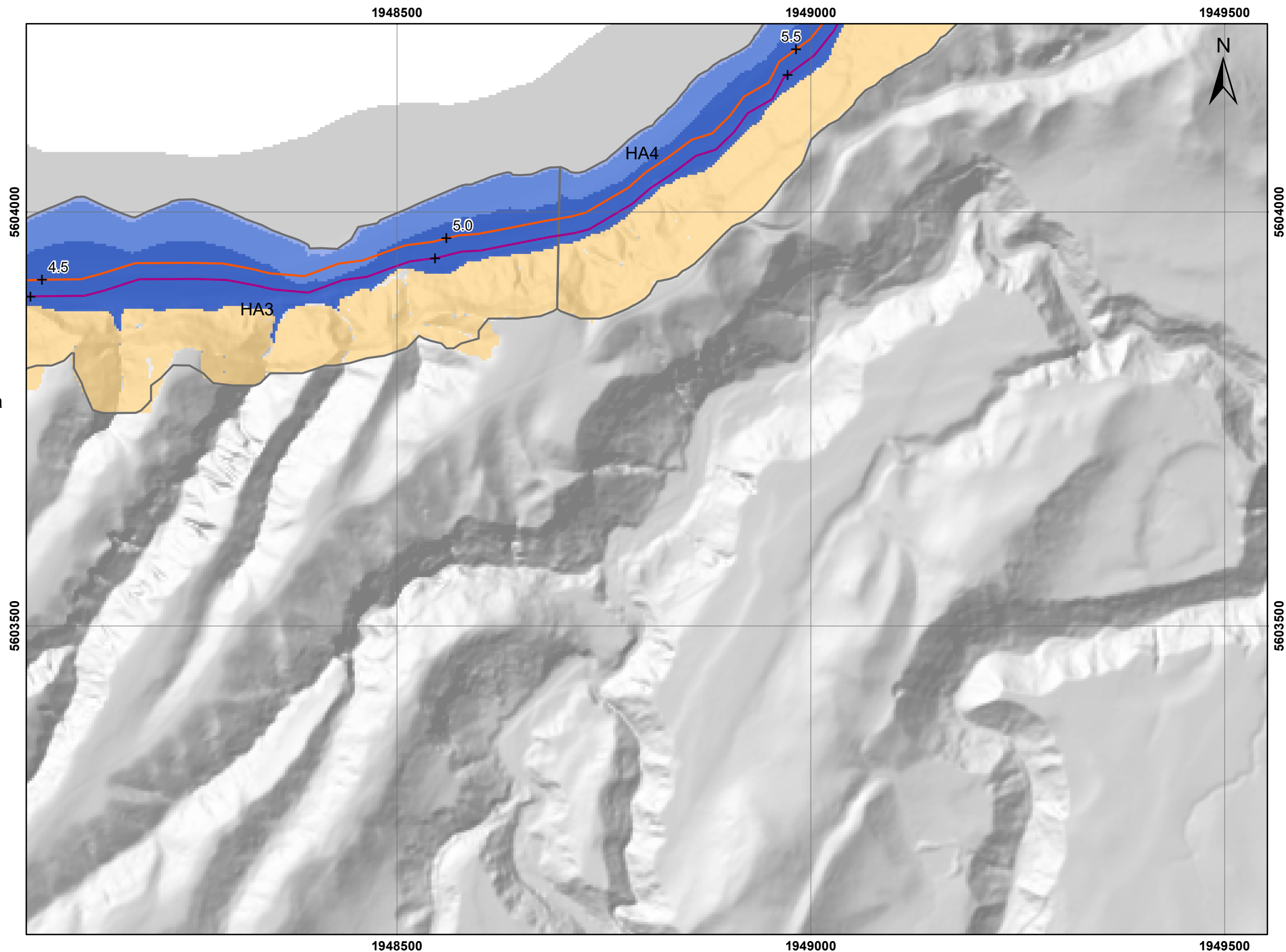
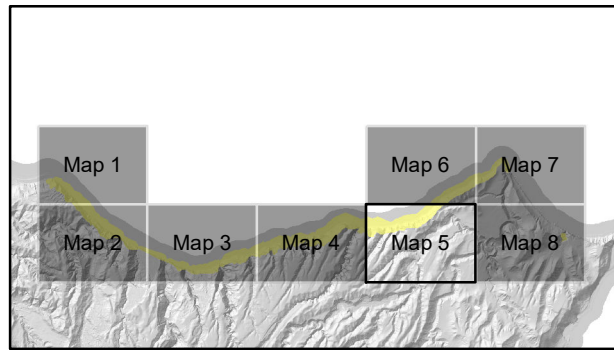
**Cape Kidnappers**


**FIGURE 4.1c**

Map 4






**FINAL**

REPORT: CR2020/28	DATE: May 2020
----------------------	-------------------




 Simulated landslide source area  
(slopes  $\geq 30^\circ$ )

**Local personal risk**

-   $10^{-1}$  to  $10^{-2}$
-   $10^{-2}$  to  $10^{-3}$
-   $10^{-3}$  to  $10^{-4}$
-   $10^{-4}$  to  $10^{-5}$
-  Less than  $10^{-5}$

 Spring tide route

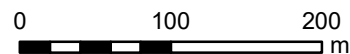
 Neap tide route

 Distance along the route (km)

 Hazard area

 DOC Reserve

SCALE BAR:



EXPLANATION:

Background shade model derived from a LiDAR based Digital Elevation Model (1m ground resolution) which was resampled to 3 m for the analysis

PROJECTION: New Zealand Transverse Mercator 2000

DRW:  
BL  
CHK:  
CM, SDV



**LOCAL PERSONAL RISK**  
**from earthquake and non-earthquake induced landslides**

**Cape Kidnappers**

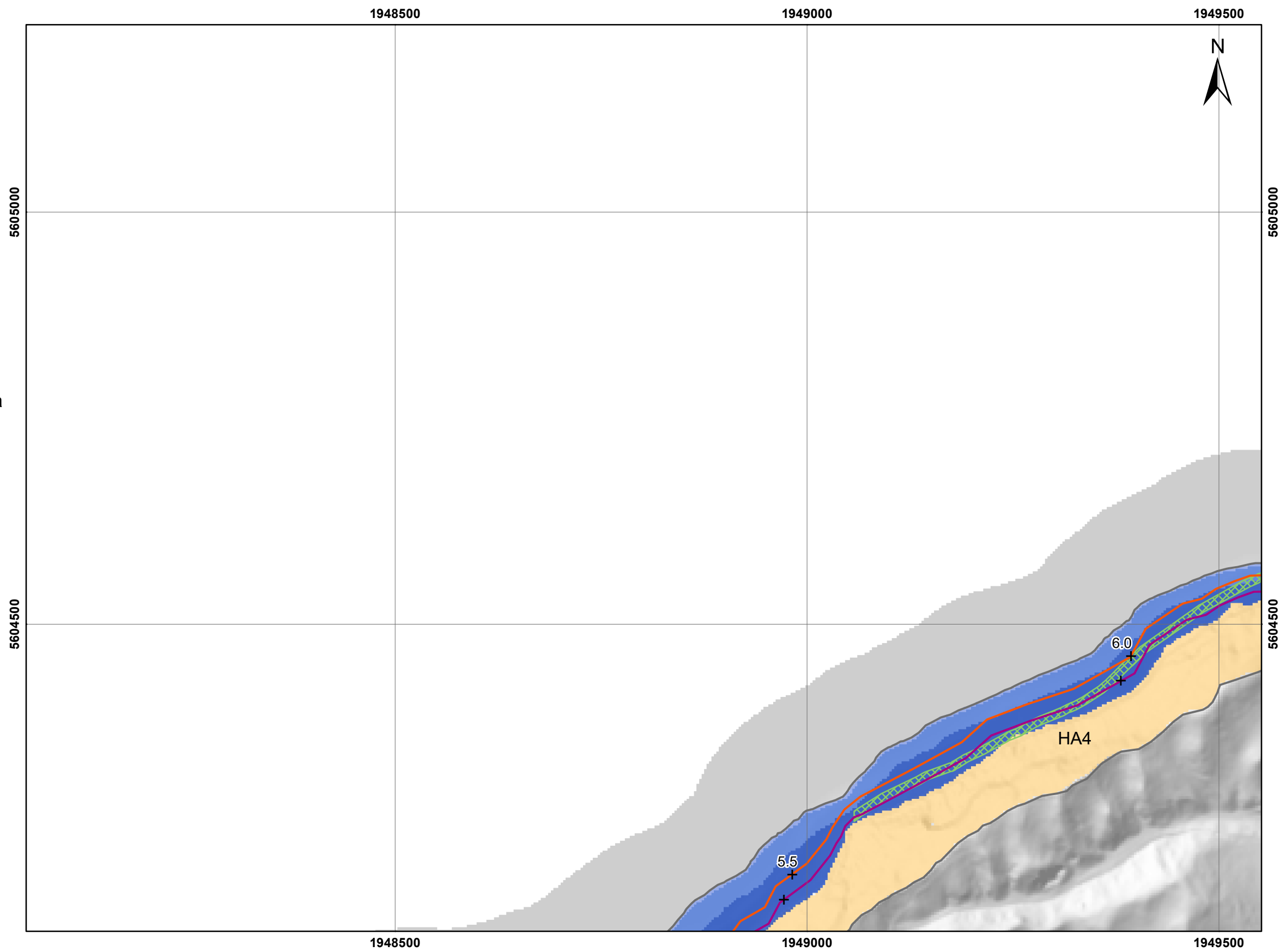
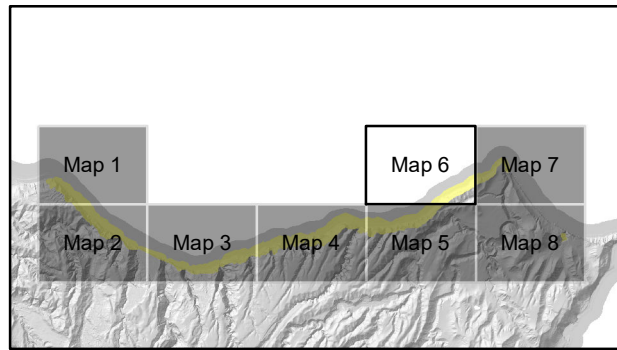
**FIGURE 4.1c**

Map 5

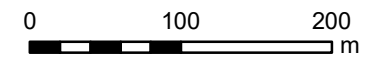
**FINAL**

REPORT:  
CR2020/28

DATE:  
May 2020



- Simulated landslide source area  
(slopes  $\geq 30^\circ$ )
- Local personal risk**
- $10^{-1}$  to  $10^{-2}$
- $10^{-2}$  to  $10^{-3}$
- $10^{-3}$  to  $10^{-4}$
- $10^{-4}$  to  $10^{-5}$
- Less than  $10^{-5}$
- Spring tide route
- Neap tide route
- + Distance along the route (km)
- Hazard area
- DOC Reserve



DRW:  
BL

CHK:  
CM, SDV



**LOCAL PERSONAL RISK**  
**from earthquake and non-earthquake induced landslides**

**FIGURE 4.1c**

Map 6

**Cape Kidnappers**

**FINAL**

REPORT:  
CR2020/28

DATE:  
May 2020

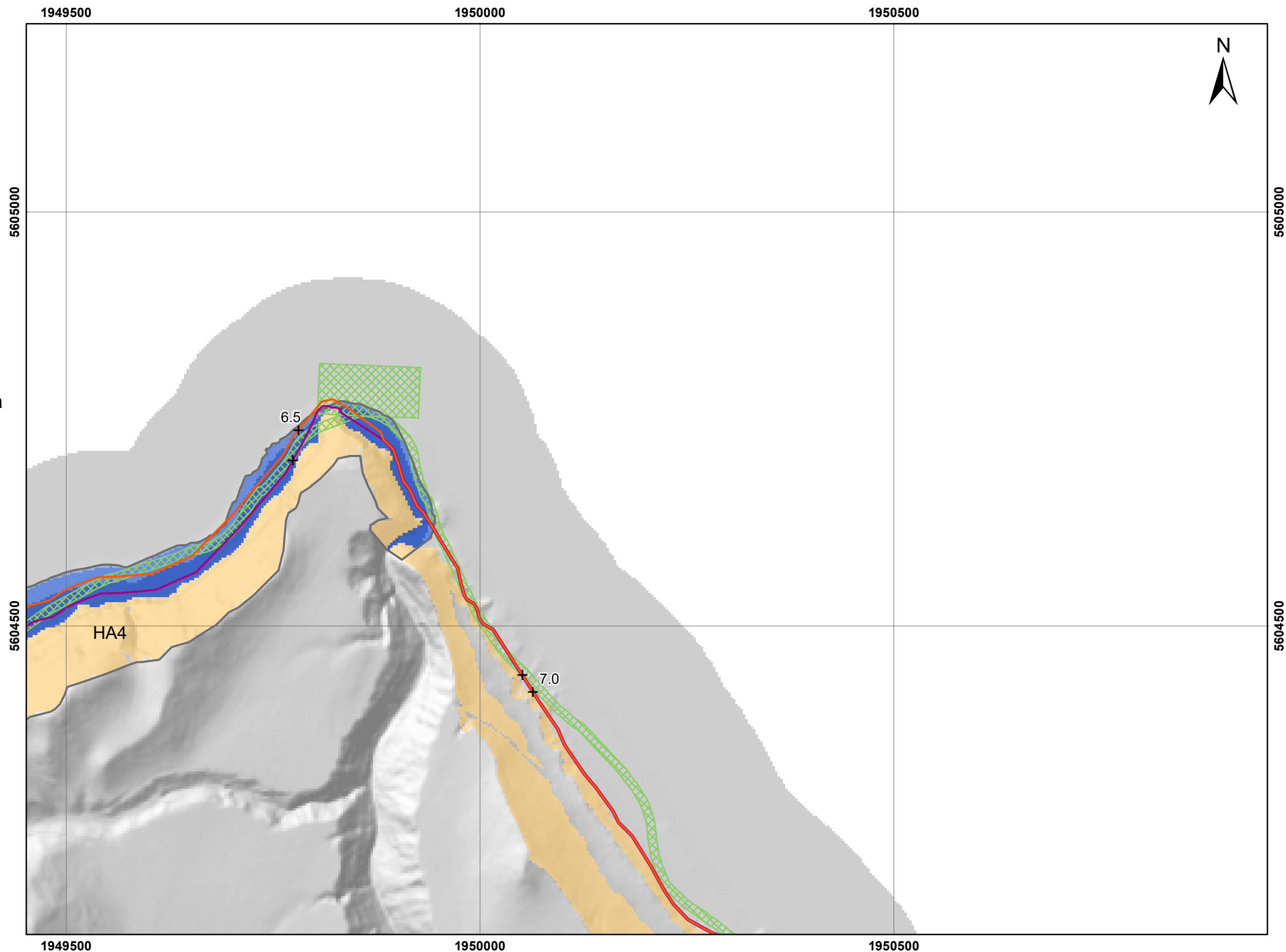
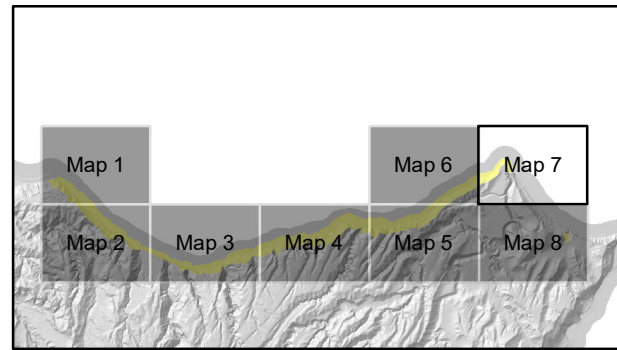
SCALE BAR:

EXPLANATION:

Background shade model derived from a LiDAR based Digital Elevation Model (1m ground resolution) which was resampled to 3 m for the analysis

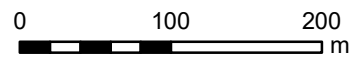
PROJECTION: New Zealand Transverse Mercator 2000





- Simulated landslide source area  
(slopes  $\geq 30^\circ$ )
- Local personal risk**
- $10^{-1}$  to  $10^{-2}$
- $10^{-2}$  to  $10^{-3}$
- $10^{-3}$  to  $10^{-4}$
- $10^{-4}$  to  $10^{-5}$
- Less than  $10^{-5}$
- Spring tide route
- Neap tide route
- + Distance along the route (km)
- Hazard area
- DOC Reserve

SCALE BAR:



EXPLANATION:

Background shade model derived from a LiDAR based Digital Elevation Model (1m ground resolution) which was resampled to 3 m for the analysis

PROJECTION: New Zealand Transverse Mercator 2000

DRW:  
BL  
CHK:  
CM, SDV



**LOCAL PERSONAL RISK  
from earthquake and non-earthquake induced landslides**

**Cape Kidnappers**

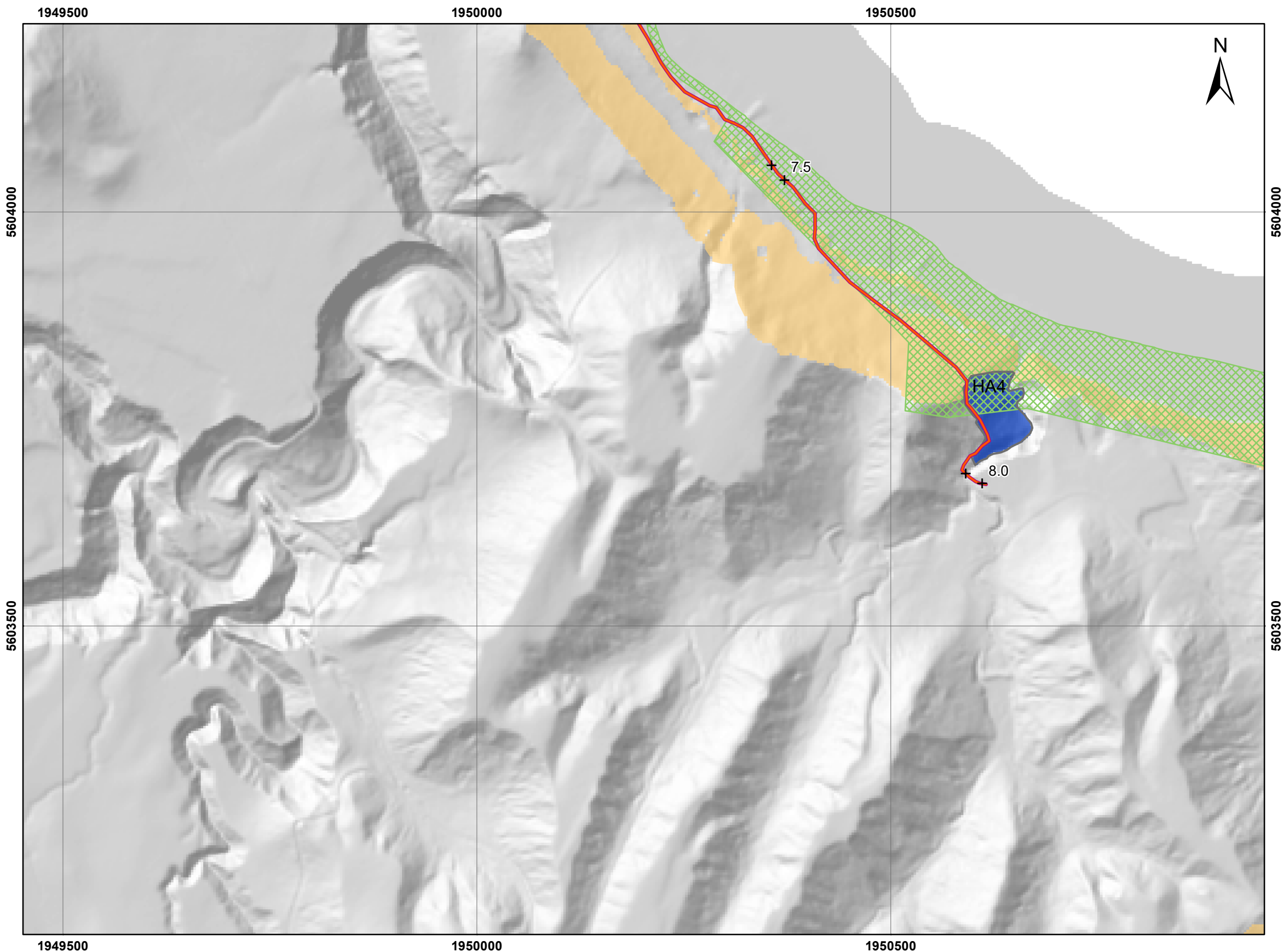
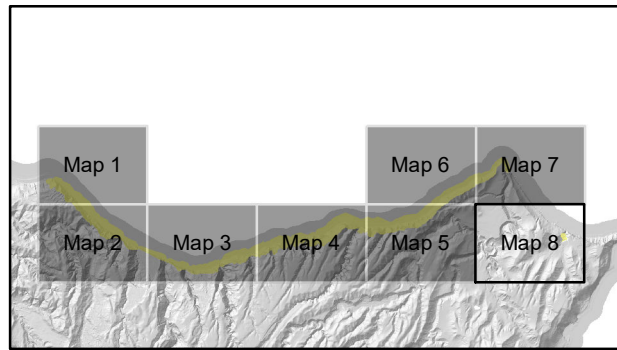
**FIGURE 4.1c**

Map 7

**FINAL**

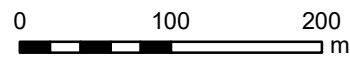
REPORT:  
CR2020/28

DATE:  
May 2020



- Simulated landslide source area (slopes  $\geq 30^\circ$ )
- Local personal risk**
- $10^{-1}$  to  $10^{-2}$
- $10^{-2}$  to  $10^{-3}$
- $10^{-3}$  to  $10^{-4}$
- $10^{-4}$  to  $10^{-5}$
- Less than  $10^{-5}$
- Spring tide route
- Neap tide route
- + Distance along the route (km)
- Hazard area
- DOC Reserve

SCALE BAR:



EXPLANATION:

Background shade model derived from a LiDAR based Digital Elevation Model (1m ground resolution) which was resampled to 3 m for the analysis

PROJECTION: New Zealand Transverse Mercator 2000

DRW:  
BL  
CHK:  
CM, SDV



**LOCAL PERSONAL RISK**  
**from earthquake and non-earthquake induced landslides**

**Cape Kidnappers**

**FIGURE 4.1c**

Map 8

**FINAL**

REPORT:  
CR2020/28

DATE:  
May 2020

### 4.1.1 General Results for the Study Area

The results show that:

1. The LPR varies along each route as a function of the proximity of the route to the steep slopes. The LPR along the Spring low tide route is marginally less than the LPR along the Neap low tide route. This is because the Spring low tide route is further away from the steep slopes.
2. In general, the LPR maps show that the representative routes are located within the LPR areas over much of their length, until 6.7 km from the start, where the topography becomes more subdued.
3. The main contributor to the LPR is from non-earthquake-induced landslides. There is about an order of magnitude difference in the LPRs calculated for earthquake- and non-earthquake-induced landslides.
4. The LPR reduces rapidly with increasing distance from the cliff bottom out towards the sea. This shows that a person, if aware that a landslide had occurred, would be best to run out towards the sea. However, at Neap tides there is very little beach to run down, and so the person may end up in the sea and potentially drown.
5. The LPR in Hazard Areas 1 and 3 are the highest and extend the furthest out into the sea from the cliff bottom. This is because these slopes are some of the highest and steepest in the study area.
6. The LPR reduces where the routes traverse the beach below the mouths of the streams and gullies. This is because the slope heights decrease in these areas, and therefore the distance debris may travel out from the cliff bottom also reduces. These results suggest that the streams and gullies are potentially safer places to be during, for example, earthquakes. However, these areas are exposed to other hazards that have been excluded in this study (e.g. debris flows), but these tend to only occur during heavy rain when few people may be on the beach.

The LPR should not be confused with the AIFR or risk per trip, as the probability of a person being present in a location and the time spent by that person in a location significantly changes the risk.

## 4.2 The Annual Individual Fatality Risk and Risk per Trip

Individual risk for a given route was calculated as follows:

- The route is mapped onto the grid cells used in the debris runout models so that each 3 m length of route is linked to a corresponding grid cell.
- The time taken to travel the route is divided by the number of cells along the route to estimate the time spent in each corresponding grid cell.
- The product of the LPR multiplied by the time spent then provides the contribution to probability of death per trip from each grid cell along the route.
- These probabilities are summed to calculate the total probability of death from walking or driving the whole route.

Estimates of the time spent for each person at risk are taken from Table 3.12. The ranges of risk per trip and AIFR values calculated for the different people at risk, taking into account the range from 'lower' to 'upper' landslide generation estimates and from 'lower' to 'upper'

exposure data, are shown in Table 4.1 and Figure 4.2 for earthquake-induced landslides and Figure 4.3 for non-earthquake-induced landslides. Note that these numbers are expressed as, for example, 1.1E-06, which means  $1.1 \times 10^{-6}$  and a 1.1 chance in 1,000,000 of dying from a landslide per trip or per year, depending on the risk units used. Approximately 16% of the Neap and Spring low tide routes within the hazard areas are on DOC conservation lands and waters (DOC Reserve).

The results show that the risk is dominated by non-earthquake-induced landslides, as these occur more frequently than strong earthquake-induced ground shaking. Past non-earthquake-induced landslides have occurred sporadically without any obvious trigger, making managing the risk from such hazards difficult.

The results also show that there is little difference (a factor of 1.4) between the AIFR estimated along the Neap and Spring low tide routes. The AIFR (and risk per trip) to a person on the Neap low tide route (closer to the cliff) is 1.4 times larger than the AIFR people are exposed to on the Spring low tide route.

Table 4.1 AIFR and risk per trip results for the Neap and Spring low tide routes, for earthquake- (EQ) and non-earthquake- (Non-EQ) induced landslides, and both combined. Lower = lower estimates of the number of landslides for earthquake and non-earthquake triggers, along with lower exposure times and vulnerability values as shown in Table 3.9. Upper = estimates of the number of landslides for earthquake and non-earthquake triggers, along with upper estimates of the exposure times and vulnerability values as shown in Tables 3.10–3.11.

Person at Risk	Trigger	From (Lower)	To (Upper)	From (Lower)	To (Upper)	Risk Units
		Neap Low Tide		Spring Low Tide		
Walker	EQ	1.1E-06	1.6E-06	7.5E-07	1.1E-06	Per trip
	Non-EQ	7.1E-06	2.9E-05	5.0E-06	2.0E-05	Per trip
	Total	8.2E-06	3.0E-05	5.7E-06	2.1E-05	Per trip
GBA passenger	EQ	5.6E-07	7.9E-07	3.8E-07	5.4E-07	Per trip
	Non-EQ	3.6E-06	1.4E-05	2.5E-06	1.0E-05	Per trip
	Total	4.1E-06	1.5E-05	2.9E-06	1.1E-05	Per trip
DOC (person most exposed)	EQ	2.6E-06	1.1E-05	1.7E-06	7.4E-06	Per year
	Non-EQ	1.6E-05	2.0E-04	1.1E-05	1.4E-04	Per year
	Total	1.9E-05	2.1E-04	1.3E-05	1.5E-04	Per year
GBA (person most exposed)	EQ	8.8E-05	1.2E-04	5.9E-05	8.5E-05	Per year
	Non-EQ	5.5E-04	2.2E-03	3.9E-04	1.6E-03	Per year
	Total	6.4E-04	2.4E-03	4.5E-04	1.7E-03	Per year
Local	EQ	6.4E-06	2.7E-05	4.3E-06	1.9E-05	Per year
	Non-EQ	4.1E-05	4.9E-04	2.8E-05	3.4E-04	Per year
	Total	4.7E-05	5.2E-04	3.3E-05	3.6E-04	Per year

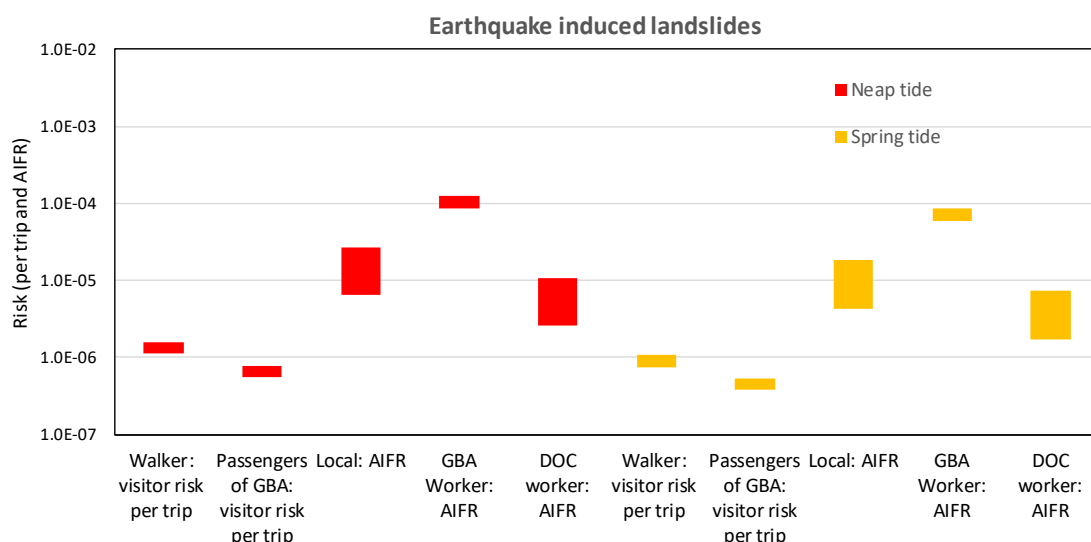


Figure 4.2 The risk per trip and AIFR: earthquake-induced landslides only.

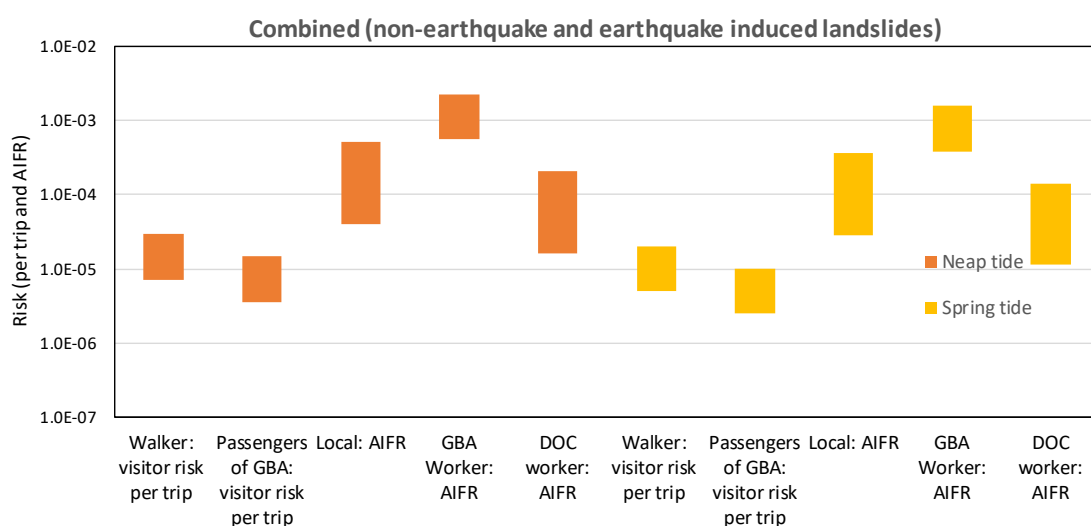


Figure 4.3 The risk per trip and AIFR: non-earthquake- and earthquake-induced landslides combined.

### 4.3 Societal Risk

The  $f/N$  curves (Figure 4.4) show the expected annual frequency of occurrence ( $f$ ) of a given number ( $N$ ) of deaths (or the expected number of deaths of a given annual frequency).

Societal risk, in the form of 'f/N curves' was calculated for tractors as follows:

1. Construct a plausible set of trips each month to match the annual number of visitors using the tractors, assuming only one trip can be completed per day due to the tides, as well as other information about hours exposed and trips per months from Table 3.12.
2. Calculate  $f/N$  pairs for each scenario and landslide.
  - a. For a given landslide and tractor/walker scenario, calculate the probability that a tractor/walker is in the path of a landslide at Spring or Neap low tides.
  - b. Estimate the number of deaths, given the number of people exposed and their vulnerability based on the different scenarios adopted.
3. Assemble  $f/N$  curves for tractors.

For walkers, the societal risk was calculated as followed:

1. Allocate walkers to groups walking together and adjust numbers to match the total number of walkers per year, assuming that most walkers are in small groups.
2. Calculate the probability of the number of deaths for each group in the path of debris, assuming that:
  - a. if one person is in the path, then the entire group are also in the path;
  - b. they are walking abreast along the beach in a row perpendicular to the cliff; and
  - c. each has the same independent vulnerability.
3. Calculate the frequency contributions from each landslide to each number of deaths for each group.
4. Assemble  $f/N$  curves for walkers.

Figure 4.4 shows the overall visitor societal risk, in terms of charts of frequency ( $f$ ) of events causing a number ( $N$ ) or more deaths, for the representative routes in the study area.

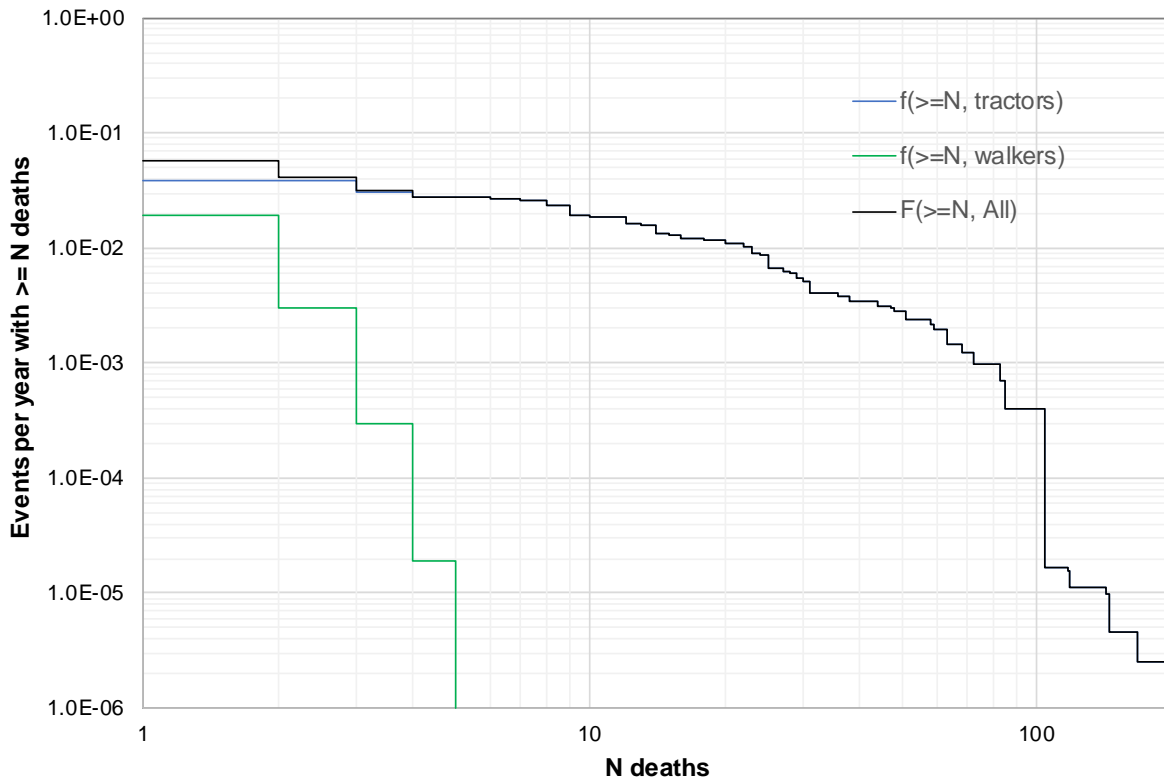


Figure 4.4 Lower overall visitor societal risk, in terms of charts of frequency ( $f$ ) of events (on the y-axis) causing a number ( $N$ ) or more deaths (on the x-axis) for the representative routes in the study area, adopting the lower estimates of the number of landslides for earthquake and non-earthquake triggers, along with lower exposure times and vulnerability values as shown in Tables 3.10–3.11. The units on the y-axis are in log scale, where 1.0E-05 is the same as 0.00001 and 1.0E+00 is the same as 1.0.

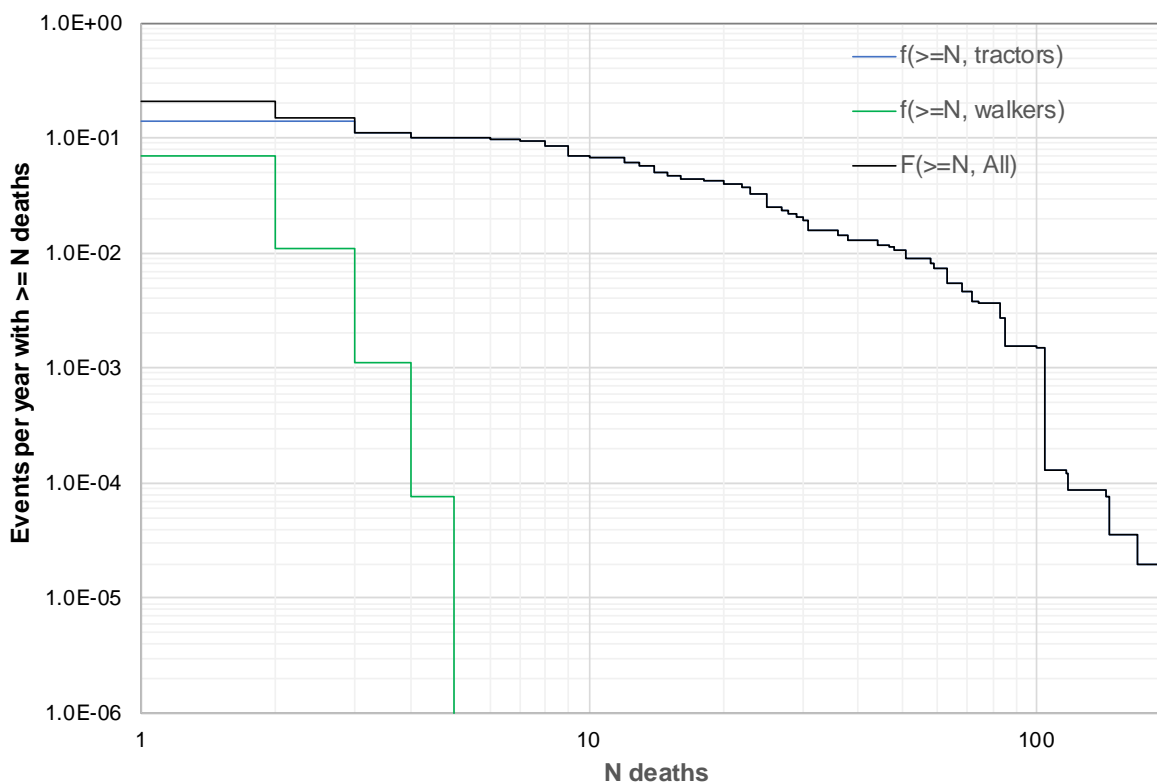


Figure 4.5 Upper overall visitor societal risk, in terms of charts of frequency ( $f$ ) of events (on the y-axis) causing a number ( $N$ ) or more deaths (on the x-axis) for the representative routes in the study area, adopting the upper estimates of the number of landslides for earthquake and non-earthquake triggers, along with upper estimates of the exposure times and vulnerability values as shown in Tables 3.10–3.11. The units on the y-axis are in log scale, where 1.0E-05 is the same as 0.00001 and 1.0E+00 is the same as 1.0.

For both lower and upper scenarios, the higher casualties on the right-hand side of Figure 4.4 are associated with earthquake Bands 3 and 4, where the probability of death along most of the routes, should these representative earthquake PGAs occur, is about one. Overall, based on the lower scenario, there is roughly a:

- 1-in-50-year chance of a fatal accident ( $N \geq 1$ ),
- 1-in-90–100-year chance of an accident killing 10–20 people or more, and
- 1-in-7000-year chance of an accident killing 100 or more people.

#### 4.4 Consistency with Actual Experience

To the authors' knowledge, there have been three documented landslide events that have hit and injured five people since 1973 – four walkers and one GBA worker. Four of these people were severely injured. This is broadly consistent with the individual risk estimates, taken in combination with the numbers of visitors annually to the study area

We note that these landslides appear to have occurred on clear days with no apparent trigger. We also note that the landslides all occurred during Spring tides, so the four walkers were walking along the beach, further away from the cliff bottom.

## 4.5 Sensitivity to Key Uncertainties

In this section, the sensitivity of the risk model to key uncertainties and the reliability of the assessments are identified.

The sensitivity of the estimated risk has been assessed to changes in the following:

- Volumes of debris triggered by both earthquake and non-earthquake triggers:
  - For earthquake-induced landslides, a lower and upper bound of landslide volumes have been used to account for any uncertainty in the relationship between PGA and the number and volume of debris avalanches generated.
  - For non-earthquake-induced landslides, a lower and upper bound of landslide volumes have been used to allow for any uncertainty in the landslide frequency (number) and magnitude (volume) estimates.
- Volume of debris passing a given distance down the slope:
  - The distribution of landslides generated in each earthquake band.
  - The area of slope inundated between the cliff bottom and the rockfall limit line and F-angle lines has been assessed by assuming the entire area is inundated by debris from each of the given landslide volume classes.
- The time spent walking or driving along the beach by the different users.
- The route a person walks along the beach between the Neap and Spring tides.
- The vulnerability of a person walking or driving along the beach.

Potentially significant uncertainties are noted and their likely implications for risk are summarised in Table 4.2. These uncertainties combine to give a total factor of difference of between 6 and 8, which is between half to an order of magnitude uncertainty on the risk estimates, in either direction. This difference is between the risk estimates that adopt the lower landslide production rates (earthquake and non-earthquake) the Spring tide route and lower estimates for the time spent on the beach, and the risk estimates adopting upper landslide production rates, the Neap tide route and the upper estimates for the time spent on the beach, which are considered to be the three most significant uncertainties in this assessment.



Table 4.2 Uncertainties and their implications for risk.

Issue	Direction and Scale of Uncertainty	Implications for Risk
a. Under-prediction of annual frequency for a given PGA by the NSHM.	Increasing. However, the contribution to risk from non-earthquake landslide triggers are higher. Time-independent model does not take into account the elapsed time since the last earthquake in 1931.	Risk due to earthquakes could be slightly underestimated.
b. Volume of debris produced in each earthquake band.	A large uncertainty in the risk estimates. However, the contribution to risk from non-earthquake landslide triggers are higher.	There is a factor of 1.4 difference between the risk estimates adopting the lower and upper numbers of landslides generated in each earthquake band.
c. Volume of debris produced by other (non-earthquake) events.	Largest uncertainty either way in the annual frequency but constrained by the geomorphology and records of past landslides in the area. The use of an 'upper' and 'lower' landslide volume per year rates appear to adequately 'bracket' the recorded data.	Factor of 4.0 difference between the risk estimates adopting the lower and upper numbers of landslides generated in each landslide volume class.
d. Numbers of landslides produced in each earthquake band.	The data is well constrained for non-earthquake-induced landslides from site-specific data. For earthquake-induced landslides, there is no data for the site. The Kaikōura earthquake landslide distributions in similar materials suggest more larger landslides could occur during an earthquake.	Factor of 1.1 uncertainty in the upward direction.
e. Volume of debris travelling downslope and inundating an area.	Quite well constrained and could be large but linked to the total volume of material leaving the slope. Physics-based simulations of debris avalanches sourcing from the lower and upper slopes would suggest about 50% of the runout zone may not be entirely inundated by debris, but debris from larger landslides sourcing from the crest of the slopes could inundate the entire runout zone between the cliff bottom and the F-angle line.	Factor of about 1.5 to 2.0 uncertainty in the upward direction.
f. The number of trips carried out per year and the time spent on a trip by DOC and GBA staff.	These parameters are constrained by the data provided to GNS Science by Stantec (2020). However, the time spent per year by DOC and GBA staff in the study area does vary, so this does have an impact on the risk.	A 50% reduction in the amount of time spent on the beach would decrease the risk by a factor of about 2.
g. The location on the beach.	The risk is higher closer to the cliff bottom and reduces with distance out from the cliff bottom to the sea. Therefore, a walk at Spring low tide is safer than Neap low tide.	There is a factor of 1.4 difference between the Neap and Spring tide routes.

Issue	Direction and Scale of Uncertainty	Implications for Risk
h. Vulnerability: Probability person killed, if struck by debris.	<p>Could make a significant difference for the moderate to large volume debris avalanches based on precedence and the possibility that a person may be aware of a landslide and take evasive action by running into the sea. However, these vulnerability values will always be large for the larger landslides, given the volumes of debris involved, and it is unlikely that people could outrun or 'dodge' such large volumes of debris, hence the recorded injuries.</p> <p>The vulnerability will also vary depending upon where a person is on the beach, i.e. it will be higher if a person is under the cliff, near the cliff toe and on the Neap low tide route, versus further away from the cliff toe on the Spring low tide route.</p>	<p>Would vary by a factor of about 1.3 to 2.0 between the values used in this report. Could be a relatively large factor of difference, but limited data is currently available.</p>
i. The difference in the vulnerability between a walker and a person on a tractor (passenger).	<p>A relatively small difference, but the passenger on a tractor is elevated off the ground and may stand a better chance of not being in the path of debris.</p>	<p>Would vary by a factor of 1.2 lower for a passenger on a tractor.</p>
j. The difference in the vulnerability between a walker on the Spring or Neap low tide routes.	<p>This was tested by adopting a reasonable lower set of vulnerability values for the Spring low tide walker and passenger and applying them to the LPR calculations for each F-angle line while keeping the cliff bottom LPR values that use the original vulnerability values the same.</p> <p>This considers that the person further out from the cliff toe has more time to notice debris coming towards them and take evasive action.</p>	<p>A factor of 1.2 decrease in risk between the original lower scenario and the one with the revised Spring low tide vulnerability values for the walker, and a 1.4 decrease for the passenger on a tractor.</p>
k. The effectiveness of HDC's current risk mitigation strategy of signage and information.	<p>The use of warning signs and the presence of security guards at the start of the walk to inform people of the risk have reduced the number of walkers visiting the gannets by about 50% (Stantec 2020).</p>	<p>A factor of 2.0 decrease in the societal risk. The risk to the individual does not change.</p>
l. The effectiveness of GBA's current risk mitigation strategy.	<p>Could be a significant uncertainty for visitors, as the risk to the individual (per trip) is dominated by non-earthquake-induced landslides and is therefore dependent on the assumptions about how effective the current mitigation strategy is in mitigating the risk from them.</p>	<p>A potentially large uncertainty, and difficult to quantify.</p>

## 5.0 RISK IN CONTEXT

There are no national or international quantitative standards setting out risk levels that are considered tolerable or intolerable for visitors to geologically active areas. It is useful, though, to compare the risk associated with visiting the gannet colonies with the risks involved from other activities in which visitors might participate in New Zealand (or elsewhere). Such comparisons are provided in Section 5.1. Section 5.2 compares the risk to DOC, HDC and GBA staff with that in other New Zealand workplaces. Finally, Section 5.3 considers where the f/N curves from Section 4.3 would sit in relation to other New Zealand experiences of multiple-fatality accidents.

Please note that the risks presented for walkers and DOC, HDC and GBA staff within the Cape Kidnappers study area do not include any consideration of the potential reduction in risk caused by the control measures that are currently in place.

### 5.1 Visitor Individual Risk in Context

The model forecasts between 0 and 2 deaths for a walker, and between 1 and 5 for a GBA passenger, based on estimates of the total number of trips made over the past 67 years. Although nobody has been killed, the model forecasts a person being hit every 40,000 to 50,000 trips for walkers and 80,000 to 100,000 trips for GBA passengers, depending on whether the trips are along the Neap or Spring low tide routes and whether the lower or upper non-earthquake-induced landslide production rates are used in the model. The difference is based on their exposure time, as the GBA passenger spends less time in the hazard area. The estimated number of people hit and injured since 1973 is five (four walkers and one GBA worker), and there have been at least as many near misses, one occurred in 2019 (Stantec 2020). The two walkers hit by debris in 2019 were very lucky to have not been killed. We believe this is mainly because they were far away from the cliff bottom, walking around an already existing pile of landslide debris.

There could have been between 56,000 and 92,000 trips made by walkers since 1973, based on DOC track counter data from 2015 and 2018. The model forecasts that there should have been between 1 and 3 people hit, given the number of trips made. For the GBA passengers, the total number of trips made is roughly estimated to be between 400,000 and 500,000 over the last 67 years. The model forecasts that there should have been between 4 and 7 people hit for the given number of trips made. For walkers, the model performs well, but for GBA passengers, the model overpredicts the number of people likely to be hit. This might be for several reasons:

1. The GBA drivers are vigilant and competent at spotting landslides and then stopping or driving away from them, effectively 'dodging' the debris.
2. The estimated number of trips made by GBA passengers over the years is too high, and/or the upper estimates of non-earthquake-induced landslide frequencies are too high.

While such risk levels are not particularly unusual in relation to some other active landscape areas in New Zealand, they are high in comparison with the risk from many other everyday leisure activities for which participants would generally be aware of significant risk, warned about it before participating and advised on what they could do to limit it.

The remainder of this section provides comparisons between the estimated risks associated with landslides in the study area and other risks faced by people at work and by tourists and visitors in New Zealand. Individual risk comparisons are presented as follows:

- with selected popular tourist activities in New Zealand, e.g. cycling, walking, rafting, jet boating and parachute and bungy jumping (Figure 5.1); and
- with selected New Zealand sport and leisure activities, e.g. golf, cricket, dancing, swimming, etc. (Figure 5.2).

Much of the comparison data used in this report were compiled by Taig and McSaveney (2015) and Massey et al. (2019). The comparisons are presented using the range of landslide risk estimated in Section 4 (adopting the lower and upper scenarios) for the two representative routes along the beach (Spring and Neap low tides).

While Figure 5.1 is a useful comparison between activities, it is not a good comparison of the risk relative to the time exposed doing each activity. If the walkers and passengers of GBA spent as much time exposed at Cape Kidnappers as the time spent overnight in Milford Sound or climbing Aoraki, then the risk per trip at Cape Kidnappers would increase significantly by a factor of about 2–4.

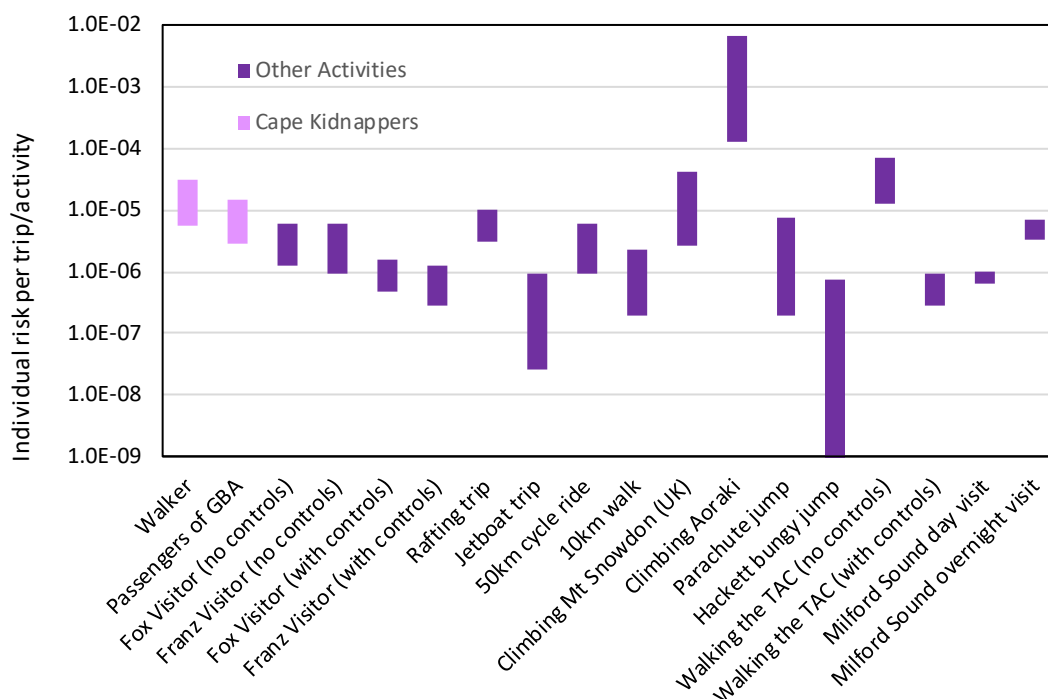


Figure 5.1 Fatality risk per single round trip for some popular adventure tourism activities compared with the fatality risk per trip to visit the gannets.

Notes: The Fox and Franz Josef data are taken from Massey et al. (2019). The rafting and jet boat figures are 90% confident levels based on Maritime New Zealand data for deaths and number of participants in commercial trips between 2001 and 2013. The cycling and walking figures are all based on average fatality rates per km travelled on New Zealand roads, based on Ministry of Transport statistics and New Zealand Travel Survey road-usage figures for 2007–2012 (the most recent available at the time of writing). The ranges shown correspond to the variability of accident rate across different broad age groups. Mt Snowdon is in Wales; risk there is dominated by casualties along a narrow ridge route to the summit. The Mt Aoraki figure is based on the number of fatalities and of visitor nights spent in huts as recorded by DOC (as not all climbers record their visits to huts, this may overstate the risk per ‘hut night’). The parachute jump statistic is the 90% confidence interval based on 1 fatality in approximately 519,000 jumps from 2009–2013 inclusive (we are grateful to the New Zealand Parachute Industry Association for providing the data from their database and note that this risk level appears consistent with that in the UK and USA). The bungy jump statistic is the 90% confidence interval based on zero fatalities in over 3 million jumps carried out at AJ Hackett Bungy in New Zealand since the first commercial bungy jump was established by them in 1988 (source – AJ Hackett web site [www.bungy.co.nz](http://www.bungy.co.nz)). The risk related to walking the Tongariro Alpine Crossing (TAC) was taken from Jolly et al. (2014). The risk reduction from putting in place the controls was estimated by DOC. The risk related to Milford Sound Tsunami hazards was taken from Taig and McSaveney (2015).

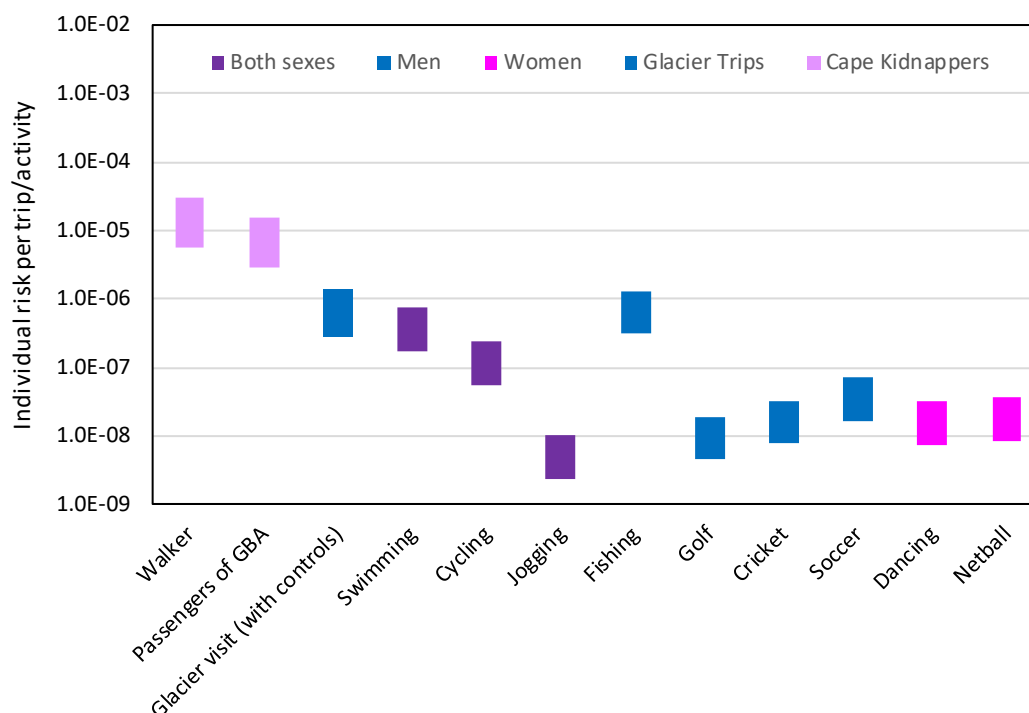


Figure 5.2 Fatality risk per day for visiting the gannets compared to the fatality risk per day from some popular New Zealand sport and leisure activities for the period January 2001 to June 2014.

Notes: We are grateful to the Accident Compensation Commission for providing us with a summary of all fatal accident claims made to them for sports-related deaths over the period January 2001 to June 2014, and to Sport New Zealand for their published data on participation levels in sport and leisure activities in New Zealand, based on their 2007–2008 survey. This survey enables reasonably reliable estimates to be made of the number of New Zealanders who participate in sport. However, it does not enable reliable estimates of how often they participate in a given sport. We have therefore made assumptions as to the frequency with which people participate in different sports in order to estimate fatality rates per day to compare with the gannet visit risk levels. Our assumption is that people participate in a given sport between once a week and once a month, except for swimming, jogging and cycling, where we assume participation rates are between twice a week and twice a month. The cycling risk estimate is lower than that of the 50 km cycle ride in Figure 5.1, as it is assumed that weekly and monthly participation involves cycling over shorter distances and not 50 km.

The comparison results show that:

- The risk levels per trip associated with visiting the gannets are slightly less than those from eruption hazards when walking the Tongariro Alpine Crossing, without DOC controls in place, but they are higher than those from visiting Fox Glacier and Franz Josef Glacier with or without DOC controls in place.
- The risk levels per trip are at the upper end of the range of the risk levels associated with other popular New Zealand tourist activities and are higher than those associated with several other ‘adventure’ activities, such as visiting the glaciers, rafting and jet boating.
- The risk per day for visiting the gannets is high compared to the fatality risk per day from some other popular New Zealand sport and leisure activities.

It should be noted that TTAC Ltd and GNS Science are currently compiling more in-depth risk comparators for DOC. For example, the cycling comparator currently shown in Figures 5.1 and 5.2 is for road cycling, whereas mountain biking is more appropriate and is included in the more in-depth comparator report currently being prepared.

## 5.2 Staff Risk in Context

This section shows the comparison between the DOC and GBA staff risk (AIFR) with workplace fatality risk for different industries, e.g. forestry, mining, transport and agricultural, etc. (Figure 5.3). The results show that:

- The fatality risk per year (AIFR) to GBA staff is high when compared to other mortality data, but, for DOC staff, it is lower than the risk those staff at Fox and Franz Josef are exposed to with the risk management controls put in place by DOC.
- The total fatalities per employee per year for GBA staff are slightly higher than those in the forestry and mining industries, two of New Zealand’s high-risk industries. However, not many GBA employees (2–3) are exposed to these levels of risk.

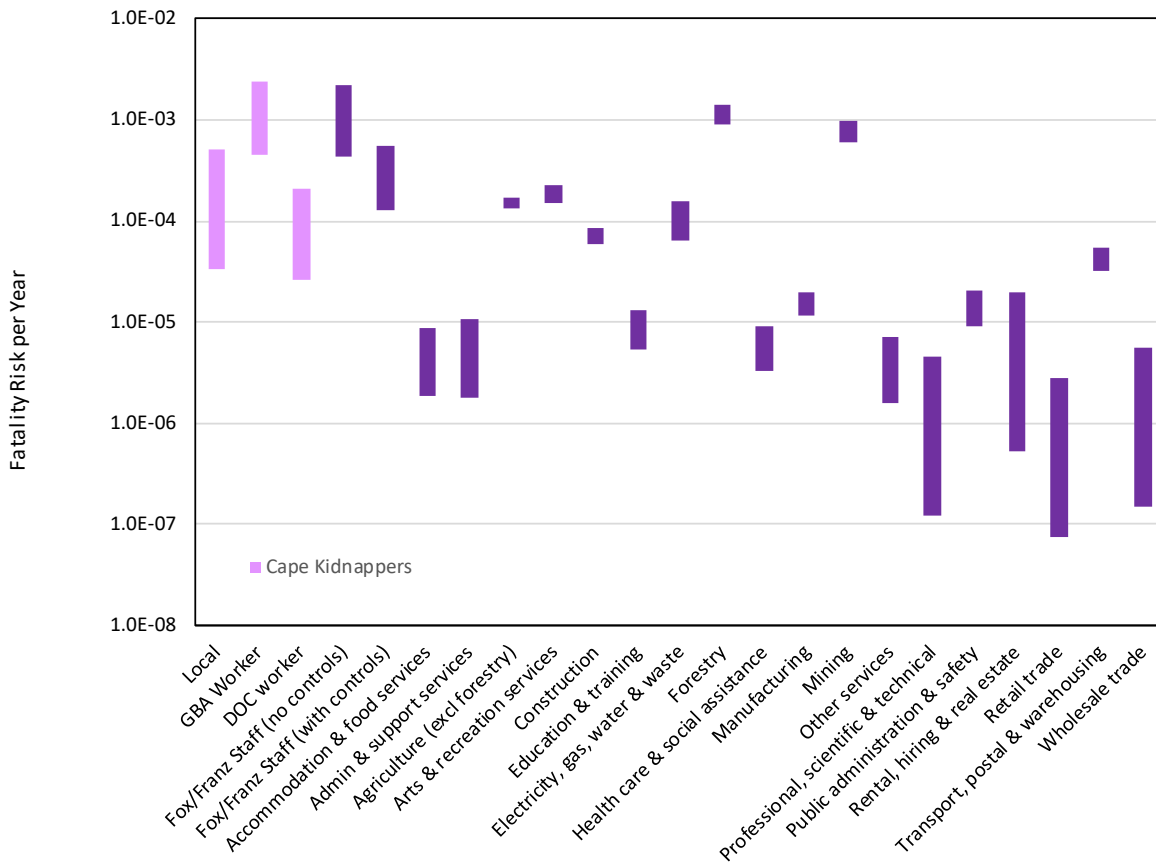


Figure 5.3 The total fatalities per employee per year for DOC and GBA staff at Cape Kidnappers compared with those from other New Zealand industries (2007–2017 Department of Labour data), shown as dark purple.

Notes: Statistics on deaths in workplaces (these include all deaths, not just those of people at work, so tend to overstate the risk to workers themselves) are collected and published by the Department of Labour (DOL, now part of the Ministry of Business, Innovation and Employment [MBIE]). These have been normalised per employee per year (based on numbers of people employed in each sector published by the Ministry of Economic Development, [MED]).

### 5.3 Societal Risk in Context

The societal risks from visiting the gannets are slightly lower than those from people visiting the Fox and Franz Josef glaciers, and those from past New Zealand earthquake, storm and flood events that have killed multiple people (Figure 5.4).

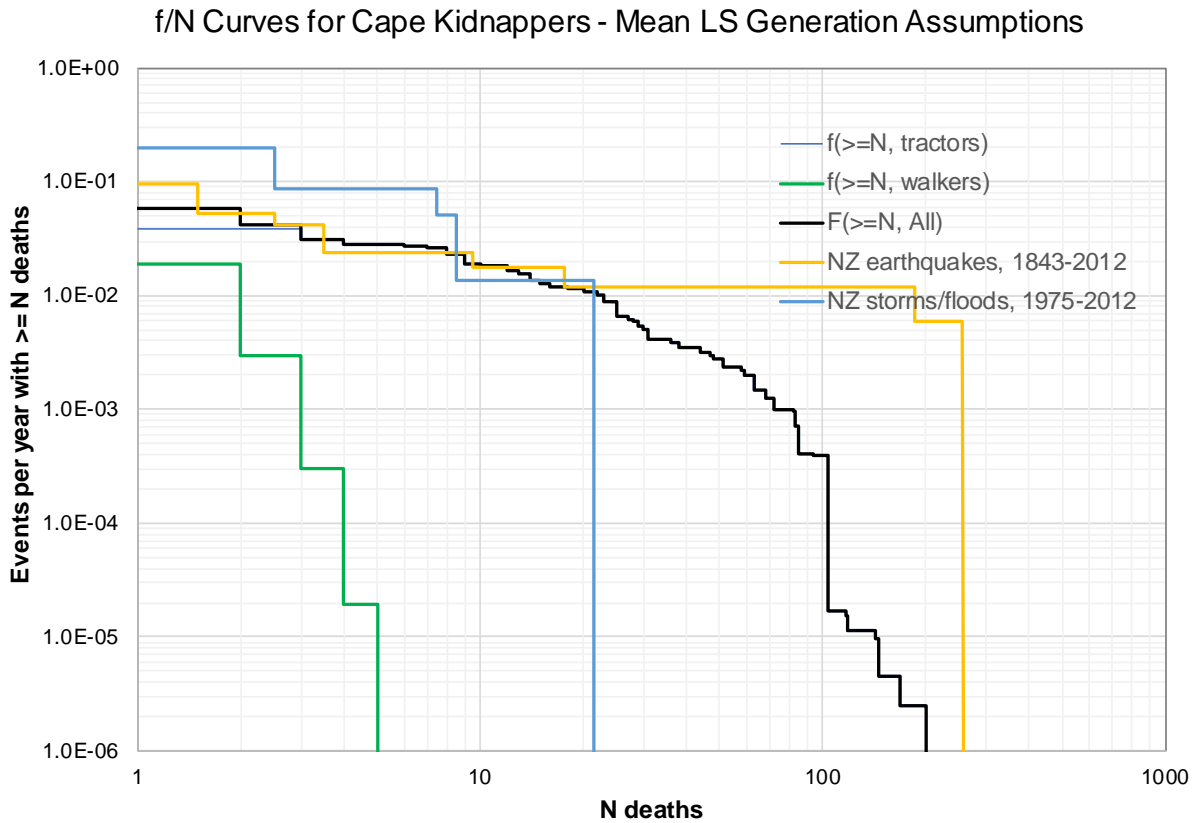


Figure 5.4 The annual frequency ( $f$ ) of events with a given number ( $N$ ) of more deaths for the study area, compared to those from New Zealand earthquakes and storms and/or floods.

## **6.0 RISK MANAGEMENT**

The people at greatest risk from landslides in the study area are GBA staff and locals, as they spend the most time in the hazard areas. GBA staff (the main operator) is the person most exposed to landslide hazards and therefore the person at highest risk. The safety of employees is regulated under the Health and Safety at Work Act 2015, which sets out to promote the management of hazards in the workplace by requiring employers to identify and control hazards that may cause harm and promote employees and others to take practicable steps to ensure their safety and the safety of others. The Act does not quantify 'safety' but does require employers to take all practical steps to identify and control hazards that may cause harm. If the hazards cannot be controlled, employers are required to take all practical steps to isolate employees from the hazard.

It is difficult to quantify the impact that the control measures, currently in place, have on reducing the risk. The risk (not hazard) from landslides can be controlled significantly by understanding, for non-earthquake-induced landslides, when they are most likely to happen and not going on the beach at those times of the year. So, what are the practical steps that could be taken on the beach to isolate people from the hazard? Some risk mitigation strategies are discussed by Stantec (2020), and some additional steps are listed below.

### **6.1 Warning Staff and Visitors that the Hazard is Present**

While the contribution to risk from earthquake-induced landslides is lower than that from non-earthquake-induced landslides, earthquakes could trigger lots of landslides at the same time. Therefore, earthquake-induced landslides could potentially kill many people, if an earthquake were to occur when a large group of GBA passengers were on the beach. The hazards associated with large earthquakes within the study area are invisible. Potential visitors and employees should be able to access information about the dangers they could be exposed to and the risks in going there. This information should be freely available to them when they are planning a travel itinerary, and similar information should be available to them on arrival at the beach and the GBA office. The recent measures adopted by HDC (informing visitors of the risk via signs and security guards) has resulted in a 50% drop in people visiting the gannets (Stantec 2020). There may be a challenge in presenting this information in a positive way, as such risks tend to be abstract for most people, and not easily understood. Some of the comparison risk graphs presented in this report might be helpful when informing people about the landslide hazards that are present within the study area. The risk levels involved are such that it is imperative that visitors are fully aware of the risk before committing to a trip.

### **6.2 Informing Staff and Visitors of the Measures in Place to Make it Safer**

One of the more positive ways of informing staff and visitors of the potential dangers within the study area is to focus on the safety measures that are in place – telling them about the evacuation routes (i.e. away from the cliff and downstream of the streams and gullies that exit onto the beach) or what will happen / be expected of them if a DOC staff or a GBA guide notices a potential landslide hazard, or if a large landslide and/or earthquake occurs. Such an approach informs staff and visitors that it is a clearly recognised hazard and also tells them that the area has an earthquake and landslide hazard.

Staff and visitors should also be informed of other risks, e.g. from tsunami and drowning hazards, which also exist in the study area.



### 6.3 Closing the Operations during Periods when the Hazard Might be Increased

GBA, DOC and HDC staff are experienced and know the study area and the weather, and other climatic conditions, well. For example, closing access to the beach when the likelihood of landslides occurring is elevated is an effective way to reduce the risk. However, knowing when the risk from landslides is elevated is not easy. In the past, most of the larger non-earthquake-induced landslides in the study area have occurred in response to no obvious trigger, such as rain. For example, periods of hot and dry weather and diurnal changes in temperature can lead to rock mass expansion and contraction, which can cause cyclic displacements and micro-cracking of the rock mass. Over time, such changes can lead to the development of landslides. In addition, many landslides appear to have been initiated by erosion from the sea. Such hazards are likely to be storm-driven, and, if the frequency of storms is increasing because of climate change, the frequency of landslides could also increase.

The GBA guides have also noted that large landslides tend to be preceded by smaller ones from the same location as areas 'switch on' and then 'switch off' again. These debris avalanche and rockfall events may occur via progressive failure, where a change in the stresses within a slope occurs (i.e. in this case, the 23<sup>rd</sup> January debris avalanche event [de Vilder et al. 2019]), resulting in stress redistribution throughout the surrounding rock mass. As this stress redistributes, this results in further cracking within the material and, subsequently, the failure of the surrounding rock mass (Eberhardt et al. 2004; Rosser et al. 2007).

However, when an area is 'switched on', meaning that the landslide activity is higher than normally observed (e.g. the January 2019 landslide was preceded by several smaller landslides), the hazard, and therefore risk, can be significantly increased.

Currently, the information recorded about landslides in the study area is not sufficiently detailed enough to establish any trends in the data. Such trends could be used to help establish the conditions under which landslides occur. Once established, such trends could become part of the Hazard Management process. We would be happy to work with DOC, HDC and GBA to set up a landslide register, which could be used to document landslides in the study area. In addition, repeat aerial drone surveys of the cliff face would provide a means to quantify the number and volume of landslides that occur in the study area between surveys. Such surveys could be carried out annually or biannually, or after a major storm or earthquake event. These surveys may also provide answers to the impact of climate change, which may result in increased erosion and landslides due to higher sea levels and increased storminess (e.g. Trenhaile 2011), on landslide activity and associated risk.

Another potential management strategy is to close the beach at Neap low tides, as this could decrease the risk by up to a factor of 2, lower than the risk estimated using the lower scenario (Table 4.2). Such a strategy could have the following benefits:

- Simple and practicable to implement.
- May not affect GBA's business too much, as people would be booking in a smaller number of larger groups.
- Reduce GBA worker time spent under the cliff (making it self-enforcing for tractors).
- May also reduce people getting trapped by the tides.

## 7.0 CONCLUSIONS

With reference to the study area boundaries as shown in Figure 1.2, the conclusions of this report are:

1. Landslides have and will continue to occur from the slopes in the study area. The main landslides hazard types affecting the representative routes along the beach to visit the gannet colonies are rockfalls and debris avalanches.
2. The risk from other natural hazards present along the beach, such as tsunami and drowning, has not been quantified. The risk from these hazards would be in addition to the risk from landslides.
3. The LPR varies along the length of each route as a function of the proximity of the route to the steep slopes (cliffs). The LPR along the Spring tide route is marginally less than the LPR along the Neap tide route. This is because the Spring tide route is further away from the steep slopes.
4. The main contributor to the risk is from non-earthquake-induced landslides. There is about an order of magnitude difference in the risks calculated for earthquake and non-earthquake-induced landslides.
5. The risk levels per trip associated with visiting the gannets are slightly less than those from eruption hazards when walking the Tongariro Alpine Crossing without risk control measures, such as monitoring volcanic unrest. They are higher than those from visiting Fox Glacier and Franz Josef Glacier with or without risk control measures in place, where the control measures mainly comprise closing the valleys during heavy rain, which is when landslides can occur.
6. The risk levels per trip are at the upper end of the range of the risk levels associated with other popular New Zealand tourist activities and higher than those associated with several other 'adventure' activities, such as visiting the glaciers, rafting and jet boating.
7. The fatality risk per day for visiting the gannets is high compared to the fatality risk per day from some other popular New Zealand sport and leisure activities.
8. The people at greatest risk from landslides in the study area are GBA staff, as they spend the most time in the hazard areas. GBA staff (the main operator) is the person most exposed to landslide hazards and therefore the person at highest risk.
9. The fatality risk per year (AIFR) to GBA staff is high when compared to other mortality data, but, for DOC staff, it is lower than the risk those staff at Fox and Franz Josef are exposed to with the risk management controls put in place by DOC.
10. The risk expressed as total fatalities per employee per year for GBA staff is slightly higher than those in the forestry and mining industries, two of New Zealand's high-risk industries. However, not many GBA employees (2–3) are exposed to these levels of risk.
11. The societal risk from visiting the gannets is slightly lower than the risk from people visiting the Fox and Franz Josef glaciers, and the risk from past New Zealand earthquake, storm and flood events that have killed multiple people.
12. While the contribution to the AIFR and the risk per trip from earthquake-induced landslides is lower than that from non-earthquake-induced landslides, earthquakes could trigger lots of landslides at the same time. Therefore, societal risk is driven by earthquake-induced landslides, as these could potentially kill many people if an earthquake were to occur when a large group of GBA passengers were on the beach.

13. One of the largest uncertainties in the risk estimates is the frequency (number) and magnitude (volume) of non-earthquake-induced landslides. Other potentially significant uncertainties are: a) the time spent walking or driving along the beach by the different users, b) the route a person walks along the beach between the Neap and Spring tides and c) the vulnerability of a person walking or driving along the beach.
14. These uncertainties combine to give a total factor of difference of between 6 and 8, which is between half to an order of magnitude difference in the uncertainty on the risk estimates, in either direction.
15. Although the risk model performs well for walkers, for GBA passengers, the model over-predicts the number of people likely to be hit and killed at those risk levels calculated adopting the upper estimates. This is thought to be because the upper estimates of non-earthquake-induced landslide frequencies are possibly too high.
16. The risk (not hazard) from landslides could be controlled by:
  - Understanding, for non-earthquake triggered landslides, when they are most likely to happen and not going on the beach at those times of the year.
  - Warning staff and visitors that the hazard is present.
  - Informing staff and visitors of the measures in place to make it safer.
  - Recommending that they take advantage of the local knowledge, and reduced exposure time, by going on an organised tour.

## 8.0 RECOMMENDATIONS

Based on the findings of this study, GNS Science recommends that HDC, DOC and GBA consider the following:

1. Warning staff and visitors that the hazard is present and informing staff and visitors of the measures in place to make it safer. This could be achieved by producing a short brochure that describes the results of this report in simple language, and the steps HDC, DOC and GBA take to manage the risk to their clients. A good example of such a brochure can be found here: <https://www.ccc.govt.nz/assets/documents/Environment/Land/gns-ph-Summary1-3web.pdf>
2. Closing operations during periods when the hazard might be increased. To do this, however, requires knowledge of when the hazard rates are likely to be elevated.
3. Currently, the information recorded by DOC and the GBA operator about landslides in the study area is not sufficiently detailed enough to establish any trends in the data, although the GBA operator has a wealth of local information about landslide conditions. Such trends could be quantified to help DOC and GBA guides to establish the conditions under which landslides occur. Once established, such trends could become part of the DOC and GBA Hazard Management process. Once a better link between landslide occurrence and weather patterns, seasons, etc. can be established, it should be possible to more effectively manage the closures.
4. Repeat LiDAR and UAV surveys of the slopes should be carried out to quantify the changes between surveys, allowing the landslide frequency and volume to be further assessed over a longer time period. The frequency of the surveys can vary. Initially, we recommend carrying out a survey later in the year, with the next in either two years' time or following a major landslide, earthquake or storm event.
5. Continuing GBA's current practice of staff visiting the area before tourist trips to observe any changes that may have occurred on the slopes adjacent to the beach, as well as putting in place a process to incorporate any visitor observations relating to landslides.
6. This risk analysis presented in this report should be reviewed, and the risk re-analysed if needed, if site conditions change or if new data becomes available, for example:
  - a. when a person is hit by a landslide.
  - b. when the repeat LiDAR/UAV surveys show a 'considerable' change or potential change of the slopes; and/or
  - c. following a major event such as a storm or earthquake.

We would be happy to work with you to set thresholds for such events, which could be used to initiate a re-analysis of the risk.

## 9.0 ACKNOWLEDGEMENTS

The authors would like to thank HDC, DOC and GBA staff for sharing their knowledge of this beautiful part of New Zealand; Sally Dellow and Regine Morgenstern (GNS Science) for reviewing this report; and Tony Taig (TTAC Ltd) for reviewing the risk-model data and calculations used in the report.

## 10.0 REFERENCES

- Australian Geomechanics Society. 2007. Practice note guidelines for landslide risk management. *Australian Geomechanics*. 42(1):63–114.
- Brideau MA, de Vilder S, Massey C, Mitchell A, McDougall S, Aaron J. In press. Empirical relationships to estimate the probability of runout exceedance for various landslide types. *5<sup>th</sup> World Landslides Forum*; 2020 Nov 2–6; Kyoto, Japan.
- Brideau MA, Massey CI, Lukovic B, Morgenstern R. 2020. Deterministic mapping of potential landslide debris inundation in the Kaikōura District. Lower Hutt (NZ): GNS Science. 37 p. Consultancy Report 2019/102. Prepared for: Canterbury Regional Council.
- Christen M, Bühler Y, Bartelt P, Leine R, Glover J, Schweizer A, Graf C, McArdell B, Gerber W, Deubelbeiss Y, et al. 2012. Integral hazard management using a unified software environment. In: *12<sup>th</sup> Congress Interpraevent; 2012 Apr 23–26; Grenoble, France*. Klagenfurt (AT): International Research Society. p. 77–86.
- Corominas J. 1996. The angle of reach as a mobility index for small and large landslides. *Canadian Geotechnical Journal*. 33(2):260–271. doi:10.1139/t96-005.
- de Vilder S, Dellow GD, Archibald GC, Morgenstern R. 2019. The 23<sup>rd</sup> January 2019 Cape Kidnappers coastal cliff collapse, Hawke's Bay, New Zealand. Lower Hutt (NZ): GNS Science. 11 p. (GNS Science report; 2019/26).
- de Vilder S, Massey CI. In press. Guidelines for natural hazard risk analysis on Public Conservation Lands and Waters – Part 3: analysing landslide risk to point and linear features. Lower Hutt (NZ) GNS Science. 45 p. (GNS Science report; 2020/52).
- Du J, Yin K, Nadim F, Lacasse S. 2013. Quantitative vulnerability estimation for individual landslides. In: *Proceedings of the 18<sup>th</sup> International Conference on Soil Mechanics and Geotechnical Engineering, Paris 2013*. p. 2181–2184.
- Eberhardt E, Stead D, Coggan JS. 2004. Numerical analysis of initiation and progressive failure in natural rock slopes – the 1991 Randa rockslide. *International Journal of Rock Mechanics and Mining Sciences*. 41(1):69–87. doi:10.1016/S1365-1609(03)00076-5.
- Finlay PJ, Mostyn GR, Fell R. 1999. Landslide risk assessment: prediction of travel distance. *Canadian Geotechnical Journal*. 36(3):556–562. doi:10.1139/t99-012.
- Heim A. 1932. Landslides & human lives. Skermer N, translator. Vancouver (CA): BiTech Publishers. 195 p.
- Hungr O, McDougall S. 2009. Two numerical models for landslide dynamic analysis. *Computers & Geosciences*. 35:978–992. doi:10.1016/j.cageo.2007.12.003.
- Hungr O, Leroueil S, Picarelli L. 2014. The Varnes classification of landslide types, an update. *Landslides*. 11(2):167–194. doi:10.1007/s10346-013-0436-y.
- Iverson RM. 2014. Debris flows: behaviour and hazard assessment. *Geology Today*. 30(1):15–20. doi:10.1111/gto.12037.

- Jolly GE, Keys HJR, Procter JN, Deligne NI. 2014. Overview of the co-ordinated risk-based approach to science and management response and recovery for the 2012 eruptions of Tongariro volcano, New Zealand. *Journal of Volcanology and Geothermal Research*. 286:184–207. doi:10.1016/j.jvolgeores.2014.08.028.
- Lee EM, Jones DKC. 2014. Landslide risk assessment. 2<sup>nd</sup> ed. London (UK): ICE Publishing. 509 p.
- Li Tianchi. 1983. A mathematical model for predicting the extent of a major rockfall. *Zeitschrift fur Geomorphologie*. 27(4):473–482.
- Loew S, Gschwind S, Gischig V, Keller-Signer A, Valenti G. 2017. Monitoring and early warning of the 2012 Preonzo catastrophic rockslope failure. *Landslides*. 14(1):141–154. doi:10.1007/s10346-016-0701-y.
- Massey CI, de Vilder S, Taig T, Lukovic B, Archibald GC, Morgenstern R. 2019. Landslide hazard and risk assessment for the Fox and Franz Josef Glacier valleys. Lower Hutt (NZ): GNS Science. 79 p. + appendices. Consultancy Report 2018/206. Prepared for: Department of Conservation.
- Massey CI, Petley DN, McSaveney MJ. 2013. Patterns of movement in reactivated landslides. *Engineering Geology*. 159:1–19. doi:10.1016/j.enggeo.2013.03.011.
- Massey CI, Townsend D, Jones K, Lukovic B, Rhoades D, Morgenstern R, Rosser B, Ries W, Howarth J, Hamling I, et al. 2020. Volume characteristics of landslides triggered by the MW7.8 2016 Kaikōura Earthquake, New Zealand, derived from digital surface difference modelling. *Journal of Geophysical Research: Earth Surface*. doi:10.1029/2019jf005163.
- Massey CI, Townsend DT, Lukovic B, Morgenstern R, Jones K, Rosser B, de Vilder S. In press. Landslides triggered by the MW7.8 14 November 2016 Kaikōura Earthquake: An update. *Landslides*.
- McDougall S. 2017. 2014 Canadian Geotechnical Colloquium: landslide runout analysis – current practice and challenges. *Canadian Geotechnical Journal*. 54(5):605–620. doi:10.1139/cgj-2016-0104.
- Olsen MJ, Massey CI, Senogles A, Leshchinsky BA, Wartman J. 2019. Predicting seismic-induced rockfall hazard for targeted site mitigation. Corvallis (OR): School of Civil and Construction Engineering, Oregon State University. Project SPR-809. Prepared for Oregon Department of Transportation Research Section and Federal Highway Administration.
- RAMMS. 2016. RAMMS – rockfall user manual: a numerical model for rockfall in research and practice, User Manual v1.6, Rockfall. Davos Dorf (CH): WSL Institute for Snow and Avalanche Research SLF. 102 p.
- Reid ME, Brien DL, LaHusen RG, Roering JJ, de la Fuente J, Ellen SD. 2003. Debris-flow initiation from large, slow-moving landslides. In: Rickenmann D, Chen CL, editors. *Proceedings of the 3<sup>rd</sup> International Conference on Debris-Flow Hazards, Davos Switzerland, September 10–12, 2003*. Reston (VA): U. S. Geological Survey. p. 155–166.
- Rosser N, Lim M, Petley D, Dunning S, Allison R. 2007. Patterns of precursory rockfall prior to slope failure. *Journal of Geophysical Research: Earth Surface*. 112(F4):F04014. doi:10.1029/2006jf000642.
- Stantec. 2020. Clifton Beach landslide hazard assessment. Stantec. 256 p. Consultancy Report.
- Stirling MW, McVerry GH, Gerstenberger MC, Litchfield NJ, Van Dissen RJ, Berryman KR, Barnes P, Wallace LM, Villamor P, Langridge RM, et al. 2012. National seismic hazard model for New Zealand: 2010 update. *Bulletin of the Seismological Society of America*. 102(4):1514–1542. doi:10.1785/0120110170.

- Taig T, McSaveney MJ. 2015. Milford Sound risk from landslide-generated tsunamis. Lower Hutt (NZ): GNS Science. 57 p. Consultancy Report 2014/224. Prepared for: Environment Southland.
- Trenhaile AS. 2011. Predicting the response of hard and soft rock coasts to changes in sea level and wave height. *Climatic Change*. 109(3):599–615. doi:10.1007/s10584-011-0035-7.

This page left intentionally blank.



## **APPENDICES**

This page left intentionally blank.

## APPENDIX 1 EARTHQUAKE-INDUCED LANDSLIDE FREQUENCY MAGNITUDE

Table A1.1 Hazard Area 1, adopting the study area landslide distribution: Landslide source volume classes and the estimated number of landslides that could be generated by the representative PGA within in each band using the data contained in Tables 3.2 and 3.3.

Landslide Volume Class (m <sup>3</sup> )	N Landslides Band 1		N Landslides Band 2		N Landslides Band 3		N Landslides Band 4	
	Lower	Upper	Lower	Upper	Lower	Upper	Lower	Upper
1	1309	2237	2421	3840	4645	7047	10,205	15,065
10	238	407	440	698	844	1281	1855	2739
100	181	310	335	531	643	975	1412	2085
1000	35	60	65	104	125	190	276	407
10,000	4	7	8	13	15	23	34	50
25,000	0.2	0.3	0.4	0.6	0.7	1.1	1.6	2.3
50,000	0.11	0.2	0.2	0.3	0.4	0.6	0.8	1.2
100,000	0.05	0.08	0.09	0.1	0.16	0.2	0.4	0.5

Table A1.2 Hazard Area 2, adopting the study area landslide distribution: Landslide source volume classes and the estimated number of landslides that could be generated by the representative PGA within in each band using the data contained in Tables 3.2 and 3.3.

Landslide Volume Class (m <sup>3</sup> )	N Landslides Band 1		N Landslides Band 2		N Landslides Band 3		N Landslides Band 4	
	Lower	Upper	Lower	Upper	Lower	Upper	Lower	Upper
1	1609	2756	2967	4714	5682	8630	12,471	18,418
10	293	501	539	857	1033	1569	2267	3349
100	223	381	411	652	786	1194	1726	2549
1000	43	74	80	127	153	233	337	498
10,000	5	9	10	16	19	29	42	61
25,000	0.2	0.4	0.5	0.7	0.9	1.3	1.9	2.8
50,000	0.13	0.2	0.2	0.4	0.5	0.7	1.0	1.5
100,000	0.06	0.10	0.11	0.2	0.20	0.3	0.4	0.7

Table A1.3 Hazard Area 3, adopting the study area landslide distribution: Landslide source volume classes and the estimated number of landslides that could be generated by the representative PGA within in each band using the data contained in Tables 3.2 and 3.3.

Landslide Volume Class (m <sup>3</sup> )	N Landslides Band 1		N Landslides Band 2		N Landslides Band 3		N Landslides Band 4	
	Lower	Upper	Lower	Upper	Lower	Upper	Lower	Upper
1	791	1365	1441	2302	2739	4174	5986	8856
10	144	248	262	418	498	759	1088	1610
100	109	189	199	318	379	578	828	1226
1000	21	37	39	62	74	113	162	239
10,000	3	5	5	8	9	14	20	29
25,000	0.1	0.2	0.2	0.4	0.4	0.6	0.9	1.4
50,000	0.07	0.1	0.1	0.2	0.2	0.3	0.5	0.7
100,000	0.03	0.05	0.05	0.1	0.10	0.1	0.2	0.3

Table A1.4 Hazard Area 4, adopting the study area landslide distribution: Landslide source volume classes and the estimated number of landslides that could be generated by the representative PGA within in each band using the data contained in Tables 3.2 and 3.3.

Landslide Volume Class (m <sup>3</sup> )	N Landslides Band 1		N Landslides Band 2		N Landslides Band 3		N Landslides Band 4	
	Lower	Upper	Lower	Upper	Lower	Upper	Lower	Upper
1	1026	1737	1927	3037	3730	5636	8236	12,134
10	187	316	350	552	678	1025	1497	2206
100	142	240	267	420	516	780	1140	1679
1000	28	47	52	82	101	152	222	328
10,000	3	6	6	10	12	19	27	40
25,000	0.2	0.3	0.3	0.5	0.6	0.9	1.3	1.9
50,000	0.08	0.1	0.2	0.3	0.3	0.5	0.7	1.0
100,000	0.04	0.06	0.07	0.1	0.13	0.2	0.3	0.4

Table A1.5 Hazard Area 1, adopting the Kaikōura earthquake landslide distribution: Landslide source volume classes, and the estimated number of landslides that could be generated by the representative PGA within in each band using the data contained in Tables 3.2 and 3.3.

Landslide Volume Class (m <sup>3</sup> )	N Landslides Band 1		N Landslides Band 2		N Landslides Band 3		N Landslides Band 4	
	Lower	Upper	Lower	Upper	Lower	Upper	Lower	Upper
1	458	848	848	1345	1626	2468	3573	5275
10	83	154	154	244	296	449	650	959
100	8	15	15	24	30	45	65	96
1000	16	29	29	46	55	84	121	179
10,000	5	9	9	15	18	28	40	59
25,000	0.7	1.4	1.4	2.2	2.6	4.0	5.7	8.4
50,000	0.3	0.6	0.6	1.0	1.2	1.8	2.6	3.9
100,000	0.1	0.1	0.1	0.2	0.2	0.3	0.4	0.7

Table A1.6 Hazard Area 2, adopting the Kaikōura earthquake landslide distribution: Landslide source volume classes, and the estimated number of landslides that could be generated by the representative PGA within in each band using the data contained in Tables 3.2 and 3.3.

Landslide Volume Class (m <sup>3</sup> )	N Landslides Band 1		N Landslides Band 2		N Landslides Band 3		N Landslides Band 4	
	Lower	Upper	Lower	Upper	Lower	Upper	Lower	Upper
1	564	965	1039	1651	1990	3022	4367	6449
10	102	175	189	300	362	549	794	1173
100	10	18	19	30	36	55	79	117
1000	19	33	35	56	68	103	148	219
10,000	6	11	12	18	22	34	49	72
25,000	0.9	1.5	1.7	2.6	3.2	4.8	7.0	10.3
50,000	0.4	0.7	0.8	1.2	1.5	2.2	3.2	4.8
100,000	0.1	0.12	0.1	0.2	0.2	0.4	0.5	0.8

Table A1.7 Hazard Area 3, adopting the Kaikōura earthquake landslide distribution: Landslide source volume classes, and the estimated number of landslides that could be generated by the representative PGA within in each band using the data contained in Tables 3.2 and 3.3.

Landslide Volume Class (m <sup>3</sup> )	N Landslides Band 1		N Landslides Band 2		N Landslides Band 3		N Landslides Band 4	
	Lower	Upper	Lower	Upper	Lower	Upper	Lower	Upper
1	277	478	504	806	959	1462	2096	3101
10	50	87	92	147	174	266	381	564
100	5	9	9	15	17	27	38	56
1000	9	16	17	27	33	50	71	105
10,000	3	5	6	9	11	16	23	35
25,000	0.4	0.8	0.8	1.3	1.5	2.3	3.4	5.0
50,000	0.20	0.4	0.4	0.6	0.7	1.1	1.5	2.3
100,000	0.03	0.06	0.06	0.1	0.12	0.2	0.3	0.4

Table A1.8 Hazard Area 4, adopting the Kaikōura earthquake landslide distribution: Landslide source volume classes, and the estimated number of landslides that could be generated by the representative PGA within in each band using the data contained in Tables 3.2 and 3.3.

Landslide Volume Class (m <sup>3</sup> )	N Landslides Band 1		N Landslides Band 2		N Landslides Band 3		N Landslides Band 4	
	Lower	Upper	Lower	Upper	Lower	Upper	Lower	Upper
1	359	608	675	1063	1306	1973	2884	4249
10	65	111	123	193	237	359	524	773
100	7	11	12	19	24	36	52	77
1000	12	21	23	36	44	67	98	144
10,000	4	7	8	12	15	22	32	48
25,000	0.6	1.0	1.1	1.7	2.1	3.2	4.6	6.8
50,000	0.27	0.4	0.5	0.8	1.0	1.5	2.1	3.1
100,000	0.04	0.07	0.08	0.1	0.16	0.2	0.4	0.5



[www.gns.cri.nz](http://www.gns.cri.nz)

#### Principal Location

1 Fairway Drive, Avalon  
Lower Hutt 5010  
PO Box 30368  
Lower Hutt 5040  
New Zealand  
T +64-4-570 1444  
F +64-4-570 4600

#### Other Locations

Dunedin Research Centre  
764 Cumberland Street  
Private Bag 1930  
Dunedin 9054  
New Zealand  
T +64-3-477 4050  
F +64-3-477 5232

Wairakei Research Centre  
114 Karetoto Road  
Private Bag 2000  
Taupo 3352  
New Zealand  
T +64-7-374 8211  
F +64-7-374 8199

National Isotope Centre  
30 Gracefield Road  
PO Box 30368  
Lower Hutt 5040  
New Zealand  
T +64-4-570 1444  
F +64-4-570 4657